18TH INTERNATIONAL CONFERENCE on Communications, Electromagnetics and Medical Applications (CEMA'24)

Sofia, Bulgaria
October 21, 2024

Organized by:
Faculty of Telecommunications of TU-Sofia, Bulgaria

NATIONAL TECHNICAL UNIVERSITY OF ATHENS, GREECE

SCHOOL OF ELECTRICAL AND COMPUTER ENGINEERING

PROCEEDINGS

OF 18TH INTERNATIONAL CONFERENCE ON COMMUNICATIONS, ELECTROMAGNETICS AND MEDICAL APPLICATIONS (CEMA'24)

Organized by:

FACULTY OF TELECOMMUNICATIONS
TECHNICAL UNIVERSITY OF SOFIA, BULGARIA

NATIONAL TECHNICAL UNIVERSITY OF ATHENS, GREECE,
SCHOOL OF ELECTRICAL AND COMPUTER ENGINEERING

NATIONAL TECHNICAL UNIVERSITY OF ATHENS, GREECE

SCHOOL OF ELECTRICAL AND COMPUTER ENGINEERING

Sofia, Bulgaria
21st October, 2024

KING 2001, Sofia

Edited by Prof. Dr. Eng. **Dimiter Tz. Dimitrov**

ISSN: 1314-2100

SCOPUS Indexing
http://suggestor.step.scopus.com/progressTracker, ID: 6B4F77263D276412.

Printed in Bulgaria
KING 2001, Sofia

P. Frangos

D. Dimitrov

K. Dimitrov

Dear Colleagues,

It is our privilege to thank all of you for your contributions submitted at 18th regular International Conference on 'Communication, Electromagnetic and Medical Applications' CEMA'24. This is a conference which should help future collaboration in the area of engineering, especially in the area of communication technologies and medical applications. This is an important scientific event not only in Balkan region, but in Europe, also. The International Conference on Communication, Electromagnetism and Medical Applications CEMA'24 is dedicated to all essential aspects of the development of global information and communication technologies, and their impact in medicine, as well. The objective of Conference is to bring together lecturers, researchers and practitioners from different countries, working on the field of communication, electromagnetism, medical applications and computer simulation of electromagnetic field, in order to exchange information and bring new contribution to this important field of engineering design and application in medicine. The Conference will bring you the latest ideas and development of the tools for the above mentioned scientific areas directly from their inventors. The objective of the Conference is also to bring together the academic community, researchers and practitioners working in the field of Communication, Electromagnetic and Medical Applications, not only from all over Europe, but also from America and Asia, in order to exchange information and present new scientific and technical contributions.

Many well known scientists took part in conference preparation as members of International Scientific Committee or/and as reviewers of submitted papers. We would like to thank all of them for their efforts, for their suggestions and advices.

On behalf of the International Scientific Committee, we would like to wish you successful presentations of your papers, successful discussions and new collaborations for your future scientific investigations.

Engineering and medicine should provide high level of living for all people.

D. Dimitrov
Conference Chairman

P. Frangos
Conference Vice Chairman

K. Dimitrov
Conference Vice Chairman

INTERNATIONAL SCIENTIFIC COMMITTEE

Chairman:

D. TZ. DIMITROV, Technical University of Sofia, Bulgaria

Vice Chairmen:

P. FRANGOS, National Technical University of Athens, Greece
K. L. DIMITROV, Technical University of Sofia, Bulgaria

Members

N. AMPILOVA,	University of Petersburg, Russia
T. AVOYAGI,	Tokyo Institute of Technology, Japan
A. BEKJARSKY,	Technical University of Sofia, Bulgaria
E. BOEMO,	University Authonoma, Barcelona, Spain
R. BRUZGIENE,	Kaunas University of Technology, Lithuania
N. DIB,	Jordan University of Science and Technology, Aman, Jordan
V. DUMBRAVA,	Kaunas University of Technology, Litvania
N. ESCUDEIRO,	ISEP, Porto, Portugal
E. GAGO-RIBAS,	University of Oviedo, Spain
V. GEORGIEVA,	Technical University of Sofia, Bulgaria
G. GOUSSETIS,	Heriot - Watt University, United Kingdom
S. V.HOEYE,	University of Oviedo, Spain
I. ILIEV,	Technical University of Sofia, Bulgaria
F. KLETT,	Franhofer Institute, Ilmenau, Germany
G. KLIROS,	Hellenic Air-Force Academy, Athens, Greece
V. KUKENSKA,	Technical University of Gabrovo, Bulgaria
L. LUBIH,	Technical University of Sofia, Bulgaria
G. MALLET,	University "Sophia Antipolis", Nice, France
G. MATSOPOULOS,	National Technical University of Athens, Greece
M. MARTINS,	Academia Militar da Amadora, DCEE, Portugal
M.– J. MORALES-GONZALES,	University of Valladolid, Spain
L. NARBUTAITE,	Kaunas University of Technology, Lithuania
K. NIKITA,	National Technical University of Athens, Greece
M. NIKOLOVA,	High Naval School, Varna, Bulgaria
A. PANAGOPOULOS,	National Technical University of Athens, Greece
J. PETROVSKA,	Medical University of Sofia, Bulgaria
H. ROTH,	University of Siegen, Germany
S. SAUTBEKOV,	Euroasian University, Astana, Kazakhstan
A. SAVOV,	Medical University of Sofia, Bulgaria
S. SAVOV,	Technical University of Varna, Bulgaria
H.-P. SCHADE,	Technical University of Ilmenau, Germany
I. SOLOVIEV,	University of St. Petersburg, Russia
L. SONG,	Technical University of Harbin, China
G. STAMATAKOS,	National Technical University of Athens, Greece
A. USHEVA,	University of Boston, USA
R. VERDONE,	University of Bologna, Italy

REVIEWERS

BALZANO, Q.	University of Maryland, USA
BEHARI, J.	Jawaharlal Nehru University ,New Delhi, India
BOEMO, E.	Technical University of Madrid, Spain
DIMITROV, D.	Technical University of Sofia, Bulgaria
DONTSCHEWA, M.	University of Applied Sciences, Dorbirn, Austria
GOUSSETIS, G.	Heriot - Watt University, United Kingdom
MALLET, G.	University "Sophia Antipolis", Nice, France
PETROVSKA, J.	Medical University of Sofia, Bulgaria
PRATO, F.	University of Western Ontario, Canada
ROTH, H.	University of Siegen, Germany
SAVOV, A.	Medical University of Sofia, Bulgaria
SCHADE, H-P.	Technical University of Ilmenau, Germany
SONG, L.	Technical University of Harbin, China
USHEVA, A.	University of Boston, USA

REGISTRATION

October, 21st, 2024, 10h – 16h

The conference registration desk will be in the Library of Technical University – Sofia
or on-line at Technical University – Sofia

CONFERENCE PROGRAM

October, 21st, 2024, Monday

OPENING CEREMONY

09h 30min – 10h
The Opening Ceremony will be on-line

SCIENTIFIC PROGRAM

FIRST SESSION

10h – 12h

Chairman: Prof. P. Frangos, *School of Electrical and Computing Engineering, National Technical University of Athens, Greece*

---

1. **DESIGN AND ARCHITECTURE OF CAN2WIFI SYSTEM FOR INTELLIGENT VEHICLE IDENTIFICATION AND ECU DIAGNOSTIC**

   Vladimir Ranchev*, Technical University – Sofia, Bulgaria*
   Rumen Yordanov*, Technical University – Sofia, Bulgaria*
   Rosen Miletiev*,Technical University – Sofia, Bulgaria*

2. **MOODSIGHT: PREDICTIVE MODELING FOR MENTAL HEALTH INSIGHTS THE IMPACT OF 0.20% CHLORHEXIDINE GEL ON THE EXTRACTION WOUND OF THIRD MOLARS BY A PRIMARY HEALING PROCESS**

   Dr. Hitesh Singh*, Dept. of Computer Science and Engineering, Noida Institute of Engineering and Technology (Affiliated to AKTU), Uttar Pradesh, India*
   Vansh Bhatt*, Dept. of Information Technology, Noida Institute of Engineering and Technology (Affiliated to AKTU), Uttar Pradesh, India*
   Dr. Vivek Kumar*, Dept. of Computer Science and Engineering, Noida Institute of Engineering and Technology (Affiliated to AKTU), Uttar Pradesh, India*
   Bhumika Rustagi*, Dept. of Information Technology, Noida Institute of Engineering and Technology (Affiliated to AKTU), Uttar Pradesh, India*
   Laraib Hussain*, Dept. of Information Technolog, Noida Institute of Engineering and Technology (Affiliated toAKTU), Uttar Pradesh, India*

3. **CROP YIELD PREDICTION USING ANN**

   Dr. Vivek Kumar*, Department of Computer Science & Engineering, Noida Institute of Engineering & Technology Gautam Buddh Nagar, Uttar Pradesh, India*
   Dr. Hitesh Singh*, Department of Computer Science & Engineering, Noida Institute of Engineering & Technology, Gautam Buddh Nagar, Uttar Pradesh*

***Laraib Hussain**, Information Technology, Noida Institute of Engineering & Technology Gautam Buddh Nagar, Uttar Pradesh ,India*

***Ratan Sen Srivastava**, Information Technology, Noida Institute of Engineering & Technology, Gautam Buddh Nagar, Uttar Pradesh, India*

***Adeeba Ali**, Information Technology, Noida institute of Engineering & Technology, Gautam Buddh Nagar, Uttar Pradesh, India*

4. ON THE FILTRATION OF COMPLEX IMAGES BY A MULTIFRACTAL METHOD

***N. Ampilova, I. Soloviev,** Saint-Petersburg State University, Russia*

5. ENTROPY LEVEL ESTIMATION OF REAL–WORLD ACOUSTIC DATA

***I. Simeonov,** Vasil Levski National Military University, Veliko Tarnovo, Bulgaria*

6. COMPARISON OF VARIOUS REGISTRATION METHODS ON MRI AND PET/PSMA MEDICAL IMAGES OF THE PROSTATE GLAND

***Diana S. Tsvetkova**, Faculty of German Engineering Education and Industrial Management, Technical University of Sofia, Bulgaria,*

***Veska Georgieva**, Faculty of Telecommunications, Technical University of Sofia, Bulgaria*

BREAK

12h – 12h 30min

SECOND SESSION

12h 30min – 14h 30min

***Chairman: Prof. V. Georgieva,** Faculty of Telecommunication, Technical University of Sofia, Bulgaria*

---

1. FLAT TERRAIN MEASUREMENTS AND PATH LOSS MODELS AT 1.0 AND 1.5 GHZ

***Nektarios Moraitis**, School of Electrical and Computing Engineering, National Technical University of Athens, Greece,*

***Panayiotis Frangos**, School of Electrical and Computing Engineering, National Technical University of Athens, Greece*

***Ileana Popescu**, School of Electrical and Computing Engineering, National Technical University of Athens, Greece*

***Alexandros Rogaris**, School of Electrical and Computing Engineering, National Technical University of Athens, Greece*

***Seil Sautbekov**, Department of Physics and Technology, Al-Farabi Kazakh National University Almaty, Kazakshtan*

6. **EFFECT OF 0.20% CHLORHEXIDINE GEL ON THE HEALING PROCESS OF TRAUMATIC LESIONS IN THE ORAL CAVITY, THAT HAVE OCCURRED AFTER REMOVABLE PROSTHETIC TREATMENT**

Desislava Konstantinova, *Department of Dental Materials Science and Prosthetic Dentistry, Faculty of Dental Medicine, Medical University – Varna, Bulgaria*

Emiliya Koleva, *Department of Electronics, Faculty of Engineering, Nikola Vaptsarov Naval Academy, Bulgaria*

Mariya Nikolova, *Department of Information Technologies, Faculty of Engineering, Nikola Vaptsarov Naval Academy, Bulgaria*

Anna Nenova-Nogalcheva, *Department of Oral Surgery, Faculty of Dental Medicine, Medical University - Varna, Bulgaria*

BREAK

14h 30min-15h

THIRD SESSION

15h – 17h

Chairman: Prof. Mariya Nikolova, *N. Y. Vaptsarov Naval Academy, Varna, Bulgaria*

---

1. **ESTIMATION OF FOREST FIRE PARAMETERS BY JOINT USE OF GEOSPATIAL DATA AND GEODETIC METHODS**

Svetlin I. Antonov, *Technical University of Sofia, Bulgaria*

Hrisimir Dochev, *Technical University of Sofia, Bulgaria*

Ivan S. Antonov, *Technical University of Sofia, Bulgaria*

2. **FRAMEWORK FOR A GAMIFIED PUBLIC TRANSPORTATION APPLICATION TO PROMOTE SUSTAINABLE TRAVEL IN SMART CITIES**

Milen Sotirov, *Nikola Vaptsarov Naval Academy, Varna, Bulgaria*

Valentina Petrova, *Nikola Vaptsarov Naval Academy, Varna, Bulgaria*

Donika Nikolova-Sotirova, *Technical University – Varna, Bulgaria*

3. **GAMIFICATION OF PUBLIC TRANSPORTATION: DEVELOPING A COMPREHENSIVE TAXONOMY FOR A MOBILE APPLICATION AND AN E-COMMERCE PLATFORM FOR REDEEMING TRAVEL POINTS**

Milen Sotirov, *Nikola Vaptsarov Naval Academy, Varna, Bulgaria*

Valentina Petrova, *Nikola Vaptsarov Naval Academy, Varna, Bulgaria*

Donika Nikolova-Sotirova, *Technical University – Varna, Bulgaria*

4. **EVALUATING THE EFFICACY OF GAMIFIED PUBLIC TRANSPORTATION SYSTEMS: A FRAMEWORK FOR EFFICIENCY AND IMPACT MODELLING**

Milen Sotirov, *Nikola Vaptsarov Naval Academy, Varna, Bulgaria*

Valentina Petrova, *Nikola Vaptsarov Naval Academy, Varna, Bulgaria*

Donika Nikolova-Sotirova, *Technical University – Varna, Bulgaria*

5. **IMPLEMENTING GRADIENT EDGE DETECTION IN FPGA: AN APPROACH TO MAXIMIZING OPERATING FREQUENCY AND MINIMIZING THE NUMBER OF CLOCK CYCLES**

***Dimitre Kromichev**, Department of Marketing and International Economic Relations, University of Plovdiv, Bulgaria*

6. **INVESTIGATING THE UPPER LIMIT OF SPEED IN TRADITIONAL NON-MAXIMUM SUPPRESSION WITH SIMULTANEOUS DYNAMIC THRESHOLD COMPUTATION IN FPGA BASED GRADIENT EDGE DETECTION**

***Dimitre Kromichev,** Department of Marketing and International Economic Relations, University of Plovdiv, Bulgaria*

CLOSING CONFERENCE

17h-17h 30min

CONTACT US:

http://rcvt.tu-sofia.bg/CEMA/eth.html

Prof. Dr. Dimiter Dimitrov

Faculty of Telecommunication
Technical University of Sofia
8, Kliment Ohridsky str.
1756 Sofia, Bulgaria
Phone:++359 2 9652278
Fax: ++359 2 9652278
E-mail: dcd@tu-sofia.bg

Prof. P. Frangos

National Technical University of Athens
School of Electrical and Computer Engineering
9, Iroon Polytechniou Str. ,
157 73 Zografou, Athens, Greece
Phone : 00 30 210 772 3694
Fax : 00 30 210 772 2281
E-mail : pfrangos@central.ntua.gr

TABLE OF CONTENTS

DESIGN AND ARCHITECTURE OF CAN2WIFI SYSTEM FOR INTELLIGENT VEHICLE IDENTIFICATION AND ECU DIAGNOSTIC

Vladimir Ranchev, Rumen Yordanov, Rosen Miletiev

Technical University of Sofia
8, Kl. Ohridski Blvd

vranchev@tu-sofia.bg

Abstract

The wireless SoCs become more reliable and energy-efficient. Considering their current miniature sizes that open many fields for various IoT (Internet of Things) applications. The compatibility and integration with automotive protocols (controllers and drivers) such as CAN give an extraordinary option for designing and implementing connected vehicle features. Within the scope of this paper, it is evaluated the design and architecture of a CAN to Wi-Fi Gateway system that enabled connected vehicles featured by using ESP32's latest SoC and small-footprint CAN-FD Controller. The proposed design confirms the performance of the system for processing the messages on the upper levels as well as vehicle identification connected features.

1. INTRODUCTION

According to the European Automobile Manufacturers' Association (ACEA), passenger cars as of Dec 2021 are on average 12 years old in the European Union, depending on the country they vary between 7 and 17 years old [1]. On the other side, every car produced since 2003 relies on Controller Area Network (CAN) networks for a primary network that connects multiple electronic control units (ECU) of the vehicle architecture [2]. It means the average passenger car in the EU vehicle fleet is equipped with a CAN network and is capable of retrofitting the connected vehicle features.

While some sensitive information and messages sent over the CAN network are encrypted or somehow protected [3], other basic data can be read without authorized access. Some of those parameters are VIN (Vehicle Identification Number), number and list of stored Diagnostic Trouble Codes (DTC), identification of available ECUs, Vehicle Speed, Fuel/Charge level, etc. The data available for the vehicle in combination with today's wireless connectivity will make the car more intelligent and real-time connected for more comfort, usability and safety features. The concept of connecting an additional Node to the CAN network which is Wi-Fi enabled is presented in Fig. 1.

The vehicle identification may be done via the service set identifier (SSID) of the Wi-Fi which is created as an Access Point (AP) with the Wi-Fi name containing the VIN itself. This will allow a standalone Wi-Fi client that is searching for corresponding SSIDs to identify the presence of a specific vehicle in a nearby place or car lot. After successful authorization for confirmation of the SSID, the system will report details for the vehicle data and status listed above.

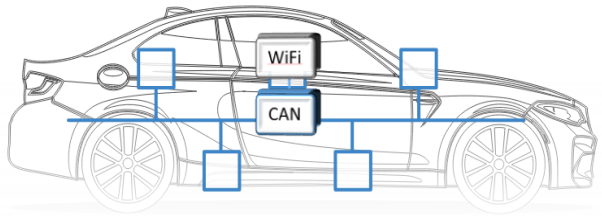

Fig. 1 Wi-Fi enabled CAN Communication

This article will propose and evaluate the hardware and software design of a system to fulfill the criteria for the performance and functionality presented in Fig. 1.

2. SYSTEM DESCRIPTION

2.1. System Design

The CAN protocol defines the lowest two layers of the OSI model as shown in Fig. 2. Several CAN-based higher-layer protocols are standardized [4] such as ISO-TP, and UDS (Unified Diagnostic Services ISO 14229).

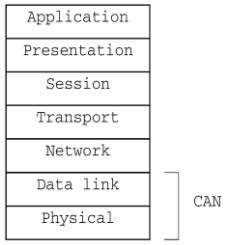

Fig. 2 The CAN protocol and OSI model. [4]

The transport protocol as well as some of the Application components has a typical time for response of 50ms. Therefore, any gateway system [5] in the middle layer (Bluetooth, Wi-Fi or other) needs to achieve latency lower than at least half of it i.e., less than 25ms.

The current research will evaluate a system built from core modules of ESP32-C6 SoC and a small-footprint external CAN FD Controller MCP2518FD. The architecture of the system is based on Wi-Fi 6 SoC which ensures fast and low latency connectivity and supports combined AP-STA mode Wi-Fi connectivity, where it is concurrently an access point and a station connected to another access point as shown in Fig. 3.

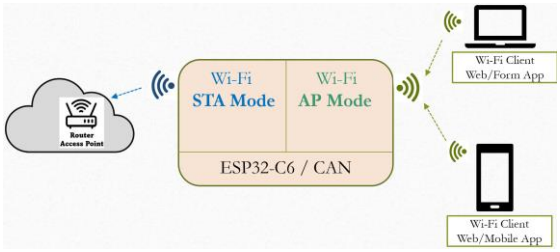

Fig. 3. Wi-Fi Combined Mode configuration of ESP32-C6

The Station (STA) mode is used for connecting to Internet AP for cloud connectivity functions. This way the system will support enhancement for a variety of cloud-intelligent functionalities like decoding VIN and providing recommendations for logged DTC (Diagnostic troubleshooting codes) and recommendations to be taken by the technician to remove faults in the vehicle.

The Access Point (AP) mode is used for P2P connection with the client(s) and will be the main focus of this work. It provides a hot spot with VIN as SSID. After authorization and access to the vehicle network, there is a Gateway from CAN to Wi-Fi (Ethernet) providing advanced wireless communication with the vehicle.

Even though the system is not targeting to expose any sensitive information about the vehicle, a certain cyber security consideration for AP-Mode will be in place to secure network access [6]. At first, there will be no WPS function to reset/disable the password for the Wi-Fi network. The system is protected with Secure Boot, Flash Encryption and Secure Storage to prevent the readout of any sensitive information from the code. Secure storage refers to the application-specific data that can be stored securely on the device, i.e., off-chip flash memory. This is typically a read-write flash partition and holds device-specific configuration data like Wi-Fi credentials, tokens, etc. A strong Wi-Fi password will be set on the system, which uses the newest security protocols including Protected Management Frames (PMF) and Wi-Fi Protected Access 3 (WPA3). As the system supports multiple clients, Client Isolation techniques will be in place to prevent direct communication between the clients. A firewall will be integrated to provide the following protections: Allows traffic only to/from the specified port, SSH/SFTP/Telnet services are disabled, filter REST (representational state transfer [7]) requests, limit requests per second, and log violations detected.

The Hardware implementation is packaged in a compact OBDII Connector for convenient integration and easy installation. This way the retrofitting is simplified to just plug it into the car OBD slot (typically located under the steering wheel on the left). There are three main blocks: SoC (Wi-Fi) compute block, CAN block, and Power Supply block as shown in Fig. 4.

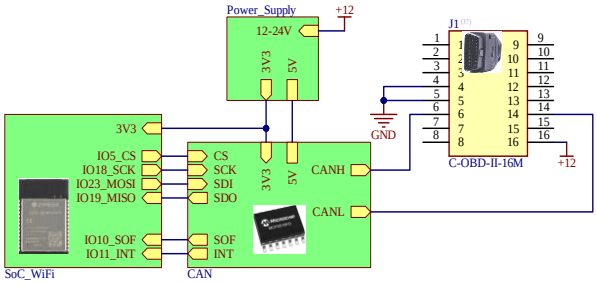

Fig. 4 Block Diagram of CAN2WiFi Architecture Design

The power supply module is responsible for efficient step-down voltage regulation from the typical 12V-24V power line of the vehicle down to the 3.3V required for the MCU. In addition, the CAN transceiver requires 5V so there shall be two stabilized voltage levels. The implementation is done in two stages. At the first stage with an Automotive grade high-frequency step-down switching regulator operating at 2MHz MP4560, there is a stable 5V power line.

By switching at 2MHz, the MP4560 may prevent EMI (Electromagnetic Interference) noise problems, such as those found in AM radio applications. An additional LDO is providing the 3.3V from the 5V power line. This way it achieves higher efficiency with minimal power heat dissipation and fewer components for achieving dual power supply lines required by the system.

As mentioned earlier the system is based on ESP32-C6-WROOM-1-N8 SoC. The selected SoC module version is with 8MB flash which storage with default partitioning is used on 30% after loading driver libraries for Wi-Fi, Webserver, RTOS, CAN Controller, and ISOTP UDS messages. The WROOM-1 type comes with an On-board PCB antenna for better miniaturization. The preloaded bootloader with FreeRTOS Kernel provides decent features for multitasking available for microcontrollers.

The CAN block is designed with a CAN Controller and CAN transceiver as separate ICs to make the system more flexible for supporting different CAN Standards. MCP2518FD is the selected external CAN FD Controller with a fast SPI Interface that is integrated into the system. It is cost-effective and comes in a small footprint package.

The selected transceiver is an ATA6560 high-speed CAN FD Transceiver which provides a physical connection with the CAN bus. It allows communication speeds up to 5Mbps and offers high resistance to electrostatic discharge and other electromagnetic disturbances. Considering the length of the CAN bus line in the vehicle this is the highest rate bus speed that can be found in the car CAN network. The ATA6563 supports Normal and Standby operational modes. In a Standby mode, the maximum current consumption is less than 12 µA.

2.2. Client – Server Architecture

The Frontend application (WEB or Mobile App) is running on the client side, and it allows the user to interact with the System whereas the backend application is running on the vehicle module. Different network protocols for accessing the CAN2WiFi system and its features as shown in Fig. 5.

The status and parameter configurations may be read/write by vehicle-specific REST API options. GET commands will provide read-out data for the current status and configuration. While some of the generic Diagnostics services such as reading VIN and logged DTC are implemented in the backend system, custom UDS requests may be directly sent by the front application using POST commands.

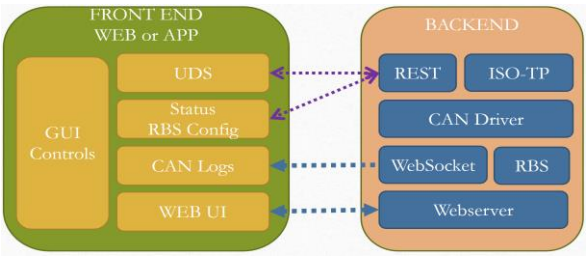

Fig. 2 Components distribution between Frontend and Backend application

The transport protocol ISO-TP is implemented in the Backend application to process the segmentation of the UDS requests and responses. The residual bus simulation (RestBUS or RSB) component is also part of the Backend application and provides a basic function for transmitting periodical CAN messages. This extends use cas es for the system to be used in certain scenarios for off-vehicle diagnosis and testing of specific ECU or when some faulty ECUs are observed. CAN driver will support full Network monitoring and logging with the support of WebSocket which will transmit requested by the Frontend CAN messages or the complete CAN communication to the Frontend application. The Frontend application will be responsible for the deserialization of specific CAN Signals based on a given .dbc or .arxml descriptor file matrix.

The CAN driver is the main component that is responsible for sending and receiving CAN messages whenever they are related to UDS segmentation or RSB. Also, it provides information on the current status of the CAN Network and detects Active or Passive error message counts. For better compatibility, most of the functionality will be available through a Webserver, so the system can be operated from various devices through a web page without needing an application to be installed.

2.3. SW Architecture Model

The implementation algorithm will follow the flowchart diagram shown in Fig. 6. After the device is powered up, the ECUs identification process on the network is initiated. The process involves sending a Tester Present Service Request (0x3E 0x00) over the range of Diagnostic Channels 0x701-0x7FF and sniffing which devices will respond. The process will be repeated if there is no response for 500ms.

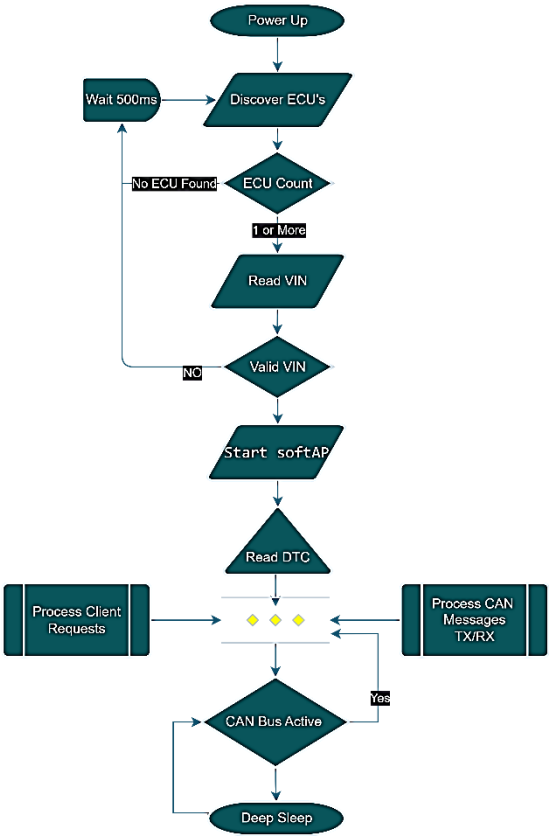

Fig. 6 Flowchart diagram of SW implementation

Once the ECUs are detected, for each of them the system will read the Vehicle Identification Number via UDS, with the use of the UDS SID 0x22 and the DID 0xF190. It is expected that all available ECUs are reporting the same VIN. After confirming the VIN, the Access Point SSID will be changed to the detected VIN.

After the Wi-Fi AP is configured, the system will read for each of the ECUs are there any DTC logged with support of the UDS Service 0x19 (Read DTC Information) request. After gathering DTC information is completed, the system enters normal multitasking mode which processes all CAN Messages received or configured for transmission and Client requests over REST or Webserver. At any point in time, if there are no requests from the client and the Bus enters into a Bus Off state (no ECU is sending messages), the CAN2WiFi will also enter Deep Sleep mode to save battery charge.

3. EXPERIMENTAL RESULTS

3.1. WEB Server (REST) Loopback

The first test measures the latency of Wi-Fi and Ethernet along with the Webserver running on the system. The test is accomplished as the PC Workstation is connected to the System with Intel(R) Wi-Fi 6 AX201 NIC via AP and sends a REST command of 7 Bytes of data. The Web Server on the system processes and returns an echo with the same data info as shown in the UML diagram in Fig. 7.

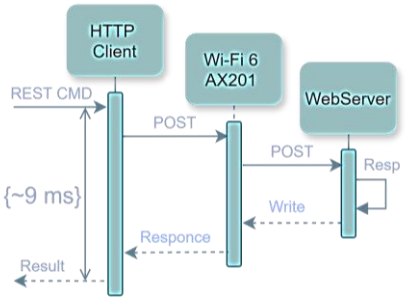

Fig. 7. REST Loopback test workflow

The test is performed with the support of the Windows Form Application developed in the .Net Core 6 framework. The system is temporarily configured in REST Loopback mode. The HTTP Client is used to send the POST Command and measure the time for response. The sequence is repeated 100 times and minimum, maximum and average times for the response are measured.

The archived results are shown in Fig. 8. The average time for response is 9ms. This is an excellent result, considering the usage of the standard library for the Webserver driver, which opens and closes the TCP connection on every request.

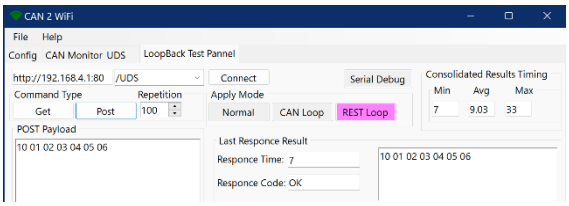

Fig. 8. REST Loopback test results

3.2. Can controller Loopback

The second test is similar, but this time a loopback is set on the CAN Controller which is configured in InternalLoopBack mode. In this mode, there is no connection to the Physical BUS layer, but any message sent is pushed to the Receive buffer (like it is received from the Physical Bus Layer) as shown in the UML diagram in Fig. 9.

The sequence is repeated 100 times in a loop and minimum, maximum and average times for the response are measured again. The obtained results are shown in Fig. 10.

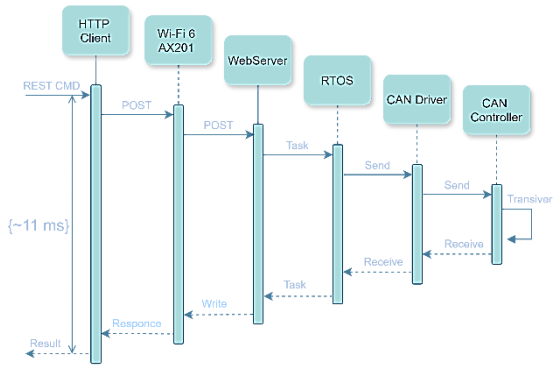

Fig. 9. CAN Loopback test workflow

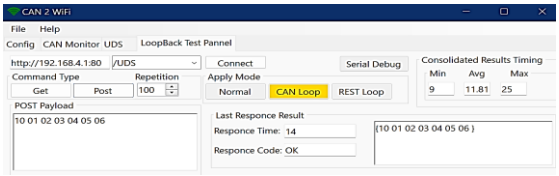

Fig. 10. CAN Loopback test results

The average time for response is calculated to 12ms. This is expected and confirms the efficiency of the RTOS scheduler which runs at 1ms tick and needs at least two ticks to send and process data between the tasks. Considering that the nominal time for response is 50ms in the upper layers, the archived result confirms that this system architecture allows upper-layer protocols to be implemented and managed on top of the CAN2WiFi Gateway on the front-end side. For internal usage to read the VIN and DTC count only the ISO-TP protocol is integrated into the design. The front-end application handles any security access if required. The system will not hold any secret key stored on the device and used for secured diagnostics communication. The Front-end client needs to implement an unlocking sequence with a seed decryption based on the car OEM model and ECU.

3.3. VIN Vehicle Identification

An in-car test is made with a Volvo brand car parked in the parking area. The device is plugged into the OBD Connector. The Android mobile device used to search for available Wi-Fi networks is put on the windshield glass next to the label of VIN on the chassis. The results are shown in Fig. 11.

Fig. 11. VIN read and Wi-Fi created for Volvo Cars

The result shows that the device can successfully read out the VIN and create an AP with the same name identification. After the Wi-Fi Authentication is made the car identification is confirmed remotely.

The extended diagnostic and data read logs, including the CAN log are made with the support of a front-end application. As a basis, it includes a list of ECUs found on the CAN-Bus, along with their VIN (in case it is supported) and Logged DTC count.

5. CONCLUSION

The proposed design and architecture of the CAN2WiFi System for Intelligent Vehicle Identification and Diagnostic confirms the expectation for performance, latency, and functionality required for the base of Intelligent Transport Enhanced Vehicles. It may be used for different types of secured modules to increase the usability, comfort, and safety of the vehicle. An example of industry appliances are Wireless Vehicle identification, Intelligent Vehicle diagnostic, GNSS/INS/IMS hybrid navigation systems for manure detection and prediction, ADAS supported systems.

6. APPENDIX AND ACKNOWLEDGMENTS

The authors would like to thank the Research and Development Sector at the Technical University of Sofia for the financial support under contract 242PD0041-07 "Research and development of electronic systems for testing and diagnostics in intelligent transport systems".

References

[1] ACEA European Automobile Manufacturers' Association,"ACEA-report-vehicles-in-use-europe-2023.pdf, January 2023, Source: acea.auto

[2] Gabriel Leen, D. Heffernan, "Expanding automotive electronic systems" February 2002, Computer 35(1): 88-93 DOI: 10.1109/2.976923, Source: IEEE Xplore

[3] Priyanka Sharma, Dietmar P. F. Möller, "Protecting ECUs and Vehicles Internal Networks" 2018 IEEE International Conference on Electro/Information Technology (EIT) At Rochester, MI, USA, USA, DOI: 10.1109/EIT.2018.8500295

[4] Karl Henrik Johansson, Martin T ̈orngren, Lars Nielsen, "Vehicle Applications of Controller Area Network" In book: Handbook of Networked and Embedded Control Systems, January 2005 DOI: 10.1007/0-8176-4404-0_32

[5] Zheng Zuo, Shichun Yang, Shichun YangBin Ma, "Design of a CANFD to SOME/IP Gateway Considering Security for In-Vehicle Networks" November 2021, Sensors 21(23):7917 DOI: 10.3390/s21237917

[6] Ramafiarisona Malalatiana, Sitraka Rakotondramanana, "Wifi Pentesting Roadmap for Classic-Future Attacks and Defenses" March 2024, American Journal of Networks and Communications 2024, Vol. 13, No. 1, pp. 44-62:7917 DOI: 10.11648/j.ajnc.20241301.14

[7] Shankey Bansal, Mohd Shajid Ansari, "Implementation of REST Architecture in ARDUINO Based Home Automation System" October 2019, Conference: ICICCI

ON THE FILTRATION OF COMPLEX IMAGES BY A MULTIFRACTAL METHOD

N. Ampilova

n.ampilova@spbu.ru

I. Soloviev

i.soloviev@spbu.ru

Saint-Petersburg State University

Abstract

In this paper we discuss the applicability of a method of multifractal analysis to filtration of images. The method allows decomposing of an initial image on non-intersecting subsets, such that every subset contains only the points which have singularity exponents from a given interval. The length of the interval is define5d arbitrarily. Every subset there correspond a binary image. The set of capacity dimensions of these subsets is a multifractal spectrum. But the using the spectra as classifying signs is not very promising, because spectra are defined on different intervals. It turns out to be more productive to consider a set of obtained binary images as a representation of the initial one. Among them there are 1-2 binary images which reveal the main structure, so they may be taken for the result of filtration. The obtained binary images may form a learning set. The results of experiments are shown for pharmaceutical solutions of Ag

1. INTRODUCTION

The study of the properties of various biological substances often uses the technique of obtaining their crystalline forms (biocrystals). In medicine, such methods of crystal growth as adding a substance to a solution of copper chloride, as well as adding a medicinal solution to an oil base, are well known.

In many cases, the properties of the substance under study can be judged by the type of crystal obtained.

For complex images fractal and multifractal techniques seems to be relevant for image analysis. That is because such structures have the property of statistical self-similarity. Multifractals are represented by a union of several non-intersecting fractals. The set of fractal dimensions of these subsets form a multifractal spectrum, which is a vector numerical characteristic.

The successful application of multifractal characteristics in the analysis of microscopic images of metal sections [1, 2] and in the study of nanostructures [3] shows that the same methods can be used in the analysis of such complex compounds as biocrystals.

Fractal methods are based on so called "power low": for a given partition of the set under study the measure of i-th element of partition is proportional to the side of the element in a power α_i, and the measure of the set is proportional the side of the element in a power of β.

If the set is a fractal then all α_i are equal, and equal to β, which is the fractal dimension of the set. For multifractals the powers α_i may be different, and we can imagine the set as a union of subsets, being each subset contains elements of the partition with the same powers.

To obtain a multifractal spectrum we should find these subsets and calculate their fractal dimensions.

The first known spectral characteristic is Regny spectra. They are calculated by the initial probability measure defined on a given partition of the set. Then initial distribution is recalculated by a definite rule which is controlled by a real parameter *q* (Regny parameter) and for each *q* a numerical characteristic — Regny dimension — is defined. The dimensions are known as generalized Regny dimensions [4].

Regny spectra are not multifractal ones in the sense of above definition. In this work we discuss another method to obtain multifractal spectrum — the calculation of “local density function” [5]. This method allows separating an initial set on nonintersecting subsets (by values of local density function

in points of the image) and constructing their graphical representations as binary images. Capacity dimensions of the subsets form multifractal spectrum.

Very often too complex structure contains a lot of unnecessary details and prevent us from finding key peculiarities of the image. A natural way for solving this problem is a filtration. This method may be easily applied for a filtration of images, because it gives a possibility to choose the image from obtained graphical representation which reveal the main structure) of the initial image.

In [6, 7] we applied both fractal and multifractal techniques and showed that for many images appearing in biology and medicine the combination of different methods allows us to obtain classifying signs.

In this work we apply this method to the analysis of images of farmaceutical solution of ions of Ag.

2. MAIN DEFINITIONS

Consider an image I in R^2 and denote the square with center x and radius r (half of the side length) by $B(x,r)$. Denote the measure of pixel intensities by μ.
Assume that

$$\mu\big(B(x,r)\big) = kr^{d(x)}(x),$$

where $d(x)$ — local density function and k is a constant.

For r small enough, then it follows

$$d(x) = \lim_{r\to 0} \frac{log\ \mu(B(x,r))}{log\ r}.$$

The function $d(x)$ characterizes the degree of heterogeneity of the pixel intensities distribution in a neighbour of x. The points x with local density α form the level set $E_\alpha = \{x \in \mathrm{I}: d(x) = \alpha\}$. In practice we calculate α_{min}, α_{max}, take $\alpha \in [\alpha_{min}, \alpha_{max}]$ and construct the sets

$$E(\alpha, \varepsilon) = \{x \in I: d(x) \in [\alpha, \alpha + \varepsilon)\},$$

where ε is a parameter given by a user. We obtain a set of binary images. Obviously, this parameter controls the number of level sets and allows the separation of the image on nonintersecting level sets. Then we calculate capacity dimensions $D_{cap}(\alpha)$ for level sets and obtain multifractal spectrum $f(\alpha) = \{ D_{cap}(\alpha)\}$.

The method really is a kind of "controlled filtration". The parameter ε is the control parameter: it defines the number of level sets. Experiments show that there are 1-2 main subsets for an image, which present main structure and have maximal capacity dimension.

So, we may consider such a subset instead of the initial image and calculate for it required characteristics. The analysis of the image obtained after filtration gives a possibility to find their main peculiarities easier.

3. EXPERIMENTS

We analyzed images of farmaceutical solutions of Ag. Two classes were considered: class A (solution contains ions), class B (without ions). In images of A there are two main structures — "flowers" and "maple-leaves". In images from B there are no structures. All the images were obtained in monochrome palette. Examples of images are given below.

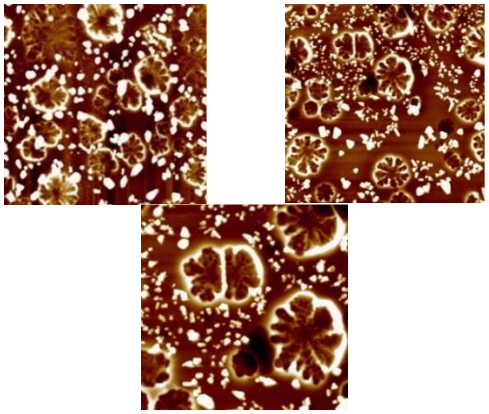

Fig. 1. Typical images of the class A: "flowers"

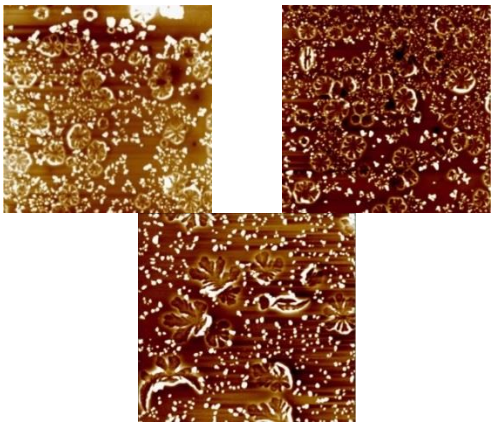

Fig. 2. Typical images of the class A: "flowers" and "maple-leaves"

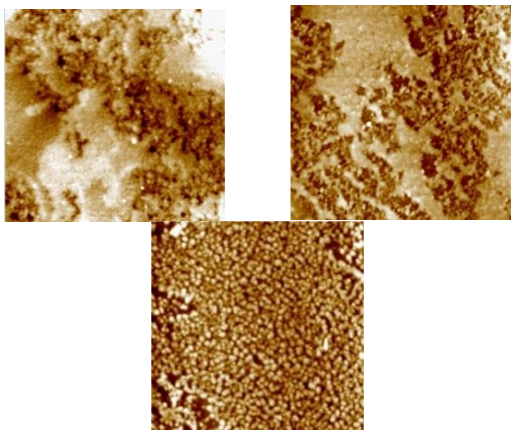

Fig. 3 Typical images of the class B

We see that images of the last class have the structure different from images of A.

After application of the described method we obtained for every image a set of binary images. The following figure illustrated the set of binary images for the first (left) image from the class A. The interval of density functions is [0.9, 4.5], value $\varepsilon = 0.4$. Images are shown for the following intervals of density function (left to right) [1.3, 2.1),[2.1, 2.5),[2.5, 2.9). Their capacity dimensions are 0.97, 1.72 and 1.51 respectively.

For brevity we do not show images containing small number of points.

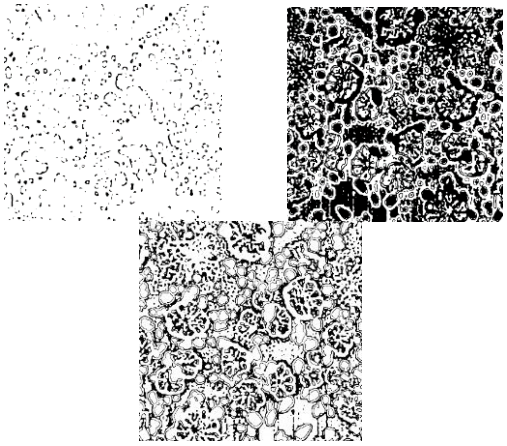

Fig. 4 Binary images of the representation for the first image of class A (Fig. 1)

It is easy to see that only two pictures reveal the structure of the initial image by the best way.

On the figures below we take for each image the binary image from the representation which has maximal capacity dimension.

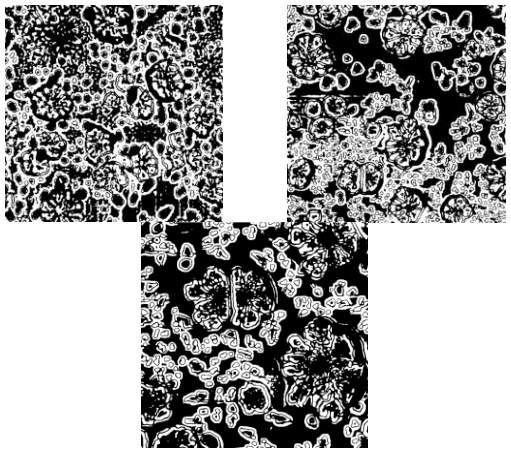

Fig. 4 Binary images for elements of Fig. 1

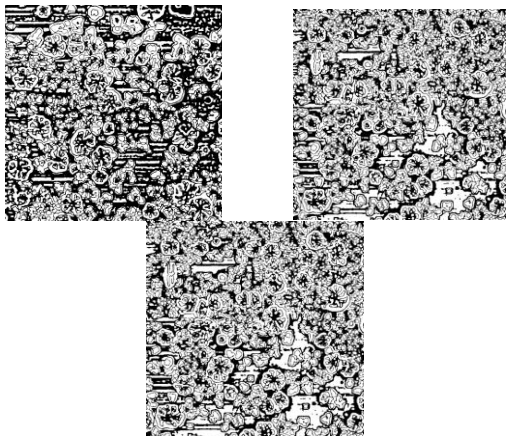

Fig. 5 Binary images for elements of Fig. 2

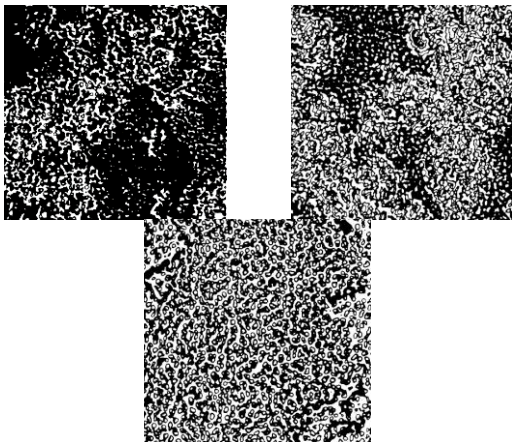

Fig. 6 Binary images for elements of the class B

4. CONCLUSION

The method of local density function seems to be a kind of "controlled filtration", because the number of binary images in decomposition of the initial image may be taken arbitrarily. The less parameter value the better approximation we obtain. But for any approximation it is enough to consider only 1-2 binary images which equivalent to the initial one.

References

[1] Vstovsky G. V. Elements of information physics M, MGIU 2002. (in Russian).

[2] Bortnikov A. Y., Minakova N. N. Texturno-fractalnii analis microscopicheskih srezov obraztsov rompozisionnih materialov zapolnennih technicheskim uglerodom, Izv TPU, 2006. №6.(in Russian).

[3] Polischuk S. V., Petrov K.A. Otsenka fraktalnyh svoystv nanostruktur po mikroskopicheskim izobrazheniyam, MNIG, 2022. №2-1 (116).(in Russian)

[4] Chhabra A. B, Direct determination of the f(α) singularity spectrum and its application to fully developed turbulence, Physical Review A.,1989,v. 40, № 9. p. 5284-5294.

[5] Y. Xu, H. Ji, C. Fermüller , Viewpoint Invariant Texture Description Using Fractal Analysis, International Journal of Computer Vision, 2009,v. 83, № 1,p. 85-100.

[6] Soloviev. Application of multifractal methods for the analysis of crystal structures , Proc. 16 Int. Conf. CEMA22, 20 Oct. 2022, Sofia, Bulgaria, p. 13-17, ISSN: 1314-2100, Sofia CEMA_2022_proc.pdf (tu-sofia.bg).

[7] N. Ampilova, I. Soloviev, V. Sergeev, On using escort distributions in digital image analysis, Journal of Measurements in Engineering, ISSN (Print) 2335-2124, ISSN (Online) 2424-4635 , v, 9, no.1, 2021, p. 58-70. https://doi.org/10.21595/jme.2021.21851 (WoS Ind.)

ENTROPY LEVEL ESTIMATIONS OF REAL-WORLD ACOUSTIC DATA

I. Simeonov

Vasil Levski National Military University, Veliko Tarnovo, Bulgaria
76, Bulgaria Blvd., 5000, Veliko Tarnovo, Bulgaria
Tel. +359 62 618724, Fax. +359 62 618899, E-mail: ivanov_ivan@nvu.bg

Abstract

Entropy estimation is important in information theory and in applications in many fields, like natural sciences, computer science etc. In this work some ways for real-world acoustic signal entropy level calculating technics, are regarded.

The ability to distinguish these levels within data sets is useful to estimate problematic component by studying their acoustic signals. Spectral entropy variations of empiric data could be improving detection in case of small signal to noise ratio.

It was shown analysis of some practical examples of acoustic recording's entropy. The results can be used in areas of real-world signal processing and applications.

1. INTRODUCTION

In recent years, extensive acoustic data has been collected through team efforts on interdisciplinary projects, and the processing of high dynamic range acoustic signals in the presence of noise has been discussed [1,2,3,4,12]. This paper is a continuation of the work in [4], focusing on specific applications and analyses using Approximate Entropy (ApEn).

In that study, several concepts and properties of mutual information and entropy were introduced, as well as an interesting approach (see the work of Zbili and Rama, 2021, [11]) used in the field of compressed sensing, based on Shannon's Source Coding Theorem. It is well-known that entropy, as a measure of the uncertainty of a random variable, takes high values for highly unpredictable variables and low values for highly predictable ones. This concept has found numerous applications in fields such as statistical physics, information theory, communication theory, biology, neuroscience, and many others [1–12]. Entropy was first introduced as a thermodynamic concept to measure molecular disorder in a closed system. Shannon entropy is one of the fundamental measures used for evaluating entropy. A brief survey of the literature on the empirical estimation of entropy can be found in Verdú, 2019 [5].

Many studies have uncovered complex dynamics and chaotic behavior in biological models, particularly those related to predator–prey interactions. The well-known continuous-time Leslie–Gower model is described in the work of Tsvetkov D. and Angelova-Slavova [6], where they prove the existence of positive ω-periodic solutions using the operator method in Banach spaces with cones.

Recently, researchers have investigated the dynamic behavior of discrete models. Vinoth et al. [7] and Hamadneh, T. et al. [8] explored the dynamic behaviors of a new Leslie–Gower discrete-time system with the Allee effect in predator populations. Rich chaotic dynamics for this system, investigated using the approximate entropy measure, can be seen in [8].

Approximate Entropy (ApEn) was initially developed to analyze medical data, such as heart rate variability, in 1991 [9]. It is known that vast amounts of data are required for accurate entropy calculation, and results can be greatly influenced by system noise, [10], which is not always feasible for experimental data. ApEn was developed by Steve M. Pincus to address these limitations.

2. APPROXIMATE ENTROPY OF EXPERIMENTAL ACOUSTIC DATA

The sound picture, i.e. experimental data is change depending on parameters as temperature, wind speed and direction, air pressure and humidity etc. In the next it was made the analysis of a set of experimental data and it was estimate unpredictability of its fluctuations by Approximate entropy calculations.

The raw data – time signals recorded from the blasts from 122 mm 2S1 howitzer ("Gvozdika"), see [4] was exported in MatLab and was calculated the Approximate entropy - ApEn correspondingly.

In the figures 1a), b) was shown signals in time domain where the second signal figure 1 b), is a part from the first and contains one burst of two pulses.

In [4] was conclude that the presence of a strong energy and noise-like component does not significantly change the spectral entropy picture.

The likelihood that similar patterns of observations are not followed by additional similar observations corresponds to a higher value of approximate entropy.

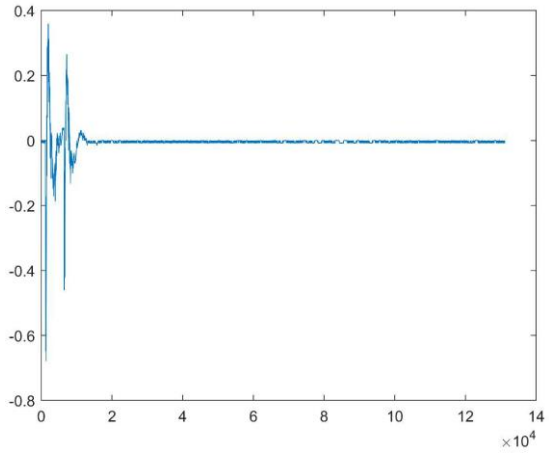

a) 131072 samples

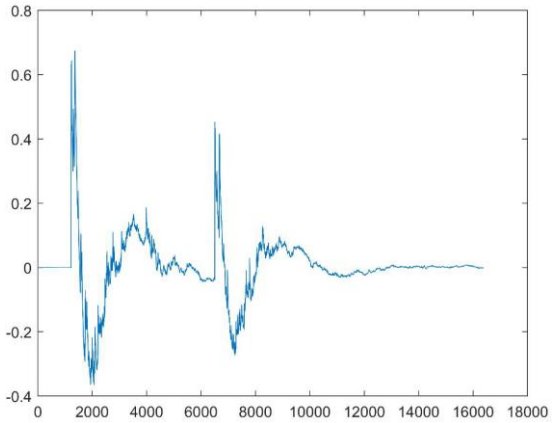

b) 16384 samples

Figure 1. a) Blast in first 0.25sec from signal waveform, [4]. All signal consists 2to17 samples, Fs=65536Hz
b) Zoom part of a), first 16384 samples

Formally, ApEn calculating steps are, [13]:

Step 1. First, it is required to fix the length of the compared patterns (embedding dimension) m, and the effective noise filter, r.

Step 2. Given a data series $\{u(i)\}$ of length N, define the sequences of length m, $x(i) = [u(i), \dots, u(i + m - 1)]$ and $x(j) = [u(j), \dots, u(j + m - 1)]$, with i being the vector acting as template and with j being the rest of the subsequences of the data series. Then, determine the distance $d[x(i), x(j)]$ as the maximum distance of the scalar components for each vector acting as template once.

Step 3. Determine the correlation integrals, i.e., the regularity or frequency, within a tolerance r, of patterns similar to a given pattern of length m. Using the sequences $x(i) = [x(1), x(2), \dots, x(N - m + 1)]$ for $i \leq N - m + 1$, calculate

$$C_i^m(r) = (number\ of\ j \leq N - m + 1\ for\ which\ d[x(i), x(j)] \leq r)/(N - m + 1).$$

Step 4. Define the functions $\phi^m(r) = (N - m + 1)^{-1} \sum_{i=1}^{N-m+1} \ln C_i^m(r)$, see Pincus work [9].

Step 5. Determine the likelihood that runs of patterns that are close for m observations remain close on the next incremental comparisons, defining the negative value of ApEn as:

$$\text{• ApEn} = \phi^{m+1}(r) - \phi^m(r) = average\ over\ i\ of \ln[conditional\ probability\ that |u(i + m) - u(j + m)| \leq r, given\ the\ fact\ that\ the\ previous\ values\ fulfill\ the\ condition |u(i + k) - u(j + k)| \leq r\ for\ k = 0, 1, \dots, m - 1].$$

The approximate entropies for the blast signal see fig. 1a,b, were found in MatLab. All these signals are parts same signal see fig1a), i.e. first 2 to 12, 2to13, 2 to 16 samples presented in fig. 2 a). For these parts was found ApEn in MatLab, see Table 1.

Some of calculations were illustrated on the fig 2b, c.

Table 1

Name of signal*	App. Entropy	Number of samples	Dim; Lag
rec9s	0,3401	2^12	2; 10
rec9ss	0,40203	2^13	2; 10
rec9sss	0,30635	2^14	2; 10
rec9ssss	0,22679	2^15	2; 10
rec9sssss	0,11706	2^16	2; 10

*All these signals are first N samples of same signal see fig1a), that consist 131071 samples

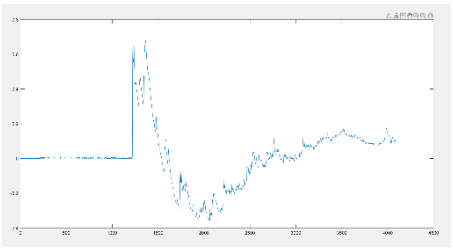

rec9s, 2to12 samp., ApEn=0,3401

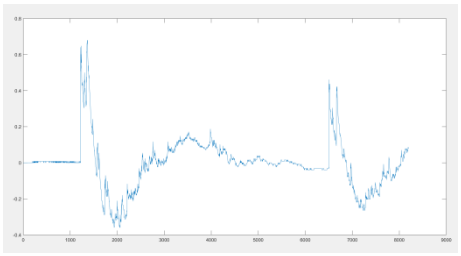

rec9ss, 2to13 samp., ApEn=0,40203

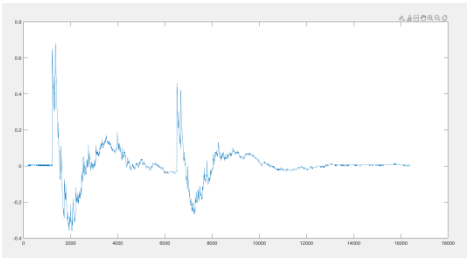

rec9sss, 2to14 samp., ApEn=0,30635

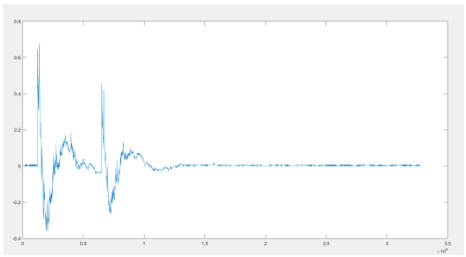

rec9ssss, 2to15 samp., ApEn=0,22679

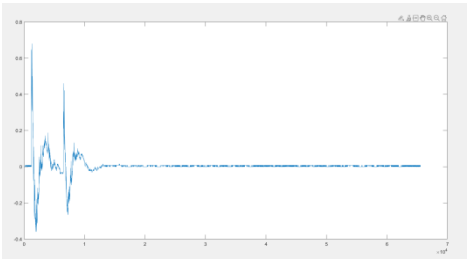

rec9sssss, 2to16 samp., ApEn=0,11706

Figure 2. a) Signals rec 9s to rec9sssss

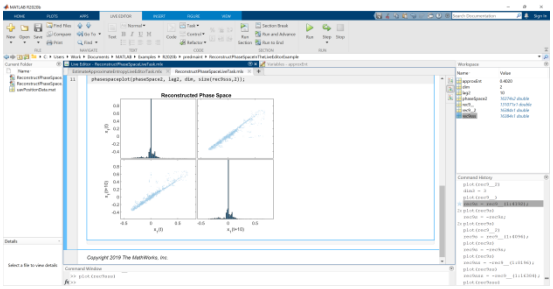

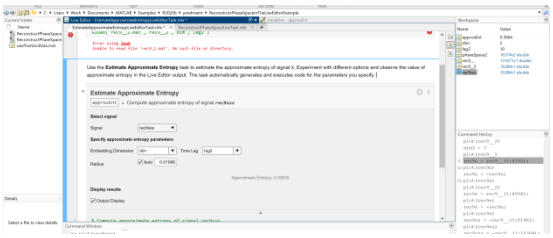

Figure 2. b) rec9sss, 2to14 samples, App. Ent. = 0,30635, dim = 2, lag = 10. Signal waveform and reconstruction the phase

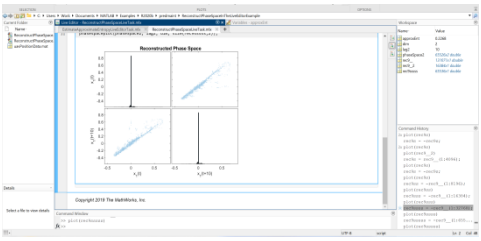

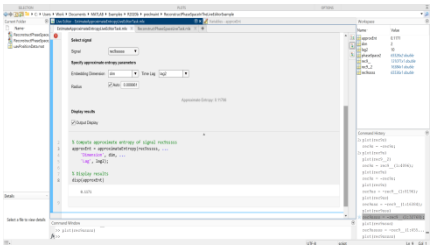

Figure 2. c) rec9sssss, 2to16 samples, App. Ent. = 0,11706, dim = 2, lag = 10.

It can be seen in Table1 that App entropy was decrease for increasing of signal time duration, i.e. number of samples.

The approximate entropy of the high regular signal is smaller than the random signal.

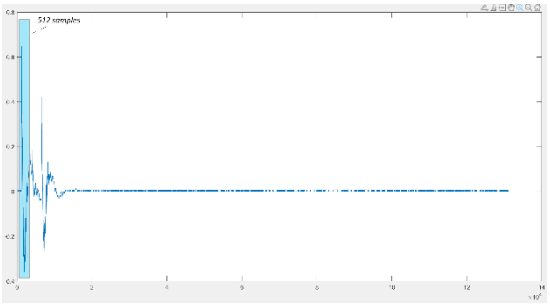

Figure 3. Small sections of 512 samples

In next part was regarded small sections, "time slices", of 512 samples, see fig.3, cute from the initial signal see fig 1a) and calculate in MatLab the ApEn. Signal waveform and corresponding reconstruction the phase space of the signal for three of slices are illustrated on fig. 4.

These sections may consist fragments, that are some reflections of first pics of blast.

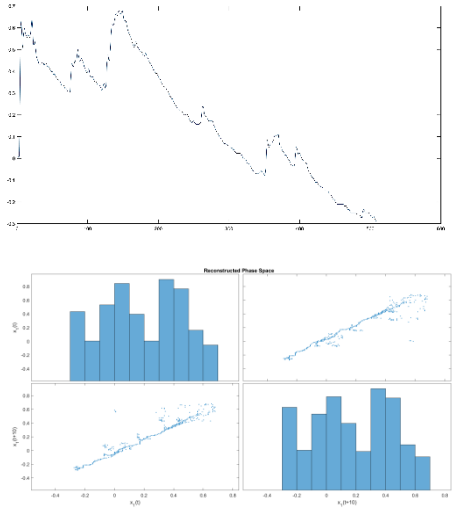

Figure 4. a) Signal waveform and reconstruction the phase space of the signal of 512 samples, i.e. rec9__ (1218:1729). Dim=2; lag=10. App. Entropy = 0,35341.

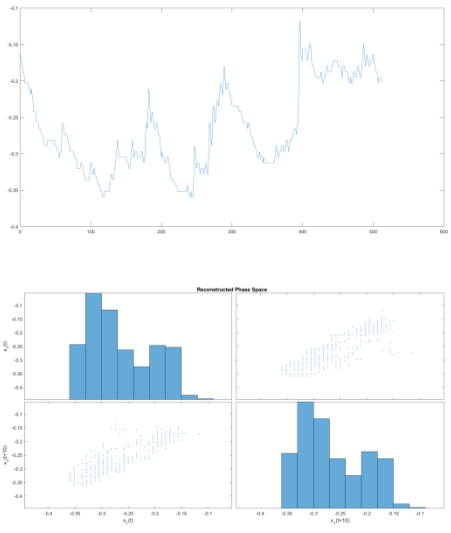

Figure 4. b) App. Entropy = 0,82006 rec9__ (1818:2329);

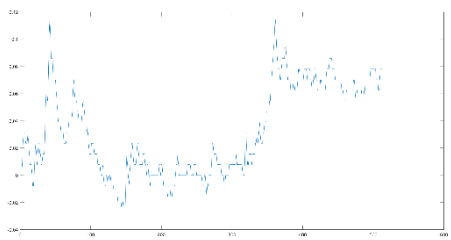

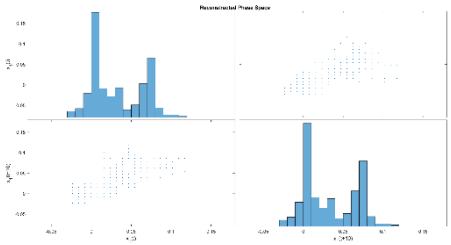

Figure 4. c) App. Entropy = 1,0354 rec9__ (2718:3229);

In Table 2 are shown results for ApEn for this 'time slices', where Dim=2, Lag =10, and consist 512 samples.

Table 2

Name of signal	Approximate Entropy	N samples
rec9s512	0,30127	(1;512)
rec9s512_	0,3339	(1024:1535)
rec9s512__	0,35341	(1218:1729);
rec9s512___	0,58698	(1518:2029);
rec9s512____	0,82006	(1818:2329);
rec9s512_____	0,59781	(2118:2629);
rec9s512______	0,87876	(2418:2929)
rec9s512_______	1,0354	(2718:3229);
rec9s512________	0,88358	(3018:3529)
rec9s512_________	1,0241	(3318:3829)

3. CONCLUSION AND FUTURE RESEARCH

It was shown that the statistics of the unpredictability of the fluctuations of a specific acoustic signal can be evaluated using approximate entropy.

For some small sections or "time slices", that were cut from the initial studied signal, an ApEn was calculated in MatLab.

As a result of these ApEn calculations, the step of increasing of ApEn was estimated when there is a decrease of the ratio signal/noise, for empirical acoustic data - recording of gun fire.

The Approximate Entropy variations through different time signal parts can be seen as a tool for the estimation of unpredictability of signal fluctuations.

ACKNOWLEDGEMENTS

I would like to thank prof. Tihomir Trifonov from Vasil Levski National Military University for his advice in acoustic signal processing. I would also like

to extend my thanks to doctor Georgi Dimkov from the Institute of mathematics, Bulgarian academy of sciences for their collaboration in many projects and for providing the hardware PULSE.

References

[1] Trifonov T., I. Simeonov, N. K. Yordanov Advanced Signal Processing Methods for Analysis of High Dynamic Range Acoustic Phenomena, *Proc. 13th Conference on 'Communications, Electromagnetics and Medical Applications' (CEMA'18)*, Sofia, Bulgaria, 18-20 Oct. 2018, pp. 52-56, ISSN: 1109-1606

[2] Trifonova, Signal Processing and Storing of High Dynamic Range Acoustic Data for Knowledge Discovery, *Proc. of 14th International Conference on Communications, Electromagnetics and Medical Applications CEMA'19*, Sofia, Bulgaria, October 17th-19th, 2019, pp. 58-62, ISSN: 1314-2100.

[3] Simeonov I., An Analysis of Uncertainty and Statistics of High Dynamic Range Acoustic Signals, *Proc. of 15th International Conference on Communications, Electromagnetics and Medical Applications CEMA'21*, Athens, Greece, October 21st, 2021, pp. 10-14, ISSN: 1314-2100.

[4] Simeonov, I., An Uncertainty and Mutual Information of Acoustic Signals with High Dynamics, *Proc. of 17th International Conference on Communications, Electromagnetics and Medical Applications CEMA'23*, Athens, Greece, November 3rd, 2023, pp. 40-43

[5] Verdú, S. Empirical estimation of information measures: a literature guide. Entropy 2019, 21, 720. https://doi.org/10.3390/e210.

[6] Tsvetkov, Dimiter & Angelova-Slavova, Ralitsa. (2020). Positive periodic solutions for periodic predator-prey systems of Leslie-Gower or Holling-Tanner type. Nonlinear Studies, 27(4), pp. 991–1002., https://arxiv.org/abs/2008.01530

[7] Seralan, Vinoth & Ramasamy, Sivasamy & Krishnasamy, Sathiyanathan & Unyong, Bundit & Vadivel, R. & Gunasekaran, Nallappan. (2022). A Novel Discrete-Time Leslie–Gower Model with the Impact of Allee Effect in Predator Population. Complexity. 2022. 10.1155/2022/6931354

[8] Hamadneh, T.; Abbes, A.; Abu Falahah, I.; AL-Khassawneh, Y.A.; Heilat, A.S.; Al-Husban, A.; Ouannas, A. Complexity and Chaos Analysis for Two-Dimensional Discrete-Time Predator–Prey Leslie–Gower Model with Fractional Orders. Axioms 2023, 12, 561. https://doi.org/10.3390/axioms12060561

[9] Pincus, S. M.; Gladstone, I. M.; Ehrenkranz, R. A. (1991). A regularity statistic for medical data analysis. Journal of Clinical Monitoring and Computing. 7 (4): 335–345. doi:10.1007/BF01619355.

[10] Pincus, Steven M. Approximate entropy as a measure of system complexity. Proceedings of the National Academy of Sciences. 1991 88 (6) 2297-2301; doi: 10.1073/pnas.88.6.2297.

[11] Zbili M and Rama S (2021) A Quick and Easy Way to Estimate Entropy and Mutual Information for Neuroscience. Front. Neuroinform. 15:596443. doi: 10.3389/fninf.2021.596443.

[12] Yordanov N., Wavelet Analysis of Acoustic Signals, *Proceedings of the Annual University Scientific Conference 2018 of the National Military University "Vasil Levski",* 14 - 15 June 2018, Vol.9, V. Tarnovo, Bulgaria, pp.1077-1084 (in Bulgarian), ISBN978-619-7246-20-9.

[13] Delgado-Bonal, A., Marshak, A., Yang, Y. et al. Analyzing changes in the complexity of climate in the last four decades using MERRA-2 radiation data. Sci Rep 10, 922 (2020). https://doi.org/10.1038/s41598-020-57917-8.

COMPARISON OF VARIOUS REGISTRATION METHODS ON MRI AND PET/PSMA MEDICAL IMAGES OF THE PROSTATE GLAND

Diana S. Tsvetkova

Faculty of German Engineering Education and Industrial Management, Technical University of Sofia, Bulgaria
1000 Sofia, "Kl. Ohridsky" str.8
E-mail: diana.tsvetkova@fdiba.tu-sofia.bg

Veska Georgieva

Faculty of Telecommunications, Technical University of Sofia, Bulgaria
1000 Sofia, "Kl. Ohridsky" str.8
T. (+359 2) 965-3293; E-mail: vesg@tu-sofia.bg

Abstract

Image registration is an essential task in medical image analysis and has been a subject of ongoing research for several decades. Multimodal medical image registration plays a crucial role in the fusion of images, particularly in detecting and treatment of prostate cancer. Progress in diverse prostate imaging methods has significantly helped in tumor detection, patient risk assessment, and overall healthcare quality.

The fusion of MRI/PET-PSMA imaging is a novel technique, that holds significant promise by combining biological and morphological data for oncological diagnosis, particularly in prostate cancer patients. Nevertheless, the lack of MRI/PET systems underscores the need for an efficient approach to merge separate PET-PSMA and MRI images acquired from the same patient.

This paper offers a comparison of various techniques regarding the registration of MRI and PET/PSMA medical images of the prostate gland. The primary goal is to contribute to the advancement of medical registration methods, particularly those that improve the diagnosis of prostate diseases.

1. INTRODUCTION

Prostate cancer remains a leading cause of death among men, highlighting the importance of accurate diagnosis and early detection. Recent advancements in prostate imaging, particularly the integration of MRI and PSMA-PET scans, have significantly enhanced tumour localization and risk assessment [1,2]. In this context, multimodal image fusion is a technique that merges two or more images from different modalities, which is particularly valuable in prostate cancer diagnostics. By integrating the functional information from PET-scanner with the anatomical detail provided by MRI imaging modality, this technique has become an effective tool for enhancing diagnostic accuracy and informing treatment strategies [3,4,5,6]. A critical component of this fusion process is image registration, which aligns images from different modalities into a common coordinate system. This alignment is essential for ensuring that the fused images provide comprehensive and precise information, enabling more effective diagnosis and intervention strategies.

As advancements continue in this field, the development of robust and accurate registration techniques will be key to improving patient outcomes. While these advancements in prostate imaging and multimodal fusion offer significant potential, they also introduce a range of technical and practical challenges that must be addressed to fully realize their benefits, particularly in the complex process of image registration

2. CHALLENGES IN MEDICAL IMAGE REGISTRATION

Challenges in medical image registration arise from both theoretical issues and the inherent characteristics of medical images, such as low contrast and poor quality. For instance, functional images like MRI, SPECT, and PET scans often suffer from lower signal-to-noise ratios, complicating the registration process [7,8].

Additionally, soft tissues and organs, such as the prostate, can shift in position due to factors like bladder or rectal filling, making accurate alignment difficult even when bone structures are aligned [7,8].

Rigid transformations, while straightforward, may be inadequate for capturing tissue deformations,

whereas free-form transformations, though more adaptable, can be unstable and challenging to regularize [7].

Furthermore, choosing between 2D-2D and 3D-3D registration involves trade-offs between computational complexity and the risk of ignoring out-of-plane deformations [8].

In addition, concerns regarding registration speed and algorithm robustness remain significant. To address these challenges, various registration techniques have been developed, as discussed in the next section.

3. COMPARISON OF PROSTATE IMAGE REGISTRATION TECHNIQUES

Multiple methods have been created for prostate image registration, each offering different advantages and drawbacks.

For instance, a study [9] compared a semi-automated clinical rigid registration technique, which relied on a urology registrar, to automated methods. While the semi-automated approach was time-consuming and less accurate, the automated rigid and non-rigid registration methods, powered by libraries within the SimpleITK package [10], demonstrated better performance and were more suitable for clinical application.

Similarly, Bharatha et al. [11] introduced a deformable registration method that improved monomodal MRI alignment but required manual segmentation, increasing processing time.

In another example, Alterovitz et al. [12] developed a 2D MR image registration technique that depended heavily on accurate segmentation, making it sensitive to errors in prostate identification.

On the other hand, Brock et al. [13] presented the MORFEUS multi-organ deformable registration approach, which was later applied by Hensel et al. [14] for MRI-to-CT registration of the prostate. However, this method faced challenges in boundary condition calculation and assigning material properties.

Despite these limitations, automated deformable registration methods have shown promise. For instance, paper [15] combined rigid and BSpline techniques, followed by a semi-automatic affine approach, achieving successful prostate image alignment.

Further advancements include Mitra et al. [16] using B-spline deformations with Normalized Mutual Information (NMI) as a similarity measure, refining accuracy by utilizing texture images derived from directional quadrature filter responses.

Other studies, such as Oguro et al. [17], have also employed the BSpline method, reporting enhanced outcomes compared to rigid methods. However, Tahmasebi et al. [18] introduced a statistical model-based approach, which, while effective in deformation modeling, required manual intervention and lengthy processing times.

Advanced automated techniques, such as those in paper [19], focused on aligning clinical MRI scans with whole-mount (WM) sections of the prostate, addressing significant deformations in the middle portion of the prostate through intensity-based volumetric registration.

Finally, modern software tools, such as the ANTS toolkit [20] and the Elastix software package [21], demonstrated accurate registration with a relatively low median in-plane error, highlighting their effectiveness in prostate image registration.

4. COMPARISON OF DEEP LEARNING TECHNIQUES IN MEDICAL IMAGE REGISTRATION

In recent years deep learning methods for image registration have seen significant growth. These techniques enhance registration accuracy, speed, and adaptability across different imaging modalities and applications Advances in computing power, larger datasets, and upgraded neural network models have all contributed to the growth in interest in these techniques. As we explore and compare these methods, it is important to consider the trends in recent research. Figure 1, taken from paper [22], compares the number of publications on classical image registration with those on deep learning-based registration over the past decade (2013–2023). The plot illustrates how image registration techniques have evolved, with a notable increase in interest in deep learning. The green line in the figure represents publications on classical image registration, while the blue line indicates those on deep learning-based approaches. This shift highlights the growing focus on neural networks and machine learning for enhancing registration performance.

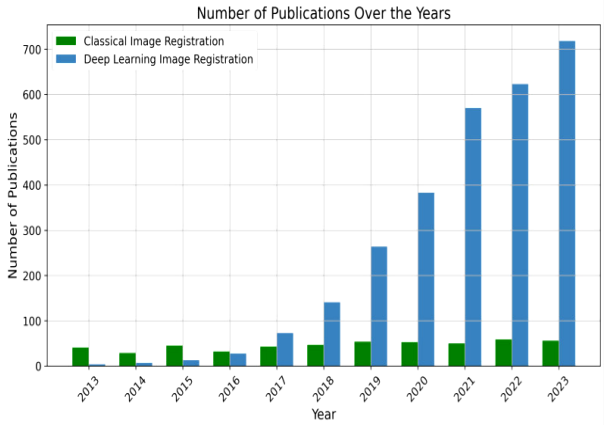

Building on these traditional methods, deep learning has introduced various techniques for medical image registration, each offering distinct advantages and drawbacks. Table 1 provides a comparative analysis, highlighting key approaches and contrasting their effectiveness, efficiency, and application suitability across different registration tasks.

Figure 1: Comparison of Classical vs. Deep Learning-Based Image Registration Publications (2013–2023)

Table 1. Comparison of Deep Learning Techniques in Medical Image Registration

Technique Group	Strengths	Weaknesses	Example(s)
Deep Similarity-Based Methods	High accuracy in complex scenarios, replaces traditional similarity measures like Mutual Information (MI).	Computationally intensive, requires large training datasets.	**Cheng et al. [23]:** Developed a deep similarity network that outperformed MI in CT-MR registration by learning complex image relationships. **Simonovsky et al. [24]:** Used a 3D similarity network for brain T1-T2 alignment, improving registration precision over traditional methods.
Reinforcement Learning (RL) Methods	Efficient in handling non-convex optimization and avoiding local maxima.	Limited by action space, complex training setup.	**Liao et al. [25]:** Applied RL for 3D-3D rigid CBCT-CT registration, achieving faster and more reliable alignment by training a CNN-based agent.
Supervised Transformation Prediction	High accuracy with well-labeled datasets, effective for specific transformations.	Dependent on ground truth data, potential for overfitting.	**Fan et al. [26]:** Developed BIRNet, which accurately predicted brain image transformations by training with dual supervision using ground truth data.
Unsupervised Transformation Prediction	Flexible, no need for ground truth labels, adaptable to various datasets.	May struggle with complex deformations, requires careful loss function tuning.	**Jiang et al. [27]:** Introduced a multi-scale unsupervised CNN framework for 3D CT lung registration, demonstrating robust performance across different datasets.
Generative Adversarial Networks (GANs)	Bridges the gap between modalities, effective for multi-modal to unimodal registration.	Challenging to train, can suffer from instability during training.	**Qin et al. [28]:** Used GANs for translating multi-modal images to unimodal, facilitating better registration with comparable results to ANTS [21] and Elastix [22].
Registration Validation via Deep Learning	Accurate error estimation without manual intervention, enhances robustness.	Limited to validation, does not directly improve registration itself.	**Eppenhof et al. [29]:** Developed a deep learning method for registration validation that accurately estimated errors without manual annotations, improving sub-voxel precision.
Other Learning-Based Methods	Versatile, applicable to a range of image registration tasks.	Computationally demanding, may require complex architectures.	**Liu et al. [30]:** Applied a Fully Convolutional Network (FCN) for multimodal to unimodal registration, achieving better accuracy than MI-based methods.

Notably, each deep learning technique offers unique advantages depending on the specific registration task. For example, while deep similarity-based methods excel in precision, reinforcement learning approaches are more efficient for complex optimization problems.

Supervised techniques work best with precisely labeled data, whereas unsupervised methods are more flexible but require careful tuning.

Although complex, GANs bridge the gap between different imaging modalities, and deep learning-based validation methods ensure the robustness of the registration.

Ultimately, selecting the right approach depends on balancing accuracy, computational resources, and the specific medical imaging challenge.

5. EVALUATION METRICS FOR REGISTRATION OF MULTIMODAL MRI/PET IMAGES OF THE PROSTATE

Visual inspection is often considered the gold standard for patient-specific verification. However, this evaluation method provides no quantifiable measure of the success of the registration process.

Evaluating the success of multimodal image registration for MRI and PET images of the prostate is an ongoing research challenge, with no universally reliable automatic metric for quality assessment. Three main evaluation categories are commonly used, each offering unique strengths and applications. These categories are discussed below.

5.1. Landmark-Based Evaluation

Landmark-based evaluation provides a direct measure of how well-known correspondences align after registration, but it only assesses accuracy at landmark locations, requiring a dense population of landmarks for better estimation of overall registration accuracy. [31]

Euclidean Distance is a example for such evaluation metric. It measures the straight-line distance between corresponding landmarks in two registered images. A decrease in distance post-registration indicates improved alignment.

Another landmark-based metric is the Target Registration Error (TRE). It measures the distance between homologous points, excluding fiducials, in two registered images and is typically expressed as Root Mean Square (RMS) error. The formula is shown in Equation.1.

$$\mathrm{TRE}_{RMS} = \sqrt{\frac{1}{N}\sum_{i=1}^{N} \|T(p_i) - q_i\|^2} \qquad \textit{(Eq.1)}$$

where p_i and q_i are the corresponding points in the two images, N is the number of points and is the $\|T(p_i) - q_i\|^2$ Euclidean distance between the transformed point and its corresponding point in the fixed image. This metric provides detailed insight into registration precision and is unaffected by patient variability, making it ideal for validation on phantoms [32].

In prostate imaging, TRE and Euclidean Distance can be calculated by measuring the distance between corresponding anatomical landmarks in registered MRI and PET images.

5.2. Segmentation-Based Evaluation

When clearly defined landmarks are not available, segmentation metrics offer a valid alternative.

Dice Similarity Coefficient (DSC) measures the overlap between two sets of data, typically represented as binary arrays. In image registration, DSC evaluates how well segmented regions from different modalities align. For example, when assessing the alignment of the prostate gland in registered MRI and PET images, DSC determines the degree of overlap between the segmented regions in both images. The Dice score ranges from 0 (no overlap) to 1 (perfect overlap), with a value close to 1 indicating near-perfect registration [33].

The 95% Hausdorff Distance (HD) measures the 95th percentile of distances between boundary points in two segmented sets, focusing on the majority of boundary points rather than outliers. After registering MRI and PET images of the prostate, 95% HD can be calculated to assess how well the boundaries of the segmented prostate gland align. This metric provides a robust measure of registration accuracy, particularly when used alongside DSC. [34]

5.3. Transformation Evaluation

When assessing the quality of a transformation or deformation field, a commonly used metric is the Jacobian determinant. It evaluates whether the transformation preserves anatomical volume or introduces distortions. A value of 1 indicates no local volume change, values greater than 1 indicate contraction, and values less than 1 suggest expansion. Negative Jacobian values indicate singularities, potentially leading to domain folding and unrealistic transformations. The Jacobian ensures topological preservation, requiring the transformation to be continuous, differentiable, and maintaining a positive determinant across the image, especially in the continuous domain [31].

6. CONCLUSION

In conclusion, various approaches to prostate image registration have been developed, each with distinct strengths and limitations. Automated methods, such as those like ANTS and Elastix, have proven more efficient and accurate than semi-automated techniques. Deformable registration methods offer improved alignment but often require manual intervention and are sensitive to segmentation accuracy. Recent advancements, including BSpline techniques and deep learning models, have further refined the process, though challenges like computational complexity and processing time persist. While visual inspection remains valuable for patient-specific verification, it provides no quantifiable measure of registration success. Instead, robust

evaluation using metrics like Euclidean Distance, Target Registration Error, Dice Similarity Coefficient, and 95% Hausdorff Distance and the Jacobian determinant are essential for assessing the accuracy of registration methods. Continued innovation in both techniques and evaluation is crucial for advancing prostate cancer diagnostics and treatment planning.

7. ACKNOWLEDGMENTS

This work was supported by the Research and Development Sector at the Technical University of Sofia, within the project №242PD0003-07/24 "Algorithms for fusion of nuclear magnetic resonance and positron emission tomography images of the prostate-specific membrane antigen".

References

[1] D. Tsvetkova, V. Georgieva, V. Hadzhiyska, and Y. Gramatikov, "Review of multimodal medical image fusion techniques and their application in prostate cancer," in Proceeding of 17th International Conference on Communications, Electromagnetic and Medical Applications (CEMA), pp.16-20, ISSN:1314-2100, 2023.

[2] A. Khan, C. M. Moore, and M. Minhaj Siddiqui, "Prostate MRI and image quality: The urologist's perspective," Eur. J. Radiol., vol. 170, p. 111255, Jan. 2024, doi: 10.1016/j.ejrad.2023.111255.

[3] A. P. Sharma et al., "Accuracy of combined multi-parametric MRI and PSMA PET-CT in diagnosing localized prostate cancer: newer horizons for a biopsy-free pathway," Eur. J. Hybrid Imaging, vol. 7, no. 1, p. 24, Nov. 2023, doi: 10.1186/s41824-023-00182-5.

[4] M. V. G. Amaral, M. T. Daher, and G. R. F. Bertolini, "Effects of adding the Kinesio Taping method to a combined exercise training program for soccer players with instability of the ankle: A randomized controlled trial," Clinics, vol. 73, Suppl. 1, p. e586s, 2018, doi: 10.6061/clinics/2018/e586s.

[5] L. Cereser, L. Evangelista, G. Giannarini, and R. Girometti, "Prostate MRI and PSMA-PET in the Primary Diagnosis of Prostate Cancer," Diagnostics, vol. 13, no. 16, p. 2697, 2023, doi: 10.3390/diagnostics13162697.

[6] I. Sonni et al., "Head-to-Head Comparison of 68Ga-PSMA-11 PET/CT and mpMRI with a Histopathology Gold Standard in the Detection, Intraprostatic Localization, and Determination of Local Extension of Primary Prostate Cancer: Results from a Prospective Single-Center Imaging Trial," J. Nucl. Med., vol. 63, no. 6, pp. 847-854, Jun. 2022, doi: 10.2967/jnumed.121.262398.

[7] D. L. G. Hill, P. G. Batchelor, M. Holden, and D. J. Hawkes, "Medical image registration," Phys. Med. Biol., vol. 46, pp. R1-R45, 2001.

[8] Y. Fu, Y. Lei, T. Wang, W. J. Curran, T. Liu, and X. Yang, "Deep learning in medical image registration: A review," Phys. Med. Biol., vol. 65, p. 20TR01, 2020.

[9] K. Rohr, H. Stiehl, R. Sprengel, T. Buzug, J. Weese, and M. Kuhn, "Landmark-based elastic registration using approximating thin-plate splines," IEEE Trans. Med. Imaging, vol. 20, pp. 526-534, 2001.

[10] K. Rohr, M. Fornefett, and H. Stiehl, "Spline-based elastic image registration: Integration of landmark errors and orientation attributes," Comput. Vis. Image Underst., vol. 90, pp. 153-168, 2003.

[11] M. Ferrant et al., "Registration of 3-D intraoperative MR images of the brain using a finite-element biomechanical model," IEEE Trans. Med. Imaging, vol. 20, pp. 1384-1397, 2001.

[12] F. El-Gamal, M. Elmogy, and A. Atwan, "Current trends in medical image registration and fusion," Egypt. Inform. J., vol. 17, no. 1, pp. 99-124, 2016.

[13] T. Liu, D. Shen, and C. Davatzikos, "Deformable registration of cortical structures via hybrid volumetric and surface warping," Neuroimage, vol. 22, pp. 1790-1801, 2004.

[14] V. Mani and Dr. Arivazhagan, "Survey of Medical Image Registration," J. Biomed. Eng. Technol., vol. 1, no. 2, pp. 8-25, 2013.

[15] D. L. G. Hill, P. G. Batchelor, M. Holden, and D. J. Hawkes, "Medical image registration," Phys. Med. Biol., vol. 46, pp. R1-R45, 2001.

[16] Y. Fu, Y. Lei, T. Wang, W. J. Curran, T. Liu, and X. Yang, "Deep learning in medical image registration: A review," Phys. Med. Biol., vol. 65, p. 20TR01, 2020.

[17] D. Yang et al., "Technical note: Dirart–a software suite for deformable image registration and adaptive radiotherapy research," Med. Phys., vol. 38, no. 1, pp. 67-77, 2011, doi: 10.1118/1.3521468.

[18] D. Yang, H. Li, D. A. Low, J. O. Deasy, and I. El Naqa, "A fast inverse consistent deformable image registration method based on symmetric optical flow computation," Phys. Med. Biol., vol. 53, no. 21, pp. 6143-6165, 2008, doi: 10.1088/0031-9155/53/21/017.

[19] T. Vercauteren, X. Pennec, A. Perchant, and N. Ayache, "Diffeomorphic demons: Efficient non-parametric image registration," Neuroimage, vol. 45, no. 1, Suppl. 1, pp. S61-S72, 2009.

[20] B. B. Avants et al., "A reproducible evaluation of ants similarity metric performance in brain image registration," Neuroimage, vol. 54, no. 3, pp. 2033-2044, 2011, doi: 10.1016/j.neuroimage.2010.09.025.

[21] S. Klein, M. Staring, K. Murphy, M. A. Viergever, and J. P. Pluim, "Elastix: a toolbox for intensity-based medical image registration," [no journal specified].

[22] F. Darzi and T. Bocklitz, "A Review of Medical Image Registration for Different Modalities," Bioengineering, vol. 11, no. 8, p. 786, Aug. 2024. doi: 10.3390/bioengineering11080786

[23] X. Cheng, L. Zhang, and Y. Zheng, "Deep similarity learning for multimodal medical images," Comput. Methods Biomech. Biomed. Eng. Imaging Vis., vol. 6, no. 3, pp. 248-252, 2018, doi: 10.1080/21681163.2015.1135299.

[24] M. Simonovsky, B. Gutirrez-Becker, D. Mateus, N. Navab, and N. Komodakis, "A deep metric for multimodal registration," in Medical Image Computing and Computer-Assisted Intervention - MICCAI 2016, Springer International Publishing, pp. 10-18.

[25] R. Liao et al., "An artificial agent for robust image registration," ArXiv, vol. abs/1611.10336, 2016.

[26] J. F. Fan, X. H. Cao, E. A. Yap, and D. G. Shen, "Birnet: Brain image registration using dual-supervised fully convolutional networks," Med. Image Anal., vol. 54, pp. 193-206, 2019, doi: 10.1016/j.media.2019.03.006.

[27] Z. Jiang, F. F. Yin, Y. Ge, and L. Ren, "A multi-scale framework with unsupervised joint training of convolutional neural networks for pulmonary deformable image registration," Phys. Med. Biol., 2019, doi: 10.1088/1361-6560/ab5da0.

[28] C. Qin et al., "Unsupervised deformable registration for multi-modal images via disentangled representations," in Information Processing in Medical Imaging, Ipmi 2019, vol. 11492, pp. 249-261, 2019, doi: 10.1007/978-3-030-20351-1_19.

[29] K. A. J. Eppenhof and J. P. W. Pluim, "Error estimation of deformable image registration of pulmonary CT scans using convolutional neural networks," J. Med. Imaging, vol. 5, no. 2, 2018, doi: 10.1117/1.JMI.5.2.024003.

[30] X. L. Liu, D. S. Jiang, M. N. Wang, and Z. J. Song, "Image synthesis-based multi-modal image registration framework by using deep fully convolutional networks," Med. Biol. Eng. Comput., vol. 57, no. 5, pp. 1037-1048, 2019, doi: 10.1007/s11517-018-1924-y.

[31] J. H. Song, "Methods for evaluating image registration," PhD dissertation, Univ. of Iowa, Iowa City, IA, USA, 2017. doi: 10.17077/etd.v0vailob.

[32] M. Fitzpatrick and J. B. West, "The Distribution of Target Registration Error in Rigid-Body Point-Based Registration," IEEE Transactions on Medical Imaging, vol. 20, no. 9, pp. 917-927, Sept. 2001. doi: 10.1109/42.952729.

[33] K. H. Zou et al., "Statistical validation of image segmentation quality based on a spatial overlap index," Academic Radiology, vol. 11, no. 2, pp. 178-189, Feb. 2004. doi: 10.1016/s1076-6332(03)00671-8. PMCID: PMC1415224.

[34] R. Karthik, R. Menaka, A. Johnson, and S. Anand, "Neuroimaging and deep learning for brain stroke detection - A review of recent advancements and future prospects," Computer Methods and Programs in Biomedicine, vol. 197, p. 105728, 2020. doi: 10.1016/j.cmpb.2020.105728.

FLAT TERRAIN MEASUREMENTS AND PATH LOSS MODELS AT 1.0 AND 1.5 GHZ

Nektarios Moraitis[1], Panayiotis Frangos[1], Ileana Popescu[1], Alexandros Rogaris[1] and Seil Sautbekov[2]

[1] School of Electrical and Computing Engineering, National Technical University of Athens (NTUA),
9, Iroon Polytechniou Str., 157 73 Zografou, Athens, Greece
Tel. : +30 210 772 3694; e-mail: pfrangos@central.ntua.gr

[2] Department of Physics and Technology, Al-Farabi Kazakh National University
Almaty, Kazakshtan
e-mail: sautbek@mail.ru

Abstract

In this paper an outdoor measurement campaign for almost flat terrain environment is undertaken for wireless mobile applications at frequencies 1.0 GHz and 1.5 GHz. The measured results are compared here both with the well – known in the literature "Two–Ray" (TR) model of wave propagation, as well as with the also well – known "Extended Hata" (EH) model. As a result, it is found here that under the conditions of this outdoor experiment the TR model is much more accurate, as compared to the measured results of ours. It is intended that further research by our research group will be conducted by our research group in the direction of comparison of our measured results with alternative analytical results which have been produced by us in previous publications of ours, in the "high frequency" regime.

1. INTRODUCTION

The problem of electromagnetic (EM) wave propagation over the flat terrain (or over a lossy medium with flat interface) is well – known in the literature as the *"Sommerfeld antenna radiation problem"*, where the interest here is for observation points over the flat interface [1-23]. However, in this paper we concentrate in comparing our outdoor experimental measurements in "high frequency" regime (here for frequencies 1.0 GHz and 1.5 GHz), which are obtained here by our research group, with approximate or empirical models of electromagnetic (EM) wave propagation [24-30]. In near future proposed research by our group, we intend to compare our outdoor experimental results measured by us here with alternative analytical results which have been produced by our research group in previous publications of ours (always in the "high frequency" regime).

This paper is organized as following: Section 2 describes the measurement equipment, as well as the procedure followed during our outdoor measurement campaign. Candidate path loss models to characterize the measured path loss are introduced and discussed in Section 3. Finally, conclusions and future research are presented in Section 4.

2. MEASUREMENT CAMPAIGN

The measurements were carried out in a football (soccer) field inside our University (NTUA) campus, in order to represent a near flat earth scenario. The field was partially covered with grass, whereas it was surrounded by tall trees. Fig. 1 illustrates the measurement environment, as well as the transmit (Tx) and receive (Rx) locations. The red circles denote the two different Tx locations, being separated about 5 m, which concurrently transmit a continuous wave (CW) signal at 1.0 GHz (Tx1), and 1.5 GHz (Tx2), respectively. It is worth noticing that under such conditions no wave interference between the two transmitted EM waves, i.e., from the two transmitting antennas, is observed, because of the fact that both transmitted waves are very narrowband, since they are CW signals.

The two (2) antennas were both mounted at a height of 2.7 m about the field surface. Two signal generators were utilized to produce the transmitted signals, which were fed, through similar 3-m low loss cables, to similar *vertically polarized* omnidirectional antennas. They both have a half power beamwidth (HPBW) of 45° in the elevation plane and a constant gain of about 0.20 dBi in the azimuth plane at the selected frequencies. The transmitted effective isotropic radiated power (e.i.r.p.),

was 16.1 dBm and 18.8 dBm, at 1.0 and 1.5 GHz, respectively.

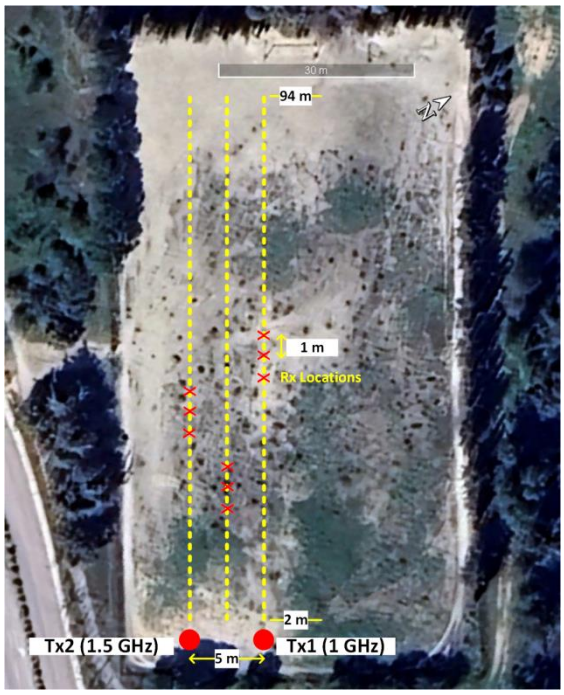

Figure 1. Measurement environment and locations

An SRM-3006 frequency selective field meter by Narda GmbH (Pfullingen, Germany) in spectrum analysis mode was employed as the receiving unit. An electric field isotropic probe was used (420 MHz - 6 GHz with a 0 dBi gain), connected to the main control unit through a 1.5-m cable. The Rx sensor was mounted on a wooden tripod at 1.7 m above the field surface. The Rx unit recorded the power samples in dBm, using a time average of 2 minutes. The Rx sensitivity was -120 dBm. The utilized Rx equipment was calibrated according to the ISO/IEC 17025:2017 standard [24]. Table I summarizes the Tx and Rx characteristics adopted in the launched measurement campaign.

TABLE I. Transmitter and receiver characteristics during the measurement campaign at each selected frequency scenario

	1.0 GHz	**1.5 GHz**
Tx power	17 dBm	20 dBm
Tx gain	0.20 dBi	
Cable loss	1.14 dB	1.42 dB
EIRP	16.1 dBm	18.8 dBm
Rx gain	0 dBi	
Rx sensitivity	-120 dBm	

The Rx recorded the signal at distinct positions from 2 m up to 94 m in three (3) parallel routes, as also shown in Fig. 1, in steps of 1 m. At each measurement position the Rx was stationary, having a line-of-sight (LOS) condition with the Tx. This entails a total number of 279 collected power samples at each frequency band.

Based on the received signal power the measured path loss *PL*, in decibels, at each Rx location can be described by:

$$PL = P_{Tx} - L_c + G_{Tx} + G_{Rx} - P_r \qquad (1)$$

where P_{Tx} denotes the Tx power in dBm, L_c indicates the cable losses, G_{Tx}, G_{Rx} stands for the Tx and Rx gains, respectively, in dBi, and P_r is the received signal power in dBm. Therefore, from (1), 279 path loss samples are resolved at each examined frequency scenario at a specific distance d_D, in meters, between Tx and Rx (length of the direct ray) that is given by:

$$d_D = \sqrt{d^2 + (h_t - h_r)^2} \qquad (2)$$

where d indicates the horizontal (ground) distance, in meters, between Tx and Rx, and h_t, h_r designate the Tx and Rx heights (2.7 and 1.7 m), respectively.

The raw data for both scenarios are shown in Fig. 2, where the received power versus distance is depicted. It should be pointed out that the distance from Tx in logarithmic scale, in meters, represents the direct distance (d_D) between Tx and Rx.

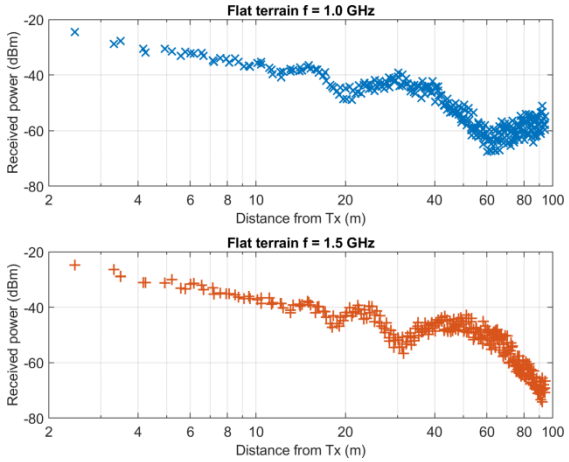

Figure 2. Received signal power at each measured location at 1 and 1.5 GHz

Clearly the power samples imply a flat terrain pattern, where power drops are encountered at specific distances. This resembles to a *two-ray pattern model*, which will be examined for its appropriateness to model the measured path loss in Section 3, below, along with appropriate Extended Hata model, as well, for comparison purposes.

3. PATH LOSS MODELS, RESULTS AND DISCUSSION

The two-ray model describes the signal propagation using two components. The direct ray between Tx and Rx and a ground reflected path ray. The path loss, in decibels, based on the two-ray model is given by [25]:

$$PL = 20\log_{10}\left(\frac{4\pi d}{\lambda}\right) - 20\log_{10}\left|1+\Gamma_V\, e^{j\Delta\varphi}\right| \quad (3)$$

where λ is the wavelength, in meters, at each selected frequency, and d is the ground (horizontal) distance between Tx and Rx, as previously mentioned. Furthermore, Γ_V denotes the vertical polarization reflection coefficient of the ground reflected path, and $\Delta\varphi$ stands for the phase difference between the direct and the ground paths. The reflection coefficient is described by:

$$\Gamma_V = \frac{-\varepsilon_r \sin\theta_i + \sqrt{\varepsilon_r - (\cos\theta_i)^2}}{\varepsilon_r \sin\theta_i + \sqrt{\varepsilon_r - (\cos\theta_i)^2}} \quad (4)$$

where θ_i, is the *"grazing angle"* of the incident wave (i.e., the angle between the incident EM wave and the flat terrain), and ε_r is the relative permittivity of the ground. Assuming a very dry ground, ε_r = 3 according to [26]. Furthermore, the grazing angle in (4), is related to the geometrical propagation characteristics according to:

$$\sin\theta_i = \left(\frac{h_t + h_r}{d_G}\right)$$
$$\cos\theta_i = \left(\frac{d}{d_G}\right) \quad (5)$$

where d_G denotes the length of the ground reflected ray, in meters, which can be calculated by:

$$d_G = \sqrt{d^2 + (h_t + h_r)^2} \quad (6)$$

Finally, the phase difference between of the path lengths between the direct and the ground reflected rays are given by:

$$\Delta\varphi = \frac{2\pi}{\lambda}(d_D - d_G) \quad (7)$$

where d_D and d_G are provided by (2) and (6), respectively.

Apart from the two-ray path loss model, the measured path loss is also compared with the *"Extended Hata"* model [27]. A rural/open area environment is assumed in this case; therefore, the path loss is given by:

$$PL = PL_U - 4.78(\log_{10}[\min\{\max\{150, f\}, 2000\}])^2 + 18.33\log_{10}[\min\{\max\{150, f\}, 2000\}] - 40.94 \quad (8)$$

where f is the operating frequency in MHz, and PL_U the path loss considering the urban environment. The latter parameter can be calculated according to:

$$PL_U = 46.3 + 33.9\log_{10}(2000) + 10\log_{10}(f/2000) - 13.82\log_{10}(\max\{30, h_t\}) + (44.9 - 6.55\log_{10}(\max\{30, h_t\}))\log_{10}(d_D) - a(h_r) - b(h_t) \quad (9)$$

where d_D is the direct ray distance, converted in kilometres, between Tx and Rx, and f the operating frequency in MHz. Further, $a(h_r)$ and $b(h_t)$, are the correction factors for the Rx and Tx, respectively, taking into account their specific heights h_r and h_t in meters. The correction factors are adopted for the rural/open area locations and can be calculated by:

$$b(h_t) = \min\{0, 20\log_{10}(h_t/30)\} \quad (10)$$

and

$$a(h_r) = (1.1\log_{10}(f) - 0.7)\min\{10, h_r\} - (1.56\log_{10}(f) - 0.8) + \max\{0, 20\log_{10}(h_r/10)\} \quad (11)$$

This model is widely used and is applicable for frequencies up to 3 GHz, and distances up to 40 km, respectively.

The results are presented in Fig. 3 where the path loss versus distance (in logarithmic scale) is provided along with the two different empirical models for comparison.

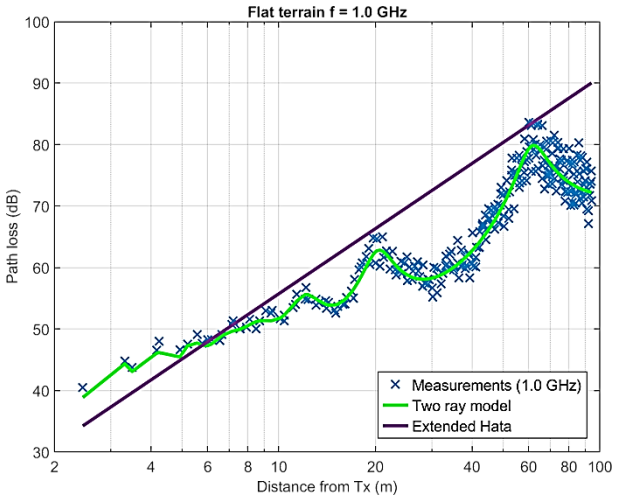

(a)

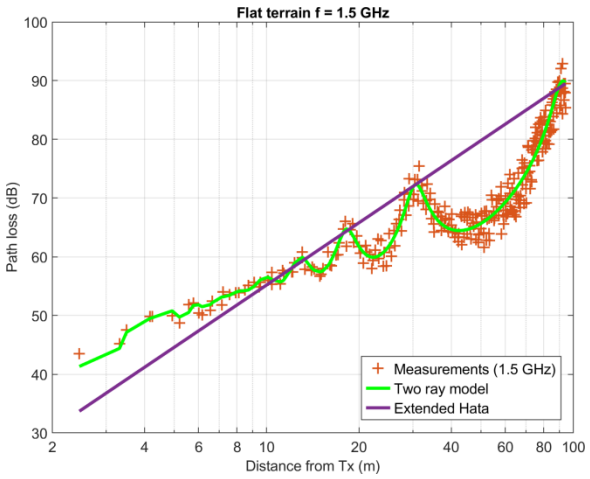

(b)

Figure 3. Path loss results versus distance. (a) 1.0 GHz and (b) 1.5 GHz

It is evident that "two-ray model" adapts better to the measured path loss, as it takes into account the geometrical characteristics of the propagating signal in the specific flat-terrain environment. On the other hand, the "Extended Hata model", predicts well the path loss in the first few meters (about 10 m for 1.0 GHz measurements, or about 15 m, for 1.0 GHz measurements), but diverges afterwards compared to the measured samples.

To compare quantitatively and validate the realized outcome, appropriate error metrics are applied, in order to analyze the statistical error of each model [28], [29]. The mean absolute error (MAE), in decibels, is given by:

$$\mathrm{MAE} = \frac{1}{N}\sum_{i=1}^{N}\left|PL_i^{meas} - PL_i^{pred}\right| \qquad (12)$$

where PL_i^{meas} and PL_i^{meas} stand for the measured and predicted path loss values, respectively, and i is the index of the measured sample. Finally, N is the total number of path loss samples (279 at each frequency scenario). The mean absolute percentage error (MAPE) is calculated according to:

$$\mathrm{MAPE} = \frac{1}{N}\sum_{i=1}^{N}\left|\frac{PL_i^{meas} - PL_i^{pred}}{PL_i^{meas}}\right| \times 100\% \qquad (13)$$

Finally, the root mean square (RMS) error, which actually represents the shadow factor is given, in decibels, by:

$$\mathrm{RMS} = \sqrt{\frac{1}{N}\sum_{i=1}^{N}\left(PL_i^{meas} - PL_i^{pred}\right)^2} \qquad (14)$$

The prediction errors are computed in the following applying (12)-(14), for each assessed path loss model. An acceptable RMS error for a path loss model is 6-7 dB for urban locations, and higher than 10 up to 15 dB, for suburban and rural/open areas [30].

Table II summarizes the numerical results of the obtained error metrics for each model and frequency scenario.

TABLE II. Statistical results between measured and predicted path loss for Two-Ray (TR) and Extended Hata (EH) models at each frequency scenario

Model	Metric	1.0 GHz	1.5 GHz
TR	MAE [dB]	**1.8**	**1.7**
	MAPE [%]	**2.6**	**2.4**
	RMS [dB]	**2.3**	**2.1**
EH	MAE [dB]	**9.6**	**7.6**
	MAPE [%]	**14.4**	**11.3**
	RMS [dB]	**10.8**	**9.1**

The results in Table II reveal that "Two-Ray" (TR) model is better applicable in a near flat-terrain environment, that is much lower errors are obtained, as compared with the "Extended Hata" (EH) model. In terms of RMS error, TR model adjusts slightly better at 1.0 GHz, nevertheless the error values between the two frequency scenarios are comparable. On the other hand, despite the high errors, EH model adapts better at 1.5 GHz, which implies that is more suitable at higher frequency applications over flat-terrain. However, at 1.0 GHz the results are discouraging, delivering an RMS error of 10.8 dB, which is higher that the acceptable value of 10 dB for rural/open areas, as suggested in [30].

Therefore, based on the above analysis, EH empirical model is not recommended for accurate path loss predictions in flat-terrain scenarios. Instead, geometrical optics (GO) models, such as "TR model", are better applicable, providing accurate path loss predictions, thus being recommendable for such flat-terrain applications.

4. CONCLUSION

In this paper we presented an outdoor experimental measurement campaign of our research group from propagation of EM waves over flat terrain (at 1.0

GHz and 1.5 GHz) and compared the experimental results with the "two – ray" model, as well as with the "Extended Hata" propagation model. It was found that the former model ("two – ray" propagation model) provides very good accuracy to the measured data (as this might be expected in the "high frequency regime", examined here).

As future work, the authors intend to assess additional path loss models of theirs (obtained by them through their previous research experience on EM propagation problems over the terrain), and validate their suitability to predict accurately the path loss in near flat-terrain scenarios.

ACKNOWLEDGEMENT

The authors would like to thank the Kazakhstan Ministry of Education and Research for a research grant, which supported this research. In addition, they would like to thank Ph.D. candidate Mr. Basil Massinas (at NTUA) for his valuable help in the preparation of this paper.

References

[1] A. N. Sommerfeld, "Propagation of waves in wireless telegraphy," Ann. Phys., 1909, 28, pp. 665-737.

[2] K. A. Norton, "The propagation of radio waves over the surface of the earth and in the upper atmosphere," Proc. Inst. Radio Eng., vol. 24, no. 10, pp. 1367-1387, Oct. 1935. doi:10.1109/JRPROC.1936.227360.

[3] A. K. Norton, "The propagation of radio waves over the surface of the earth and in the upper atmosphere," Proc. Inst. Radio Eng., vol. 25, no. 9, pp. 1203-1236, Sep. 1937. doi:10.1109/JRPROC.1937.228544.

[4] J. Wait, "Launching a surface wave over the earth," Electron. Lett., vol. 3, no. 9, pp. 396-397, Sep. 1967. doi:10.1049/el:19670307.

[5] R. J. King, "Electromagnetic wave propagation over a constant impedance plane," Radio Sci. 1969, 4, pp. 255-268, doi:10.1029/RS004i003p00255.

[6] T. K. Sarkar, W. Dyab, M. N. Abdallah, M. Salazar-Palma, M. V. S. N. Prasad, S. W. Ting, and S. Barbin, "Electromagnetic macromodeling of propagation in mobile wireless communication: Theory and experiment," IEEE Antennas Propag. Mag., 2012, 54, pp. 17-43, doi:10.1109/MAP.2012.6387779.

[7] J.G.V. Bladel, The Sommerfeld Dipole Problem. In Electromagnetic Fields, J. Wiley and Sons, Inc.: Hoboken, NJ, USA, 2007; Section 9.3, pp. 448–452.

[8] G. Tyras, Field of a Dipole in a Stratified Medium. In Radiation and Propagation of Electromagnetic Waves; Academic Press, Inc., New York, NY, USA, 1969; Section 6, pp. 133–160.

[9] Y. Rahmat-Samii, R. Mittra, P. Parhami, "Evaluation of Sommerfeld Integrals for Lossy Half-Space Problems". Electromagnetics, 1981, 1, pp. 1–28, doi: 10.1080/02726348108915122.

[10] R. E. Collin, "Hertzian dipole radiating over a lossy earth or sea: some early and late 20th-century controversies". IEEE Antennas Propag. Mag., 2004, 46, pp. 64–79, doi:10.1109/MAP.2004.1305535.

[11] K. A. Michalski, "On the efficient evaluation of integral arising in the sommerfeld halfspace problem". IEE Proc.-Microwaves, Antennas Propag., 1985, 132, pp. 312–318, doi:10.1049/ip-h-2.1985.0056.

[12] G. Pelosi, J. L. Volakis, "On the Centennial of Sommerfeld's Solution to the Problem of Dipole Radiation Over an Imperfectly Conducting Half Space", IEEE Antennas Propag. Mag., 2010, 52, pp. 198–201, doi: 10.1109/MAP.2010.5586629.

[13] J. R. Wait, "The Ancient and Modern History of EM Ground-Wave Propagation.", IEEE Antennas Propag. Mag., 1998, 40, pp. 7–24, doi:10.1109/74.735961.

[14] A. Baños, Dipole Radiation in the Presence of a Conducting Half-Space, Pergamon Press, Oxford, UK, 1966; pp. 151–158.

[15] S. S. Sautbekov, R.N. Kasimkhanova,; P.V. Frangos, "Modified Solution of Sommerfelds's Problem:, In Proceedings of the CEMA'10 Conference, Athens, Greece, 7–9 October 2010; pp. 5–8. Available online: http://rcvt.tu-sofia.bg/CEMA/proceedings/CEMA_2010_proc.pdf (accessed on May 2021).

[16] S. Sautbekov, "The Generalized Solutions of a System of Maxwell's Equations for the Uniaxial Anisotropic Media. In Electromagnetic Waves Propagation in Complex Matter"; IntechOpen Limited: London, UK, 2011; Chapter 1, pp. 1–24, doi:10.5772/16886.

[17] K. Ioannidi, C. Christakis, S. Sautbekov, P. Frangos, and S. K. Atanov, "The Radiation Problem from a Vertical Hertzian Dipole Antenna above Flat and Lossy Ground: Novel Formulation in the Spectral Domain with Closed–Form Analytical Solution in the High Frequency Regime," Int. J. Antennas Propag. (IJAP), 2014, Special Issue on 'Propagation of Electromagnetic Waves in Terrestrial Environment for Applications in Wireless Telecommunications', doi:10.1155/2014/989348.

[18] S. Bourgiotis, K. Ioannidi, C. Christakis, S. Sautbekov, P. Frangos, "The Radiation Problem from a Vertical Short Dipole Antenna Above Flat and Lossy Ground: Novel Formulation in the Spectral Domain with Numerical Solution and Closed-Form Analytical Solution in the High Frequency Regime", Proceedings of CEMA'14 Conference, Sofia, Bulgaria, 16–18 October 2014; pp. 12–18, Available online: http://rcvt.tu-sofia.bg/CEMA/proceedings/CEMA_2014_proc.pdf (accessed on May 2021).

[19] S. Bourgiotis, A. Chrysostomou, K. Ioannidi; S. Sautbekov and P. Frangos, "Radiation of a Vertical Dipole over Flat and Lossy Ground using the Spectral Domain Approach: Comparison of Stationary Phase Method Analytical Solution with Numerical Integration Results",

Electronics and Electrical Engineering Journal, 2015, 21, pp. 38–41, doi:10.5755/j01.eee.21.3.10268.

[20] A. Chrysostomou, S. Bourgiotis, S. Sautbekov, K. Ioannidi, and P. Frangos, "Radiation of a Vertical Dipole Antenna over Flat and Lossy Ground: Accurate Electromagnetic Field Calculation using the Spectral Domain Approach along with Redefined Integral Representations and corresponding Novel Analytical Solution," Electronics and Electrical Engineering Journal, 2016, 22, pp. 54–61, doi:10.5755/j01.eie.22.2.14592.

[21] S. Sautbekov, S. Bourgiotis, A. Chrysostomou, and P. Frangos, "A Novel Asymptotic Solution to the Sommerfeld Radiation Problem: Analytic Field Expressions and the Emergence of the Surface Waves," PIER M, 2018, 64, pp. 9–22, doi:10.2528/PIERM17082806.

[22] S. Bourgiotis, P. Frangos, S. Sautbekov and M. Pshikov, "The Evaluation of an Asymptotic Solution to the Sommerfeld Radiation Problem using an Efficient Method for the Calculation of Sommerfeld Integrals in the Spectral Domain", 'Electronics' Journal, MDPI Publisher, 1, https://doi.org/10.3390/electronics1010000, https://www.mdpi.com/journal/electronics, Special Issue on 'Propagation of Electromagnetic Waves in Terrestrial Environment for Applications in Wireless Telecommunications and Radar Systems', June 2021.

[23] J. Fikioris, Introduction to Antenna Theory and Propagation of Electromagnetic Waves; National Technical University of Athens: Athens, Greece, 1982. (In Greek).

[24] International Organization for Standardization, "General requirements for the competence of testing and calibration laboratories," ISO/IEC 17025:2017, Geneva, Switzerland, Nov. 2017.

[25] T. S. Rappaport, Wireless Communications: Principles and Practice. (2nd ed.), Prentice Hall, Upper Saddle River, New Jersey, 2002.

[26] Electrical Characteristics of the Surface of the Earth, document ITU-R P.527-6, International Telecommunication Union, Geneva, Switzerland, Sep. 2021.

[27] Monte Carlo simulation methodology for the use in sharing and compatibility studies between different radio services or systems, document ITU-R SM.2028-2, International Telecommunication Union, Geneva, Switzerland, Jun. 2017.

[28] E. Östlin, H. J. Zepernick, and H. Suzuki, "Macrocell path-loss prediction using artificial neural networks," IEEE Trans. Veh. Technol., vol. 59, no. 6, pp. 2735-2747, Jul. 2010.

[29] Y. Zhang, et al., "Path loss prediction based on machine learning: Principle, method, and data expansion," Appl. Sci., vol. 9, no. 9, pp. 1-18, May 2019.

[30] J. D. Parsons, The Mobile Radio Propagation Channel. 2nd ed., New York: Wiley, 2000.

RADIATION OF A VERTICAL HERTZIAN DIPOLE ABOVE A LOSSLESS MEDIUM WITH FLAT INTERFACE: CALCULATION OF THE TRANSMITTED ELECTROMAGNETIC (EM) FIELD BY USING A GEOMETRICAL OPTICS (GO) NOVEL IMAGE THEORY APPROACH

S. Sautbekov[(1)], P. Frangos[(2)], F. Karagiannopoulos[(2)], B. Massinas[(2)] and N. Moraitis[(2)]

[(1)] Department of Physics and Technology, Al-Farabi Kazakh National University
Almaty, Kazakshtan
e-mail: sautbek@mail.ru

[(2)] School of Electrical and Computing Engineering, National Technical University of Athens,
9, Iroon Polytechniou Str., 157 73 Zografou, Athens, Greece
Tel. : +30 210 772 3694; e-mail : pfrangos@central.ntua.gr

Abstract

In this paper we examine the problem of the radiation of a vertical Hertzian dipole over a lossless medium with flat interface in high frequency regime. Here the goal is to calculate the electromagnetic (EM) field value below the flat interface. For this purpose, a novel Geometrical Optics (GO) method is adopted here, and in this paper the first step to the problem solution is presented by calculating the position of the virtual image for given coordinates of the observation point below the flat interface. In order to accomplish the above, Snell's law and simple trigonometric relations for the given geometry of the problem are used.

1. INTRODUCTION

The problem of electromagnetic (EM) wave propagation over the flat terrain (or over a lossy medium with flat interface) is well – known in the literature as the 'Sommerfeld antenna radiation problem' [1-23]. Even in more cases the interest may be for observation points over the flat interface [1-14], also the problem solution below the flat interface can be formulated [see e.g. 15-22], and this is performed in an exact EM wave formulation [15-22]. On the contrast, in this paper we examine the problem of calculating the EM field value for an observation point below the flat interface (z<0), where we assume that the medium at the region z<0 (see Fig. 1) is a *lossless* and non-magnetic medium, that is ε_{r2} (relative dielectric constant) o medium 2 is real ($\varepsilon_{r2} > 1$) and $\mu_{r2} = 1$ (μ_{r2} is the relative magnetic constant of medium 2, below the interface). The source of EM radiation in this paper (see also Fig. 1) is assumed to be a vertical Hertzian dipole (i.e. dipole of length much smaller from the wavelength of EM radiation, $2l << \lambda$).

Furthermore, here we assume that the frequency of EM radiation from the vertical Hertzian dipole is sufficiently high, so that in this paper we can use a 'Geometrical Optics' (GO) approach, i.e. a 'ray optics – high frequency' approximation method.

Finally, in this paper we will just concentrate on the calculation of the exact position of the 'virtual image' for an observation point B lying in the region z<0 (see Fig. 1). Once the location of the image point C has been specified, then the value of EM field at the observation point B below the interface (Fig. 1) can be easily calculated by standard image theory approached (see e.g. [23]).

2. PROBLEM GEOMETRY AND SNELL'S LAW OF REFRACTION

The geometry of the problem is shown in Fig. 1, above, where we examine here only the two – dimensional (2D) case (i.e. calculations only on the yz-plane, or x=0 plane / one can easily extend our proposed method to the three – dimensional (3D) space). The radiating vertical Hertzian dipole is at height $z_0 = h$ above the lossless dielectric medium with flat interface [which lies in the region z<0 , i.e. lossless and non – magnetic medium for z<0 , that is ε_{r2} = dielectric constant = real ($\varepsilon_{r2} > 1$), $\mu_{r2} = 1$, index of refraction $n_2 = (\varepsilon_{r2})^{1/2} > 1$].

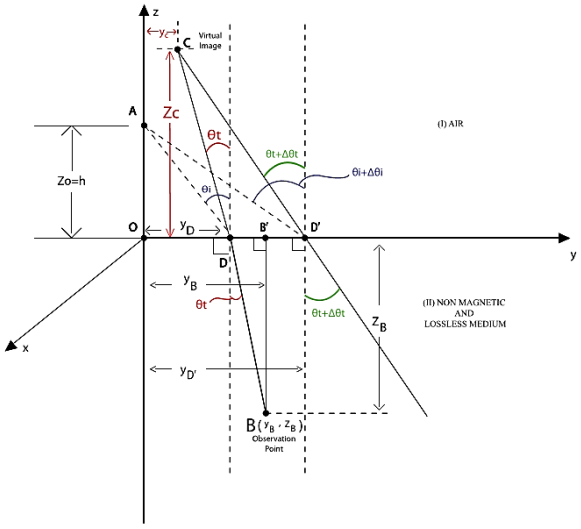

Figure 1. Geometry of the problem

Considering a particular point of refraction D (see Fig. 1) the well – known *Snell's law for refraction* holds (see e.g. [23]):

$$sin\theta_t = \frac{n_1}{n_2} \cdot sin\theta_i = \sqrt{\frac{\varepsilon_{r1}}{\varepsilon_{r2}}} \cdot sin\theta_i \qquad (1)$$

Furthermore, let us consider a second incident ray AD' at a point D' close to point D, that is: DD' << OD. Then, we obtain a second refracted ray D'F (besides the first one, which is DBE ray), which intersects the first ray at point C (which is the location of the '*virtual image*'. For this second ray, also Snell's law for refraction holds, that is:

$$sin(\theta_t + \Delta\theta_t) = \frac{n_1}{n_2} \cdot sin(\theta_i + \Delta\theta_i) = \\ = \sqrt{\frac{\varepsilon_{r1}}{\varepsilon_{r2}}} \quad sin(\theta_i + \Delta\theta_i) \qquad (2)$$

Next, the geometric problem that we have to solve is as following:

Step 1: Given the coordinates (y_B, z_B) of the observation point B, we will calculate the coordinate y_D for given coordinates of the source (y = 0, z = z_0 = h) and of the observation point B. This task will be presented at Section 3, below (see Fig. 1, and in particular Fig. 2).

Step 2: Once the coordinate y_D of the refracting point D is calculated (Section 3), the coordinates (y_C, z_C) of the '*virtual image*' C can be calculated by simple geometry (see Section 4 / that is see Fig. 1, and, in particular, Fig. 3).

3. CALCULATION OF POSITION OF THE UNIQUE REFRACTING POINT, GIVEN THE COORDINATES OF THE OBSERVATION POINT

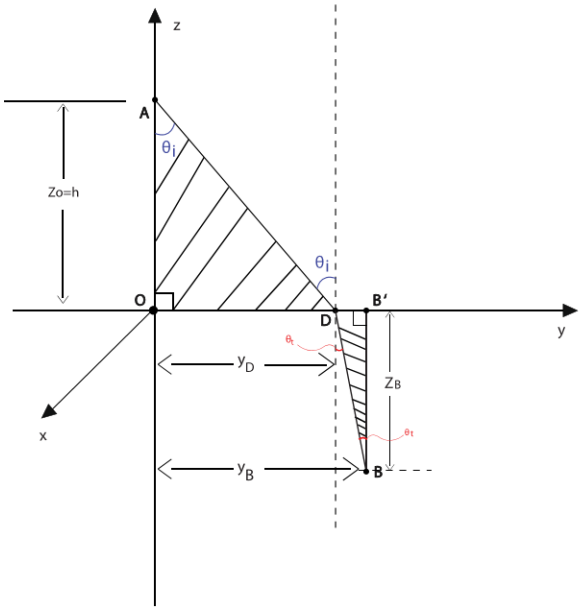

Figure 2. Problem geometry with coordinates of the observation point (B)

From simple *geometrical considerations* of Fig. 2, and working along the horizontal (Oy – axis) we have:

$$DB' = \; y_B - h \cdot \tan\theta_i = \; z_B \tan\theta_t \qquad (3)$$

where $y_D = h \tan\theta_i$.

Therefore, from eq. (3):

$$\tan\theta_t = \frac{y_B - h \cdot \tan\theta_i}{z_B} \qquad (4)$$

which is a function between the unknown quantities θ_t and θ_i (quantities h, y_B and z_B are considered known, here). Moreover, we repeat here (just for our convenience) *Snell's law for refraction*, eq. (1):

$$\sin\theta_t = \sqrt{\frac{\varepsilon_{r1}}{\varepsilon_{r2}}} \cdot sin\theta_i \qquad (1)$$

Furthermore, since $\tan\theta_t$ appears at eq. (4), we can easily transform eq. (1) to a form, where $\tan\theta_t$ (instead of $\sin\theta_t$) appears (this can be very easily performed, by using elementary trigonomteric calculus). Then, in this way, *Snell's law for refraction*, instead of eq. (1), takes the form:

$$B(\theta_i) = tan^2(\theta_t) = \frac{1}{1 - \frac{\varepsilon_{r1}}{\varepsilon_{r2}} \cdot sin^2(\theta_i)} - 1 \qquad (5)$$

while, by just squaring eq. (4), we obtain:

$$C(\theta_i) = tan^2\theta_t = \left(\frac{y_B - h\cdot\tan\theta_i}{z_B}\right)^2 \quad (6)$$

Note here that $C(\theta_i)$, eq. (6), is a *monotonic* function, *decreasing* with θ_i . where $DB' = y_B - y_D = y_B - h\cdot\tan\theta_i > 0$, then $\tan\theta_i < (y_B / h)$, and where $0 \le \theta_i \le \pi/2$, while $B(\theta_i)$, eq. (5), is a *monotonic* function, *increasing* with θ_i

$(0 \le \theta_i \le \pi/2)$. Then, by using, e.g. MATLAB, we can easily calculate the angle θ_i (Fig. 2) for which $B(\theta_i) = C(\theta_i)$, yielding the solution $\theta_i = \theta_i^0$. Once θ_i^0 has been calculated (numerically, as described just above), one can easily calculate, successively, the following quantities:

$$y_D = h\cdot\tan\theta_i^0 \quad (7)$$

$$\sin\theta_t^0 = \sqrt{\frac{\varepsilon_{r1}}{\varepsilon_{r2}}}\cdot sin\theta_i^0 \quad (8)$$

(which is Snell's law, once again), and

$$DB' = y_B - y_D \quad (9)$$

[see Fig. 2 and eq. (3)].

4. CALCULATION OF THE COORDINATES OF THE IMAGE POINT

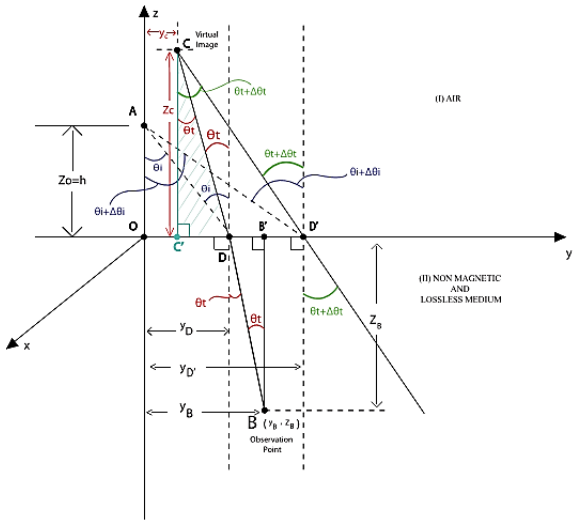

Figure 3. Geometry for the calculation of the image point coordinates (C)

Finally, given the calculation of the quantities mentioned at Section 3, above, *the calculation of the coordinates (y_C, z_C) of the 'virtual image' C* can be easily performed by simple trigonometric calculations on triangle CC'D (1st refracted ray of Fig. 3) and triangle CC'D' (2nd refracted ray of Fig. 3), that is by working (simple trigonometric calculations) in half – space z>0. Then, it can be easily proved that the coordinates (y_C, z_C) of the 'virtual image' C are provided by the following equations:

$$y_C = y_D - \frac{\sin(2\theta_t^0)}{2}\cdot\frac{\Delta y_{2rays}}{\Delta\theta_t^0} \quad (10)$$

and

$$z_C = \frac{\Delta y_{2rays}}{\Delta\theta_t^0}\cdot cos^2\theta_t^0 \quad (11)$$

where

$$\frac{\Delta y_{2rays}}{\Delta\theta_t^0} \approx CD \approx CD' \quad (12)$$

where Δy_{2rays} = DD' = chosen small quantity (known, DD' << OD), θ_t^0 has been calculated from eq. (8) and $\Delta\theta_t^0$ is θ of the 2nd ray, rewritten here for our convenience:

$$\sin(\theta_t^0 + \Delta\theta_t^0) = \sqrt{\frac{\varepsilon_{r1}}{\varepsilon_{r2}}}\cdot\sin(\theta_i^0 + \Delta\theta_i^0) \quad (13)$$

and where angle $(\theta_i^0 + \Delta\theta_i^0)$ is calculated by (see Fig. 3):

$$\theta_i^0 + \Delta\theta_i^0 = tan^{-1}\left(\frac{y_D + \Delta y_{2rays}}{z_0}\right) = known \quad (14)$$

Then, from eq. (13), $\Delta\theta_i^0$ is also known.

Finally, note that because of eq. (12) and CD ≈ CD' [for small DD', as explained below eq. (11), above], the *coordinates (y_C, z_C) are 'almost independent' of the chosen length DD'= =Δy_{2rays}, provided DD' << OD*, as explained above.

5. NUMERICAL EXAMPLE: CALCULATION OF THE POSITION OF THE REFRACTING POINT (D) AND OF THE 'VIRTUAL IMAGE' (C) FOR GIVEN SOURCE AND OBSERVATION POINT COORDINATES

Referring to Fig. 2, in this numerical example we choose: z_0 = h = 10 m (position of the radiating Hertzian dipole, i.e. of the source of EM radiation), (y_B = 10 m, z_B = = -5 m, hence $|z_B|$ = 5 m), i.e. the coordinates of the observation point, and ε_{r2} = 1.6. Then, by calculating at MATLAB eqs. (5) and (6), i.e. the quantity $B(\theta_i)$ [Snell's law for refraction] and quantity $C(\theta_i)$ [equation coming from the geometry of Fig. 2], and setting

$$B(\theta_i) = C(\theta_i) \quad (15)$$

we find that eq. (15) holds for $\theta_i = 36.32^0$ [once again, we emphasize here that we look here for angles θ_i in the interval $(0^0, 90^0)$ for which $C(\theta_i)$ is a *decreasing function* of θ_i, see eq. (6) and remarks below that].

Then, from eq. (7) we find: $y_D = OD = 7.35$ m (see Fig. 2), and from eq. (9): $DB' = OB' - OD = y_B - y_D = 2.65$ m.

Furthermore, by choosing (see Fig. 3): $DD' = \Delta y_{2rays} = 3$ m (which is 'much smaller' than OD = 7.35 m, that is DD'<<OD, while we chose here DD' = 3m > DB' = 2.65 m, as it is the case in Fig. 3), we make the following successive calculations:

Moreover, from eq. (14): $\theta_i^0 + \Delta\theta_i^0 = 45.99^o$, therefore $\Delta\theta_i^0 = 9.66^o$. Further, from eq. (8), i.e. Snell's law: $\theta_t^0 = 27.92^o$, and from eq. (13): $\theta_t^0 + \Delta\theta_t^0 = 34.65^o$, therefore: $\Delta\theta_t^0 = 6.73^o$. Finally, from eqs. (10) and (11) we calculate the *coordinates of the 'virtual image'*: $y_C = -3.22$ m, $z_C = 24.01$ m.

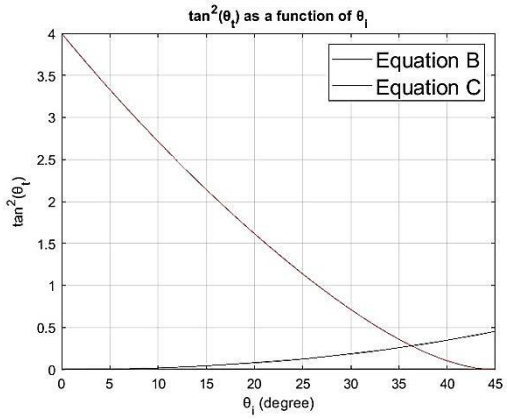

Figure 4. Graphs of monotonic functions $B(\theta_i)$, eq. (5), which is variant form of *Snell's law,* and $C(\theta_i)$, eq. (6), which comes from problem geometry

6. CONCLUSION – SHORT DISCUSSION – FUTURE RESEARCH

In this paper we considered the problem of a vertical short (i.e. Hertzian) dipole antenna in air radiating above a flat interface. Below the flat interface a lossless dielectric medium lies (unbounded for z<0), with dielectric constant ε_r (ε_r = real).

In high frequencies the solution to the above EM problem can be solved in an *approximate fashion* by applying the *'Geometrical Optics' (GO)* approach, that is '*ray representation'* of the EM waves. In this paper, as a first step, the refraction of rays on the flat interface is considered (by applying the well – known '*Snell's law of refraction'*) and for given position (coordinates) of the radiating dipole (above the flat interface) and of the observation point (below the flat interface) the coordinates (y_C, z_C) of the '*virtual image'* C of the radiating source are calculated.

The above solution is based, for given coordinates of the observation point below the flat interface, on the calculation of the position of the unique refraction point D on the interface. In this way, by applying our proposed method, a *unique* position (y_C , z_C) for the '*virtual image'* C is calculated (our formulation described above is a 2D formulation of the problem, where one can easily extend that to a 3D problem formulation).

Concerning corresponding *future research* by our group to this paper (in the near future), the well – known EM radiation formula from a vertical Hertzian dipole will be used, so that by applying *standard image theory techniques* an approximate EM formula at the receiver position (below the flat interface) will be derived (i.e. approximate value of the EM field at that point).

Finally, regarding *possible applications* of this research can be, for example, for the calculation of EM field values below the surface of the sea or of lakes, when a vertical antenna radiates above sea or lake surface (the rather small value of sea or lake water conductivity can be neglected, as a first approximation, provided that the depth below sea or lake surface is sufficiently small).

7. ACKNOWLEDGMENT

The authors would like to thank the Kazakshtan Ministry of Education and Research for a research grant, which supported this research.

References

[1] A. N. Sommerfeld, "Propagation of Waves in Wireless Telegraphy", Ann. Phys. 1909, 28, pp. 665–737.

[2] K. A. Norton, "The Propagation of Radio Waves over the Surface of the Earth and in the Upper Atmosphere", Proc. Inst. Radio Eng. 1936, 24, pp. 1367–1387, doi:10.1109/JRPROC.1936.227360.

[3] A. K. Norton, "The Propagation of Radio Waves over the Surface of the Earth and in the Upper Atmosphere", Proc. Inst. Radio Eng., 1937, 25, pp. 1203–1236, doi:10.1109/JRPROC.1937.228544.

[4] J. Wait, "Launching a surface wave over the Earth", Electronics Letters 1967, 3, pp. 396–397, doi: 10.1049/el:19670307.

[5] R. J. King, "Electromagnetic Wave Propagation Over a Constant Impedance Plane", Radio Sci. 1969, 4, pp. 255–268, doi: 10.1029/RS004i003p00255.

[6] T. K. Sarkar; W. Dyab, M.N. Abdallah; M. Salazar-Palma, M.V.S.N. Prasad, S.W. Ting, S.Barbin, "Electromagnetic Macro Modelling of Propagation in Mobile Wireless Communication: Theory and Experiment", IEEE Antennas Propag. Mag., 2012, 54, pp. 17–43, doi:10.1109/MAP.2012.6387779.

[7] J. G .V. Bladel, The Sommerfeld Dipole Problem. In Electromagnetic Fields, J. Wiley and Sons, Inc.: Hoboken, NJ, USA, 2007; Section 9.3, pp. 448–452.

[8] G. Tyras, Field of a Dipole in a Stratified Medium. In Radiation and Propagation of Electromagnetic Waves; Academic Press, Inc., New York, NY, USA, 1969; Section 6, pp. 133–160.

[9] Y. Rahmat-Samii, R. Mittra, P. Parhami, "Evaluation of Sommerfeld Integrals for Lossy Half-Space Problems". Electromagnetics, 1981, 1, pp. 1–28, doi: 10.1080/02726348108915122.

[10] R. E. Collin, "Hertzian dipole radiating over a lossy earth or sea: some early and late 20th-century controversies". IEEE Antennas Propag. Mag., 2004, 46, pp. 64–79, doi: 10.1109/MAP.2004.1305535.

[11] K. A. Michalski, "On the efficient evaluation of integral arising in the sommerfeld halfspace problem". IEE Proc.-Microwaves, Antennas Propag., 1985, 132, pp. 312–318, doi:10.1049/ip-h-2.1985.0056.

[12] G. Pelosi, J. L. Volakis, "On the Centennial of Sommerfeld's Solution to the Problem of Dipole Radiation Over an Imperfectly Conducting Half Space", IEEE Antennas Propag. Mag., 2010, 52, pp. 198–201, doi: 10.1109/MAP.2010.5586629.

[13] J. R. Wait, "The Ancient and Modern History of EM Ground-Wave Propagation.", IEEE Antennas Propag. Mag., 1998, 40, pp. 7–24, doi:10.1109/74.735961.

[14] A. Baños, Dipole Radiation in the Presence of a Conducting Half-Space, Pergamon Press, Oxford, UK, 1966; pp. 151–158.

[15] S. S. Sautbekov, R. N. Kasimkhanova,; P. V. Frangos, "Modified Solution of Sommerfelds's Problem:, In Proceedings of the CEMA'10 Conference, Athens, Greece, 7–9 October 2010; pp. 5–8. Available online: http://rcvt.tu-sofia.bg/CEMA/proceedings/CEMA_2010_proc.pdf (accessed on May 2021).

[16] S. Sautbekov, "The Generalized Solutions of a System of Maxwell's Equations for the Uniaxial Anisotropic Media. In Electromagnetic Waves Propagation in Complex Matter"; IntechOpen Limited: London, UK, 2011; Chapter 1, pp. 1–24, doi: 10.5772/16886.

[17] K. Ioannidi,; C. Christakis, S. Sautbekov, P. Frangos, S.K. Atanov, "The Radiation Problem from a Vertical Hertzian Dipole Antenna above Flat and Lossy Ground: Novel Formulation in the Spectral Domain with Closed–Form Analytical Solution in the High Frequency Regime". Int. J. Antennas Propag. (IJAP), 2014, Special Issue on 'Propagation of Electromagnetic Waves in Terrestrial Environment for Applications in Wireless Telecommunications', doi:10.1155/2014/989348.

[18] S. Bourgiotis, K. Ioannidi, C. Christakis, S. Sautbekov, P. Frangos, "The Radiation Problem from a Vertical Short Dipole Antenna Above Flat and Lossy Ground: Novel Formulation in the Spectral Domain with Numerical Solution and Closed-Form Analytical Solution in the High Frequency Regime", Proceedings of CEMA'14 Conference, Sofia, Bulgaria, 16–18 October 2014; pp. 12–18, Available online: http://rcvt.tu-sofia.bg/CEMA/proceedings/CEMA_2014_proc.pdf (accessed on May 2021).

[19] S. Bourgiotis, A. Chrysostomou, K. Ioannidi; S. Sautbekov and P. Frangos, "Radiation of a Vertical Dipole over Flat and Lossy Ground using the Spectral Domain Approach: Comparison of Stationary Phase Method Analytical Solution with Numerical Integration Results", Electronics and Electrical Engineering Journal, 2015, 21, pp. 38–41, doi:10.5755/j01.eee.21.3.10268.

[20] A. Chrysostomou, S. Bourgiotis, S. Sautbekov, K. Ioannidi and P. Frangos, "Radiation of a Vertical Dipole Antenna over Flat and Lossy Ground: Accurate Electromagnetic Field Calculation using the Spectral Domain Approach along with Redefined Integral Representations and corresponding Novel Analytical Solution", Electronics and Electrical Engineering Journal, 2016, 22, pp. 54–61, doi:10.5755/j01.eie.22.2.14592.

[21] S. Sautbekov, S. Bourgiotis, A. Chrysostomou and P. Frangos, "A Novel Asymptotic Solution to the Sommerfeld Radiation Problem: Analytic Field Expressions and the Emergence of the Surface Waves", PIER M, 2018, 64, pp. 9–22, doi: 10.2528/PIERM17082806.

[22] S. Bourgiotis, P. Frangos, S. Sautbekov and M. Pshikov, "The Evaluation of an Asymptotic Solution to the Sommerfeld Radiation Problem using an Efficient Method for the Calculation of Sommerfeld Integrals in the Spectral Domain", 'Electronics' Journal, MDPI Publisher, 1, https://doi.org/10.3390/electronics1010000, https://www.mdpi.com/journal/electronics, Special Issue on 'Propagation of Electromagnetic Waves in Terrestrial Environment for Applications in Wireless Telecommunications and Radar Systems', June 2021.

[23] J. Fikioris, Introduction to Antenna Theory and Propagation of Electromagnetic Waves; National Technical University of Athens: Athens, Greece, 1982. (In Greek).

ELECTROMAGNETIC POLLUTION ANALYSIS IN SOME SCHOOLS OUTDOOR ENVIRONMENTS

Tamar Nozadze, Davit Kharshiladze, Giorgi Ghvedashvili

Ivane Javakhishvili Tbilisi State University, Department of Electric and Electronic Engineering,
Laboratory of Applied Electrodynamics and Radio Engineering,
3, Chavchavadze Ave. 0176, Tbilisi, Georgia

E-mail: tamar.nozadze@tsu.ge,
E-mail: davitkharshiladze26@gmail.com,
E-mail: giorgi.ghvedashvili@tsu.ge

Abstract

Goal of the presented paper is to conduct electromagnetic (EM)-background research through direct measurements in the most sensitive locations (schools) in Tbilisi. Regular measurements/monitoring were conducted.

Based on the obtained results was determined whether the measured EM field values are in compliance with the existing safety limits and whether the environment in which especially children have to live is safe from the point of view of EM pollution.

1. INTRODUCTION

Electronic devices, which operation is accompanied by electromagnetic radiation, are introduced in modern life at an increasing pace. The background of these EM waves around us is increasing day by day. As the number of mobile phone users increases, so does the number of base stations, which in turn increases the background EM field (EM pollution). On the other hand, a high quality of connection must be ensured for the operation of mobile phones. In case of a weak connection, the devices automatically increase the transmission power [1], [2], which has an undesirable effect on both biological objects and electronic devices nearby. Added to this are many other EM radiations, and obviously, all this requires control, since in the near future, the increase of the EM background at such a rate may lead to uncontrollable processes.

Current safety standards limit the level of EM radiation to those cases that pose a threat to human health, while there may be some other biological effect, impact, but it is not considered dangerous to health [3]. The influence of RF radiation on living organisms is manifested in the form of direct and indirect thermal as well as non-thermal effects. Biological effects depend on the internal EM field. In order to characterize the internal EM field, the coefficient of absorption (SAR-Specific Absorption Rate, W/kg) is introduced, which shows the energy absorbed by the unit of mass in the unit of time. The SAR limit recommended by The Council of the European Union is 2.0W/kg averaged over 10 grams of tissue for the body [3].

A high-value EM field can interfere with the operation of implanted pacemakers and regularly interrupt the delivery or generation of impulses, which can lead to the death of the patient [4].

Scientists believe that the decline in the number of pollinators can cause serious problems, more immediate and larger than global warming [5]. It turned out that the birds living in the telephone towers abandoned the nest within a week. Eggs laid in nests near transmission towers did not hatch [6]. It has been established that EM radiation can also have a negative effect on plant crops. Many studies show that EM field can inhibit seed germination and slow down root growth [7].

All of the above is the signal that an ecosystem is undergoing adverse changes due to EM pollution, which will manifest in the near future and will definitely have an adverse effect on human health/ quality of life. It is important to note that if the necessary precautions against EM pollution will not be taken, EM exposure will increase day by day and more serious disorders will be revealed in people as well as in the ecosystem in general.

All ecosystems of the earth are interconnected. If one component of an ecosystem is disrupted the whole system will be affected (could cause cascading effects). The study of these problems is an important challenge for scientists today because the existing studies are incomplete and insufficient.

The presented study aims to investigate the EM background level in urban areas of Georgia (Tbilisi school locations). It is important to determine the level of EM radiation and conduct periodic monitoring. Because each of us has the right to know whether the environment where we live is safe from the point of view of EM pollution; whether the safety norms are followed or not.

2. RESEARCH METHODOLOGY

Schools, hospitals, shopping malls are locations were the concentration of users may vary according the day of the week and time within the day. Therefore, the value of the EM field in the environment can be different. In terms of EM background assessment, measurements were made during the day in public schools locations (on the school perimeter where special permission is not required). Periodic monitoring was carried out in order to assess the trend (tendency) of EM field values at selected locations, for visibility, appropriate diagrams were constructed based on the results obtained. Measurements were made in the period from January to June, 2024. Periodic measurements were carried out two times over the weekend. The interval between each measurement was varied according to weather conditions.

The measurement methodology used in the study was based on the recommendations specified in the standards and guidelines. According to the ICNIRP guidelines, exposure to RF EM fields is quantified in terms of electric field (V/m), magnetic field (A/m) and power density (W/m^2). HF-B8G was used as a measuring device Figure 1.

For measurements, the 1MHz-8GHz frequency range is selected, within which the measuring device allows to provide non-ionizing radiation definition with an isotropic antenna.

In order to initially avoid the influence of weather (humidity), measurements were always carried out under the same weather conditions, only during cloudless periods.

All measurement was conducted at the same time period of the day, to avoid time difference influence on measurement [8]. Measurement points were selected at a height of about 1.5 meters from the ground, as the level of average human height. The duration of measurements at each location is determined by 5-6 minutes. Several measurements were conducted at various locations around of the interested areas (schools) and were selected maximum value of the measured EM field.

Figure 1. Measuring device (HF-B8G: Professional High Frequency and RF Meter)

Measurements of EM field values in selected places on weekdays and weekends at different intervals were carried out in different locations to study the dependence of the pollution level on the number of mobile phone users (active sources) and the effect of time. Analysis of the values obtained by measurement was carried out and compliance with safety norms was determined. The data obtained from the field measurement device were processed and clearly identified which locations of the schools of Tbilisi are noteworthy according to the level of pollution.

3. RESULTS AND DISCUSSIONS

EM waves emitted from base stations are rapidly increasing due to the development of modern technology capabilities and cause unwanted EM pollution of the environment. It should be noted that people living near base stations are constantly under the influence of EM radiation and in many cases are not aware of the unwanted effect. For EMF exposure there are some reference levels set by international organizations such as WHO, ICNIRP, FCC, IEEE and the countries follow the ICNIRP reference levels Figure 2.

Council Recommendation1999/519/EC	42V/m(4.75W/m^2)	59V/m(9.25W/m^2)
ICNIRP Guidelines,April1998	42V/m(4.75W/m^2)	59V/m(9.25W/m^2)

Figure 2. International EM safety reference standard

For research 25 public school locations were chosen Figure 3. The study focused on measuring the

radiated energy and determining whether the locations of the selected schools are safe in terms of electromagnetic pollution; research showed that an increasing trend is observed EM field values, which can be explained by the change of season (winter to spring) Figure 4.

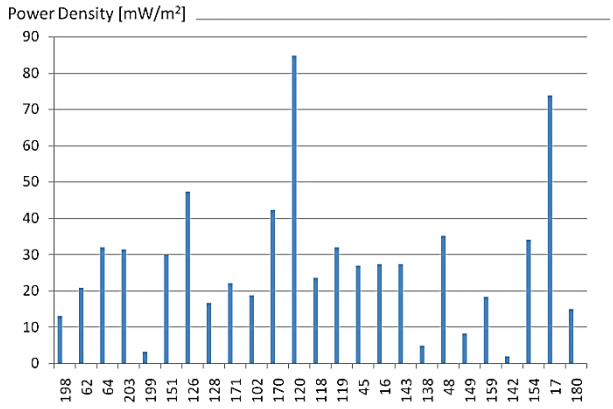

Figure 3. EM power density values by the school numbers (measured on weekdays)

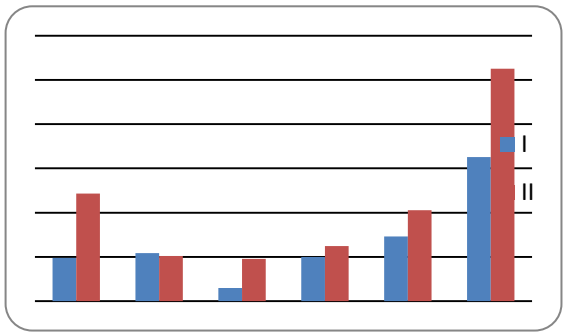

Figure 4. Power density values for each selected public school areas measured on weekends

In this study, measurements of the EM field power density in the city of Tbilisi are used to estimate the electromagnetic radiation level. It is indicated [10] that the radiation density can be considered safe up to the level of 10 μW/cm^2. The research shows that the values of EMF intensity in selected locations of Tbilisi are within 1-105 mW/m^2.

Was obtained that one location recorded relatively high radiation value (school number 54) Figure 4, while the rest were within the acceptable range according to both global and local standards Figure 3. [10]. Therefore, where the measured value is higher, it is desirable to take measures to reduce the values of the EM field intensity below the threshold value. Also, by analyzing the results obtained during the study period, it was determined that for this stage there was no significant difference between the EM field values obtained by measurements on weekdays and weekends. Which can be explained by the fact that the measurements were made on the schools outer perimeter.

4. CONCLUSION

The interim results of the study are presented in the presented paper. The study of these problems is an important challenge for scientists today, because the existing studies are incomplete and insufficient. Research in this direction continues and we will be able to make general conclusions about EM pollution in Tbilisi school locations based on the measurement results.

It should be noted that although people are developing means of defence to protect themselves from physical threats, they cannot do the same against the effects of EM fields, which are rapidly increasing day by day and are imperceptible. The studies conducted so far have shown that in the modern world it is impossible to completely avoid the effects of EM fields. Finding ways to protect against the effects of EM pollution is extremely important. As the above review revealed, the adverse correlation between EM pollution and human health and the ecosystem in general is clear.

ACKNOWLEDGMENT

Research is financially supported by Shota Rustaveli National Science Foundation of Georgia (SRNSFG) [grant number **YS-23-131**]

References

[1] T. Nozadze, V. Jeladze, R. Zaridze, 'Mobile Antenna Matching Study Considering Different Holding Positions at 2100 MHz Frequency', XXVIth International Seminar/Workshop on Direct and Inverse Problems of Electromagnetic and Acoustic Wave Theory DIPED2020, Tbilisi, Georgia, September 15-18, 2020

[2] T. Nozadze, V. Jeladze, M. Tsverava, V. Tabatadze, M. Prishvin, R. Zaridze, "EM Exposure Study on an Inhomogeneous Child Model Considering Hand Effect", 2017 IEEE First Ukraine Conference on Electrical and Computer Engineering (UKRCON), Kyiv, Ukraine, May 29 - June 2, 2017, pp. 51-54

[3] Abdul-Al, M., Amar, A.S. I., Elfergani, I., Littlehales, R. , Ojaroudi Parchin, N. , Al-Yasir, Y., See, C.H., Zhou, D., Abidin, Z. Z. , Alibakhshikenari, M., Zebiri, C., Elmegri, F., Abusitta, M., Ullah, A., Abdussalam, F. M. A., Rodriguez, J., McEwan, N.J., Noras, J.M., Hodgetts, R., Abd-Alhameed, R. A." Wireless Electromagnetic Radiation Assessment Based on the Specific Absorption Rate (SAR): A Review Case Study". Electronics. 11(4), 511, 2022.

[4] Jana Mydlováa , Ivana Gálováa, Mariana Beňováa . "Impact of Electromagnetic Fields in Transport on Active Implantable Medical Devices". Transportation Research Procedia 40 (2019) 1497–1503.

[5] Sundar Santhosh Kumar. "Colony Collapse Disorder (CCD) in Honey BeesCaused by EMF Radiation". Bioinformation. 2018; 14(9): 521–524

[6] Alfonso Balmori. "Electromagnetic Pollution as a Possible Explanation for the Decline of House Sparrows in Interaction with Other Factors". Birds 2021, 2(3), 329-337

[7] B. Blake Levitt, Henry C. Lai and Albert M. Manville II. "Low-level EMF effects on wildlife and plants: What research tells us about an ecosystem approach". Front. Public Health, 25 November 2022 Sec. Radiation and Health Volume 10 - 2022

[8] N. As, B. Dilek, M. Şahin, Y. Karan, "Electromagnetic pollution measurement in the RTE university campus area", Global Journal on Advances in Pure & Applied Sciences , Vol. 3 , pp.65-72, 2014.

[9] https://cpcb.nic.in/uploads/healthreports/Newsletters_68_mobiletower.pdf

[10] Order No 297/N of 2001 of Minister of Labor, Health and Social Affairs of Georgia on Environmental Quality Requirements | AMP EID

A SYSTEM FOR DIGITIZING ANALOG SIGNALS, COMPRESSION AND ENCRYPTION

Dilyana Dimitrova

Department of Information Technologies
Nikola Vaptsarov Naval Academy
73 Vasil Drumev Str., Varna, Bulgaria
Email: di.dimitrova@naval-acad.bg

Abstract

This paper investigates the digitalization and encryption of audio signals using the AES symmetric cryptographic algorithm, focusing on their application in modern communication systems. Digitalization transforms analog signals into discrete digital form, crucial for efficient data processing and transmission in diverse industries. A-law compression optimizes signal bandwidth and storage efficiency while maintaining quality. Results demonstrate analog-to-digital conversion of sinusoidal signals and voice using an 8-bit ADC, confirming minimal signal loss with higher quantization levels. AES encryption secures the digitized and compressed signal, ensuring data integrity and privacy. Future research will explore signal recovery methods and automated encryption techniques using Simulink. This study underscores the importance of digitalization and encryption technologies in advancing communication systems reliability and security.

Keywords: digitalization, ADC, encryption, AES, signals, cryptography

1. INTRODUCTION

In today's rapidly advancing technological landscape, the digitalization of signals and voice plays a central role in numerous aspects of our everyday life and industrial applications. Digitalization refers to the process of converting analog signals, which are continuous and variable, into digital signals, which are discrete and binary. This transformation is crucial for many reasons, spanning from enhanced data processing capabilities to improved storage and transmission efficiency.

Digitalization facilitates the integration and interoperability of various devices and systems. In an era where the Internet of Things (IoT) is becoming widespread, the seamless connectivity between smart devices, sensors, and control systems is made possible through digital communication. This connectivity enables real-time monitoring, data analysis, and automation, driving efficiency and innovation across industries such as healthcare, transportation, and manufacturing.

Digital signals can be easily compressed, encrypted, and stored, offering significant advantages in terms of data management and security. Techniques like A-law compression, commonly used in Europe, allow for efficient use of bandwidth and storage space while maintaining high-quality signal replication. Encryption ensures that digital information can be transmitted securely, protecting sensitive data from unauthorized access and cyber threats.

In the field of voice communication, digitalization has transformed how we interact and communicate. From mobile phones to voice over Internet Protocol (VoIP) services, the conversion of voice to digital signals has enabled clearer, more reliable, and more versatile communication methods. Features such as voicemail, call forwarding, and video conferencing have become standard, enhancing personal and professional communication.

In paper [1] authors propose an encryption technology for voice transmission in mobile networks using the 3DES-ECC algorithm. It combines speech signal acquisition, 3DES, and ECC algorithms for speech data encryption. In [2] is presented speech to text conversion system that also encrypts the text using the Advanced Encryption Standard (AES) algorithm. In [3] authors introduce a k-shuffle based audio scrambling technique that produces cipher audio with variable audibility, beneficial for perceptual video encryption algorithms, showing resistance to certain types of attacks.

The absence of an analog-to-digital converter that uses A-law compression and encryption of the signal following the literature review underscores the relevance of the issue.

The models in this paper present source digitization and A-law compression. A possibility for signal encryption is provided. For this purpose, two examples of digitization are examined – a sinusoidal signal, to clearly observe the signal transformation, and voice. The analog-to-digital converter is a fundamental block that enables the conversion of information from analog to digital form and its transmission to digital devices. Without analog-to-digital conversion, the world today would be very different. An A-law compression is selected because it is used in Europe.

The main aim of the paper is to explore and demonstrate the processes of analog-to-digital conversion and A-law compression in the context of digitizing signals, specifically sinusoidal signals and voice. Additionally, the paper aims to highlight the significance of these processes in enhancing signal quality, reducing noise, and improving the efficiency of digital signal transmission. The study also investigates the application of encryption techniques, particularly using symmetric cryptographic algorithms like AES, to secure the digitized and compressed signals. Overall, the paper seeks to provide insights into the technical aspects and practical applications of digital signal processing in telecommunications and related fields.

2. SOURCE DIGITALIZATION

2.1. Components of the block diagram

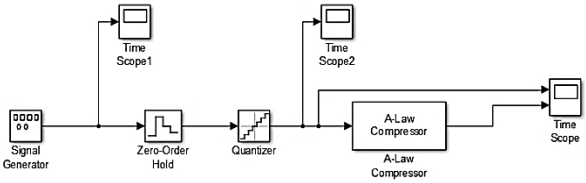

Figure 1. Block diagram of an ADC with A-law signal compression

Figure 1 presents a block diagram of analog-to-digital conversion with A-law signal compression made in Simulink. The following blocks are used:

- Signal Generator: Used to generate a sinusoidal signal, which will then be converted to digital.
- Zero-Order Hold: This block samples the signal at specific time intervals, Δt. According to the Kotelnikov-Nyquist theorem [4], if we have a signal with a frequency band from f_{min} to f_{max} and take the reciprocal of the doubled maximum value of the frequency band, the time interval Δt should be less than or equal to this value to transmit it accurately to the receiver without distortion. This can be presented with the formula (1).

$$\Delta t \leq \frac{1}{2f_{max}} \quad (1)$$

- Quantizer: It discretizes the signal by amplitude and rounds it to the nearest allowed level. Rounding to an integer leads to distortion of the original signal and errors at the receiving end. There is a quantization step between two allowed levels, which is uneven, and the quantization is even.
- A-law Compressor: It uses an algorithm that, instead of even steps between quantization levels, uses uneven — smaller steps for lower levels and larger steps for higher levels. This compresses the signal's dynamic range and improves its quality. Lower levels are important because they carry more information. The A-law is a logarithmic compression law used in Europe.
- Several oscilloscopes that visually display the analog-to-digital conversion process.

2.2. Results from the Source digitalization simulation

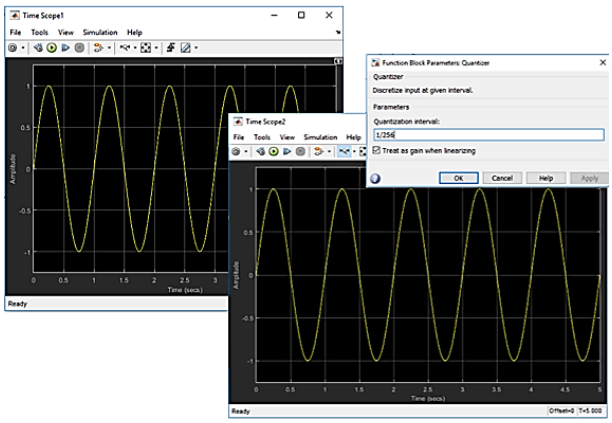

Figure 2. Graph of the analog signal from oscilloscope Time Scope1 and the digital signal from Time Scope2 with a quantization interval of 1/256

According to ITU-T standard G.711 for pulse-code modulation (PCM) [5] of speech frequencies, the best signal digitization is achieved using 256 quantization levels because it uses 8 bits for encoding (digitizing) speech. Therefore, the quantization interval in this case will be equal to 1/256. After ex-

amining the oscilloscope graphs with this value, it was found that there is no visual difference between the analog and digital signals, as it is shown on Fig. 2, indicating that the conversion was performed with almost no loss.

To clearly observe the conversion of the analog signal to digital, and after testing different values that are powers of two, a noticeable difference in the graph without zooming in was seen at a quantization interval value of 1/32.

In Fig. 3, the analog signal and the digital signal are superimposed, and the A-law compressed signal, shown in red, clearly demonstrates that the quantization interval is non-uniform for the latter. The purpose of the compression is to improve the quality of the transmitted signal. In conclusion of the experiment, lower levels are more probable and carry more information, so they are quantized with a smaller step. The opposite is true for higher levels, so they are quantized with a larger step.

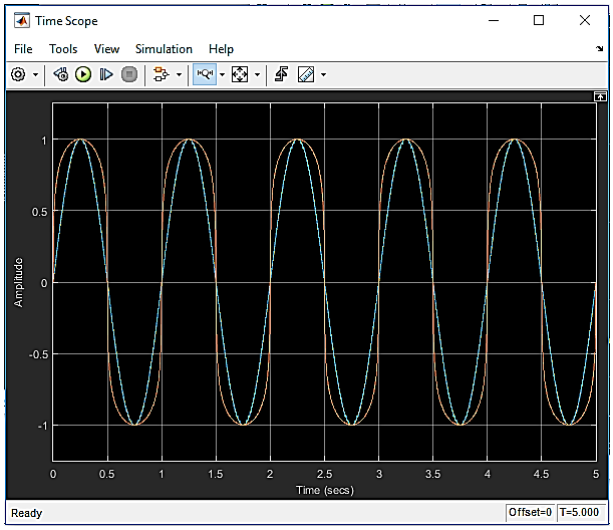

Figure 3. Graph of the signal before and after analog-to-digital conversion and after A-law compression from the Time Scope oscilloscope

3. DIGITIZATION OF VOICE

3.1. Components of the block diagram

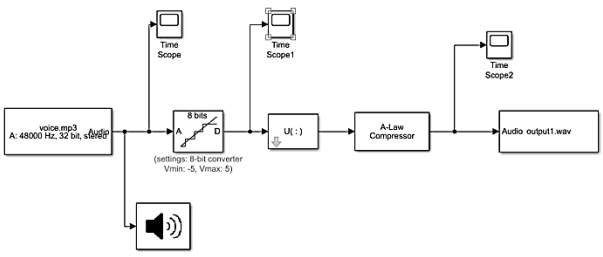

Figure 4. Block Diagram of Voice Digitization

In Fig. 4, a block diagram of voice digitization is presented. Its purpose is to demonstrate how speech is converted from analog to digital form and what happens to the signal after A-law compression. The following elements are used:

- Block that Loads an Audio File (From Multimedia file): The file contains my voice, with a format of m4a or MPEG audio encoding. The signal is dual-channel since it is stereo and was recorded using my phone's built-in microphone.
- Analog-to-Digital Converter (Idealized ADC quantizer): Built-in ADC block is used to convert quickly the voice from analog to digital form, as using separate elements for analog-to-digital conversion from the first diagram takes too much time to perform the simulation. According to ITU-T standard G.711 for pulse-code modulation (PCM) of speech frequencies [5], 256 levels or 8 bits are used for signal quantization by level for voice digitization. An 8-bit ADC is used for this purpose.
- Block for Converting 2-D Signal to 1-D: This block converts the two-dimensional stereo signal into a one-dimensional signal, as the A-law compression block requires a one-dimensional signal.
- A-law Compressor Block (A-law Compressor): The same as the first experiment.
- To Audio Device Block: Used for playback of the audio file.
- Oscilloscopes: Used for graphical visualization of analog-to-digital conversion and A-law compression.

3.2. Results from the Voice digitalization simulation

In Fig. 5, two graphs depict the digital signal of the voice after processing by the ADC and an enlarged view of it. These clearly show the analog-to-digital conversion. The signal is in two colors because it is dual-channel.

Fig. 6 presents graphs of the signal after A-law compression. The wide dynamic range of speech is not well encoded by standard ADCs and their linear coding, as the quantization step is the same, leading to errors during analog signal reconstruction. For this purpose, A-law compression is used, where

low frequencies are quantized with a smaller step and high frequencies with a larger one, reducing the dynamic range of speech, minimizing quantization noise, and enhancing the quality of the transmitted digital signal.

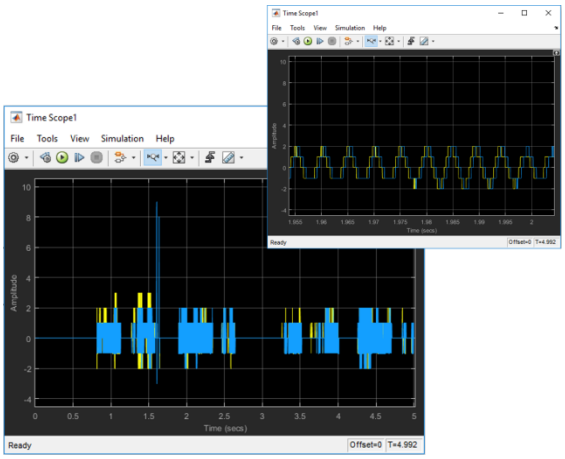

Figure 5. Graphs of the digitized signal (voice) from the Time Scope1 oscilloscope

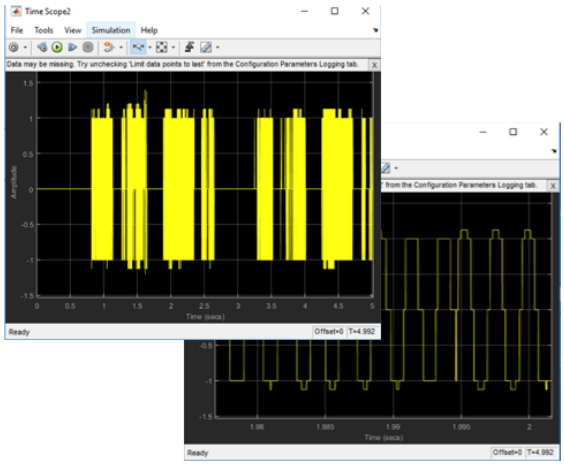

Figure 6. Graphs of the signal after A-law compression from Time Scope2 oscilloscope

4. ENCRYPTION

For encrypting the digitized and compressed signal, various cryptographic algorithms can be used, with symmetric cryptographic algorithms like AES being recommended for encrypting large volumes of information. During the experiment, the symmetric cryptographic algorithm AES was utilized.

There are several approaches that can be implemented for encrypting the digitized and compressed signal. In this specific solution, the compressed signal was first saved into a WAV file using the built-in Simulink block "To Multimedia File". Subsequently, a MATLAB function was written to convert this WAV file into a binary file. The binary file was then encrypted using external software. The decryption and information recovery processes were successful. As this paper is focused on digitizing the source signal, recovering the signal at the receiver will be the subject of future work.

Another potential approach for encrypting the digitized and compressed signal involves creating a Simulink function that automates the described procedures, which also remains a subject for future investigation.

4. CONCLUSION

During the study, graphical analog-to-digital conversion and A-law compression of sinusoidal signals and speech were observed. It was found that using higher levels of quantization provides better digitization of the analog signal. In the first case, 32 levels were used to observe the digitization process more closely. Comparing this with 256-level quantization, the digital signal showed no visible difference from the analog signal on the graph, indicating minimal loss during inverse conversion. In the second scheme, voice analog-to-digital conversion was performed using an 8-bit ADC according to G.711 standard, applying the same principles as in the first scheme. A-law compression was utilized in both cases to improve the quality of the transmitted digital signal. To secure the digitized and compressed signal, a range of cryptographic algorithms can be applied, with symmetric methods such as AES preferred for their effectiveness with large data sets. In this experiment, AES was specifically employed to encrypt the signal, ensuring robust protection.

The report is in implementation of the National Scientific Program "Security and Defense", adopted with RMS No. 731/21.10.2021, and financed by the Ministry of Education and Science of the Republic of Bulgaria according to Agreement No. D01-74/19.05.2022.

References

[1] Chang, Z., Woźniak, M. Encryption technology of voice transmission in mobile network based on 3DES-ECC algorithm. Mobile Netw Appl 25, 2398–2408 (2020). https://doi.org/10.1007/s11036-020-01617-0

[2] Agarwal, A., Raj, P.M., & Katiyar, S. (2019). Secured Audio Encryption using AES Algorithm. International Journal of Computer Applications.

[3] Alhassan, S., Iddrisu, M. M. & Daabo, M. I. Securing audio data using K-shuffle technique. Multimed Tools Appl **78**, 33985–33997 (2019). https://doi.org/10.1007/s11042-019-08151-6

[4] V. V. Zamaruiev, "The use of Kotelnikov-Nyquist-Shannon sampling theorem for designing of digital control system for a power converter," 2017 IEEE First Ukraine Conference on Electrical and Computer Engineering (UKRCON), *Kyiv,* UKraine, 2017, pp. 522-527, doi: 10.1109/UKRCON.2017.8100305.

[5] International telecommunication union. "recommendation g.711: pulse code modulation (pcm) of voice frequencies." accessed june 20, 2024. https://www.itu.int/rec/t-rec-g.711/.

APPLICATION AND IMPORTANCE OF 0.20% CHLORHEXIDINE GEL DURING THE ADAPTATION PERIOD AFTER PROSTHETIC TREATMENT WITH DIFFERENT REMOVABLE PROSTHESES DEPENDING ON THE AGE OF THE PATIENTS

Anna Nenova-Nogalcheva

Department of Oral Surgery, Faculty of Dental Medicine
Medical University - Varna, Bulgaria
Varna 9002, 55 Marin Drinov str.
E-mail: anenova@yahoo.com

Desislava Konstantinova

Department of Dental Materials Science and Prosthetic Dentistry
Faculty of Dental Medicine, Medical University – Varna, Bulgaria
Varna 9002, 55 Marin Drinov str.
E-mail: dr.konstantinova@gmail.com

Mariya Nikolova

Department of Information Technology, Faculty of Engineering
Nikola Vaptsarov Naval Academy, Bulgaria
Varna 9026, 73 V. Drumev str.
E-mail: mpn@abv.bg

Emiliya Koleva

Department of Electronics, Faculty of Engineering
Nikola Vaptsarov Naval Academy, Bulgaria
Varna 9026, 73 V. Drumev str.
E-mail: e.koleva@nvna.eu

Abstract

The paper presents a study of the effects of 0.20% chlorhexidine gel on the healing process of wounds during the adaptation period after prosthetic treatment, taking into account the location and type of placed prosthesis as well as the age of the patients. The condition of the patients was monitored 24, 48 and 96 hours after the placement of the prosthesis. The results of a statistical analysis of data from the adaptation period are presented.

It is concluded that the gel does not affect the size of the lesions, in dependance to the location of the placed prosthesis. Patients with partial and total dentures, that have applied gel, have undergone a faster healing process of the lesion compared to the standard treatment. It was evidenced that there is no relation between the age of the patients and the size of the lesion after prosthetics.

1. INTRODUCTION

The trend of aging of the population and the increased life expectancy of the elderly people in Bulgaria and worldwide, increase the need for prosthetic treatment [1,2,3]. The partial and total plaque prostheses are a method of choice for these patients, in order to rehabilitate their masticatory apparatus and increase their quality of life overall. Some of the most commonly observed lesions on the oral mucosa during the adaptive period, after prosthetic treatment with removable prosthesis are prosthetic stomatitis, traumatic ulcers, fibrous hyperplasia and oral candidiasis [4,5,6,7,8]. The subjective symptoms vary depending on the localization of the lesion in the oral cavity and lead to the inability to use the prosthesis [9].

Purpose: To study the effects of 0.20% chlorhexidine gel on the healing process of traumatic lesions in the oral cavity, that occurred after removable prosthetic treatment, depending on the age of the patients, the location and the type of prosthesis.

2. MATERIAL AND METHODS

The study was conducted in two dental practices, specializing in prosthetic and surgical dentistry on the territory of the city of Varna, Bulgaria, in the period from November 2021 to April 2022.

52 Patients aged 64 to 74 with removable dentures took an informed part in the study. They were divided into two groups in accordance to the instructions they received regarding the adaptation period. The participants in the first group received only standard instructions regarding influencing the traumatic lesions after the prosthetic treatment. The second group of patients received a recommendation for an application of 0.20% chlorhexidine gel three times a day, after performing oral hygiene in addition to the standard instructions.

The lesion size was measured in all of the study's participants 24, 48 and 96 hours after the placement of the prosthetic structures.

2.1. Sample size

52 patients have undergone prosthetic treatment with partial or total plate prostheses. A descriptive statistic is presented in table 1 about the general characteristics of the patients. The mean age of all participants was 69.4. Half of them (26) are male. The last three columns contain information related to the size of the wound, measured in mm one day, two days and four days after the placement of the prosthesis.

Table 1. Descriptive statistics

Descriptives

	Gender	Age	24 hours	48 hours	96 hours
N	52	52	52	52	52
Mean	1.50	69.4	4.35	2.12	0.827
Median	1.50	69.0	4.00	2.00	1.00
Std deviation	0.505	2.31	2.09	1.77	1.15
Min.	1	64	1	0	0
Max.	2	74	8	6	5

For the purposes of this study, the patients were divided into 2 groups. The first group – Study Group (SG) consists of patients who used 0.20% chlorhexidine gel after prosthetic treatment. The second group – Control Group (CG) included patients, who received only standard instructions after the placement of the prostheses.

Half of the patients (9) in the SG had prosthetic structures made for the upper jaw, while the remaining patients had a prosthetic structure for the lower jaw. In the Control group, 9 of the patients had prostheses placed on the upper jaw and 7 on the lower jaw. The patients, who had prostheses placed on both jaws were 9 in both groups.

2.2. Statistical analysis

Descriptive statistics were obtained. Tests for the statistical assumptions of normality and homogeneity of variance were made for the variables, where needed. The differences between the different groups were assessed using Student's t test or the Mann-Whitney U test [10, 11] depending on parametric or non-parametric data for continuous variables. A correlation analysis was also used. Excel [12], Matlab [13], and Jamovi [14] software programs were applied to process the obtained data.

3. RESULTS

The study evaluates the influence of 0.20% chlorhexidine gel applied on oral lesions, that have occurred immediately after prosthetic rehabilitation, taking into account different factors like age and type of prosthetic construction – upper or lower, partial or total prosthesis.

3.1. The effect of the location of prosthesis – upper or lower jaw, on wound size in patients

Tables 2 and 3 present summarized information about the studied data about the age and size of the wound, depending on the location placement of the prosthesis for the two groups of patients.

Table 2. Mean age and mean wound size for LJ, UJ and LJ&UJ for Study group

		Study group			
	prostheses	Age	Wound size at 24h [mm]	Wound size at 48h [mm]	Wound size at 96h [mm]
mean	UJ	68,89	3,44	1,33	0,78
	LJ	67,44	3,67	1,44	0,56
	UJ&LJ	70,33	5,78	3,00	1,56

UJ: Upper jaw; LJ: Lower jaw

Table 3. Mean age and mean wound size for LJ, UJ and LJ&UJ for Control group

		Control group			
	prostheses	Age	Wound size at 24h [mm]	Wound size at 48h [mm]	Wound size at 96h [mm]
mean	UJ	69,67	3,56	1,89	0,44
	LJ	69,14	4,71	2,43	1,00
	UJ&LJ	70,67	5,00	2,67	0,67

UJ: Upper jaw; LJ: Lower jaw

Tables 2 and 3 show that the mean values of the wound size in patients with a maxillary prosthesis were smaller than those with a mandibular one, with the exception of patients in SG after 96 hours. A Mann-Whitney U test was used to confirm the hypothesis for a difference in wound size, depending on the prosthetic site. The need for the use of the test arises due to the lack of normal distribution of the data about the wound size and the small sizes of the samples.

The sizes of the lesions were analyzed after 24, 48 and 96 hours for the upper and lower jaw for both patient groups separately. The results of the tests carried out ($p>0.05$) show that there was no significant difference between the size of the lesion in dependance of the placement of the prosthesis on the upper or lower jaw in both groups of patients during the entire healing process.

Figure 1 shows the mean wound size 24, 48 and 96 hours after the placement of prostheses on the upper and lower jaw respectively for SG and CG.

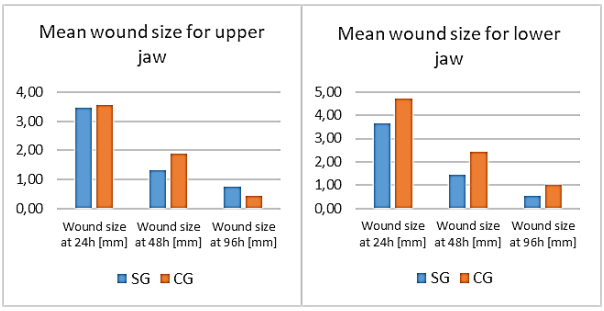

Figure 1. Mean wound size after prosthetic treatment of the upper and lower jaw

Figure 1 demonstrates a trend, that the average wound sizes of the gel applying patients were smaller than of those who followed standard treatment plans.

It remains to be established whether the gel has an effect on the wound sizes, depending on the location of the prosthetic placement. The results from the conducted tests, shown in table 4 and table 5, do not confirm the observation of a statistically significant difference ($p>0.05$).

Table 4. Test results, about the difference of the wound size in CG and SG when UJ prothesis is used

		Statistic	df	p
24 hours	Student's t	-0.125	16.0	0.902
48 hours	Mann-Whitney U	30.0		0.359
96 hours	Mann-Whitney U	38.0		0.837

Table 5. Test results, about the difference of the wound size in CG and SG when LJ prothesis is used

		Statistic	df	p
24 hours	Student's t	-1.03	14.0	0.322
48 hours	Mann-Whitney U	19.0		0.190
96 hours	Mann-Whitney U	20.5		0.221

3.2. Study of the influence of the gel on the healing process of lesions in partial and full prostheses

Tables 6 and 7 present the average values of the sizes of the lesions after the placement of partial and full acrylic prostheses of the patients respectively.

Table 6. Average values of the sizes of the lesions after the placement of partial dentures

Group	Wound size at 24h [mm]	Wound size at 48h [mm]	Wound size at 96h [mm]
SG	3,56	1,34	0,67
CG	4,06	2,13	0,69

Table 7. Average values of the sizes of the lesions after the placement of total dentures

Group	Wound size at 24h [mm]	Wound size at 48h [mm]	Wound size at 96h [mm]
SG	5,78	3	1,56
CG	5	2,67	0,67

From tables 6 and 7, it can be established that the differences in the average values of the size of the wound in every group SG and CG separately during the healing process are not significantly different. In patients with partial dentures, the differences range from 0.02mm in 96 hours to 0.79mm in 48 hours and in those with complete dentures – from 0.33mm in 48 hours to 0.89mm in 96 hours. Due to the characteristics of the data, the Mann-Whitney U test had to be used once again. The results of the tests ($p>0.05$) confirmed that there is no significant difference with and without the application of the gel for 24, 48 and 96 hours in both groups of patients.

When comparing the data in tables 6 and 7, it is noticeable that the wound is larger in patients with total dentures compared to those with partial ones, in the beginning of the healing process – after 24 and 48 hours in comparison with the size of the wound after 96 hours.

The results of the Mann-Whitney U test in the examination of the wound sizes of patients that have not used gel with partial and full dentures confirmed

that there are no significant differences in sizes at 24, 48 and 96 hours ($p>0.05$). In the SG patients however, there is a statistically significant difference in wound sizes at 24 and 48 hours, regardless of the type of prosthesis, with the wound being larger in the case of total dentures. It can be concluded that the gel has a positive effect when used for a longer time.

3.4. The effect of the age on wound size in patients

Figure 2 provides a summary of the average age of the patients by wound size.

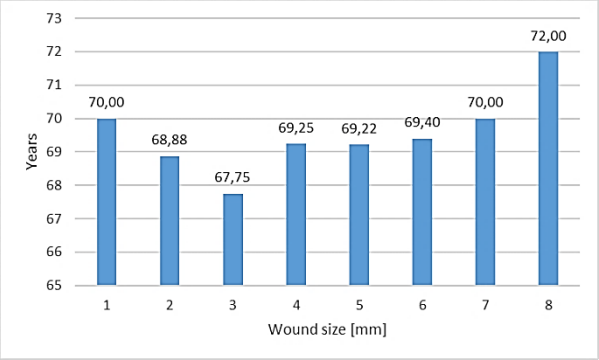

Figure 2. Mean age referred to the wound size

The influence of the age of the patients from both groups – SG and CG, on the course of the wound healing process was studied using the Spearman correlation method.

In both groups of patients – those who applied and those who did not apply 0.20% chlorhexidine gel on the wound, after 24, 48 and 96 hours, no relationship between age and the size of the wound was found. All p-values are greater than 0.05.

7. CONCLUSION

The adaptation period after prosthetic treatment with removable dentures can be positively affected by following the instructions given out by the attending physician. Our study shows a statistically significant difference in wounds sizes at 24 and 48 hours in patients who have applied gel, regardless of the type of prosthesis – partial or total. There is no relation between the age of the patients and the size of the ulcers

The application of 0.20% chlorhexidine gel on oral lesions has a positive effect in the healing process, with long-term use. Age has no statistical correlation to the size of the lesion.

References

[1] G. Marois, A. Bélanger and W. Lutz, "Population aging, migration, and productivity in Europe", Proceedings of the National Academy of Sciences, 117(14), 2020, pp. 7690-7695, https://doi.org/10.1073/pnas.1918988117

[2] M. Luy, M. Zannella, C. Wegner-Siegmundt, W. Lutz and G. Caselli, "The impact of increasing education levels on rising life expectancy: a decomposition analysis for Italy, Denmark, and the USA", Genus, 75, 2019, pp.1-21, https://doi.org/10.1186/s41118-019-0055-0

[3] J. Aburto, F. Villavicencio, U. Basellini, S. Kjærgaard and J. Vaupel," Dynamics of life expectancy and life span equality", Proceedings of the National Academy of Sciences, 117(10), 2020, pp. 5250-5259, https://doi.org/10.1073/pnas.1915884117

[4] T. de P. Mascarenhas, "Lesões bucais associadas ao uso de prótese total", Saúde.com, 7(2), 2011, pp. 133-142

[5] A. Oliveira, H. Carvalho, B. Tramontani, T. Sayed, L. Santos, G. Oliveira and M. Cantisano. Filgueiras, "Lesões bucais associadas ao uso de prótese total.", Revista Brasileira de Odontologia, 73(2), 2016, pp.130, https://doi.org/10.18363/rbo.v73n2.p.130

[6] N. Veiga, A. Herdade, L. Diniz, B. Brites, S. Pinto, et al., "Oral lesions associated with removable prosthesis among elderly patient's, Portugal", Int J Dent Oral Health, 3(1), 2016, http:// dx.doi.org/10.16966/2378-7090.218

[7] B. Khanal, S. Sapkota, S. Thakur and R. Chaulagain, "Evaluation of traumatic ulcerations frequency and site in post-insertion adjustment recall visits in complete denture patients visiting a dental college in Chitwan", Journal of Chitwan Medical College, 13(3), 2023, pp.18-20, https://doi.org/10.54530/jcmc.1373

[8] P. Kivovics, M. Jáhn, J. Borbély and K. Márton, "Frequency and location of traumatic ulcerations following placement of complete dentures", Int J Prosthodont, 20(4), 2007, pp.397-401, https://doi.org/10.1038/bdj.2007.1051

[9] LI Kupp, PJ Sheridan, "Denture sore mouth", DermatolClin, 21(1), 2003, pp.115–22, https://doi.org/10.1016/S0733-8635(02)00099-2

[10] M. Fay and M. Proschan, "Wilcoxon-Mann-Whitney or t-test? On assumptions for hypothesis tests and multiple interpretations of decision rules.", Statist. Surv. 4, 2010, pp.1 - 39, https://doi.org/10.1214/09-SS051

[11] K. Kishore and V. Jaswal, "Statistics Corner: Wilcoxon–Mann–Whitney Test", Journal of Postgraduate Medicine, Education and Research, 56(4), 2022, https://doi.org/10.5005/jp-journals-10028-1613

[12] H. Guerrero, "Analysis of Quantitative Data. In: Excel Data Analysis". Springer, Cham., 2019, https://doi.org/10.1007/978-3-030-01279-3_3

[13] A. King and R. Eckersley, "Statistics for Biomedical Engineers and Scientists: How to Visualize and Analize Data", Elseiver Ltd., 2019, pp. 1– 52, pp. 77–113, 132-167, https://doi.org/10.1016/C2018-0-02241-0

[14] M. Şahin and E. Aybek, "Jamovi: An Easy to Use Statistical Software for the Social Scientists", International Journal of Assessment Tools in Education, 6(4), 2020, pp. 670-692, https://doi.org/10.21449/ijate.661803

EFFECT OF 0.20% CHLORHEXIDINE GEL ON THE HEALING PROCESS OF TRAUMATIC LESIONS IN THE ORAL CAVITY, THAT HAVE OCCURRED AFTER REMOVABLE PROSTHETIC TREATMENT

Desislava Konstantinova

Department of Dental Materials Science and Prosthetic Dentistry
Faculty of Dental Medicine, Medical University – Varna, Bulgaria
Varna 9002, 55 Marin Drinov str.
E-mail: dr.konstantinova@gmail.com

Emiliya Koleva

Department of Electronics, Faculty of Engineering
Nikola Vaptsarov Naval Academy, Bulgaria
Varna 9026, 73 V. Drumev str.
E-mail: e.koleva@nvna.eu

Mariya Nikolova

Department of Information Technologies, Faculty of Engineering
Nikola Vaptsarov Naval Academy, Bulgaria
Varna 9026, 73 V. Drumev str.
E-mail: mpn@abv.bg

Anna Nenova-Nogalcheva

Department of Oral Surgery, Faculty of Dental Medicine
Medical University - Varna, Bulgaria
Varna 9002, 55 Marin Drinov str.
E-mail: anenova@yahoo.com.bg

Abstract

The paper presents a study on the influence of 0.20 % chlorhexidine gel on the healing process of lesions in the oral cavity, that have occurred after the placement of removable acrylic prostheses. A statistical analysis of the data for prosthetic patients has been carried out. The results of the study show that the use of 0.20% chlorhexidine gel has a beneficial effect on the healing process in patients with a lesion size of less than 5mm. The relation between the sex of the patients and the size of the ulcers was investigated. The influence of gender was confirmed in patients applying the gel, 96 hours after the prosthetic placement. The findings are that the healing of lesions in women was faster than in men.

1. INTRODUCTION

The most common soft tissue injuries resulting from treatment with removable full plate prostheses are ulcus traumaticus and ulcus decubitale [1, 2]. Pressure ulcers on the oral mucosa are commonly observed during the adaptation period, after the placement of removable dental prosthetics [2, 3]. The subjective symptoms vary depending on the localization of the lesions in the oral cavity [4, 5]. The most common ones are pain when consuming food and drinks, pain when speaking due to the movement of the masticatory and mimic facial muscles, pain during palpation and inability to use the prosthesis [6].

Purpose: To study the effects of 0.20% chlorhexidine gel on the healing process of traumatic lesions in the oral cavity, that occurred after removable prosthetic treatment, as well as the influence of gender on the speed of the healing process.

2. MATERIAL AND METHODS

The study was conducted in two dental practices, specializing in prosthetic and surgical dentistry located in the city of Varna, Bulgaria, for the period

from November 2021 to April 2022. 52 patients who have undergone a prosthetic treatment with removable acrylic prostheses were selected and they participated after signing an informed consent in accordance with the requirements of the Declaration of Helsinki for human and animal research.

2.1. Sample size

52 patients of both sexes with removable prosthetic structures took part in the study. Inclusion criteria were expression of written informed consent to participate in the study and indications for fabrication of a removable plaque prosthesis. The mean age of the patients is 69 years, with there being an equal number of men and women.

The participants of the study were separated into two groups – Study and Control groups for the goals of this research. The general characteristics of the patients are described in table 1.

Table 1. Baseline characteristics of patients

Characteristics	Control group (n=25)	Study group (n=27)
Age (years)	69.88 ± 0.89	68.89±0.95
Sexes:		
Male	14	12
Female	11	15
Prostheses:		
UJ	9	9
LJ	7	9
LJ&UJ	9	9

UJ: Upper jaw; LJ: Lower jaw;

Each participant in the first group - Control group (CG), received written instructions, how to conduct the adaptation period after the prosthetic treatment. The participants in the second group - Study group (SG) received the same instructions, with the addition of 0.20% chlorhexidine gel to apply to the traumatic lesion after each main meal. The patients were monitored 24, 48 and 96 hours after the placing of the prosthetic structures.

2.2. Statistical analysis

The methods of descriptive statistics, hypothesis testing and correlation analysis were used. Different statistical tests are made depending on the distribution of the data [7]. The results of the tests are used in the research to decide whether the data at hand sufficiently support a particular hypothesis. The significance level of the tests is 5%. Jamovi [8] and Matlab [9] were used for data processing and statistical analysis. The variables included in the analysis are the size of lesion, measured in mm at 24 h, 48 h and 96 h after placement of the prosthetic structures and the sex of the patients.

3. RESULTS

Different types of data analyses were performed to investigate the influence of 0.20% chlorhexidine gel during the healing process, depending on the gender of the participants and the size of the lesion after the placement of the removable prosthetic structures (partial or total plaque prosthesis). Tables 2 and 3 present descriptive statistics for the study data for the size of the lesion, measured 24, 48 and 96 hours after the prosthesis placement for both patient groups.

Table 2. Descriptive statistics for Study group

	Wound size at 24h [mm]	*Wound size at 48h [mm]*	*Wound size at 96h [mm]*
Mean	4,30	1,93	0,96
Median	4	2	0
Mode	5	0	0
Std Deviation	2,15	1,92	1,45
Minimum	1	0	0
Maximum	8	5	5

Table 3. Descriptive statistics for Control group

	Wound size at 24h [mm]	*Wound size at 48h [mm]*	*Wound size at 96h [mm]*
Mean	4,40	2,32	0,68
Median	4	2	1
Mode	3	1	1
Std Deviation	2,08	1,60	0,69
Minimum	1	0	0
Maximum	8	6	3

3.1. Examination of the influence of the gel on the size of the lesion during the healing period for the Study and Control groups

A Spearman correlation coefficient is used to assess the strength of the relation between the wound size 24 h, 48 h and 96 h after the placement of the prosthetic construction for the Study and Control groups. The Spearman's correlation coefficient for SG *(rho = .75, n = 27, p <0.001)* said to be a mod-

erate correlation between the size of the gel treated wound at the beginning of the healing process and at the 96th hour. It can be established that the application of 0.20% chlorhexidine gel is beneficial to the healing process of the oral mucosal injuries, that are often observed during the adaptation period after the placement of the removable prosthetics.

It was found that in cases in which the gel was used, there was a statistical relationship between the size of the primary lesion and its size after 96 hours i.e. the gel has a beneficial effect on the healing process.

The results *(rho = .33, n = 25, p =0.107>0.05)* for the CG show that there is no statistically significant correlation in the size of wounds at 24 hours and 96 hours. There isn't sufficient evidence to suggest that there is a correlation. This proves that the healing process of the lesion among patients from the control group proceeds individually and with a different speed during the adaptation period. According to the results we have obtained 48h after the placement of the prosthetics, in 40.7% of patients, the lesion, which was treated with the gel has healed and in the Control group, where there was no gel applied – only 8%.

The data shows that after 96 hours the healing process is complete in 55.6% of patients who have applied the gel and 40% of patients who have not applied it.

After a detailed analysis of the data, it was observed that in patients with a lesion size under 5 mm, the healing of the wound was faster when it is treated with 0.20% chlorhexidine gel. To prove this hypothesis, the Mann-Whitney U test was applied for all three measurements of the wound, since the statistical assumption of normality was not met. The results of the application of the test are presented in table 4.

Table 4. Mann-Whitney U test for patients with a wound of under 5 мм

		U	p
24 hours	Mann-Whitney U	84.0	0.520
48 hours	Mann-Whitney U	38.5	0.004
96 hours	Mann-Whitney U	56.0	0.015

The p-value shows that the gel has an impact on the healing process 48 and 96 hours after the placement of the partial and full dentures ($p<0.05$).

3.2. Research of the influence of the gel on the healing process of the lesions depending on the gender of the patients

The aim is to examine the size of the wound 24, 48 and 96 hours after the placement of the prosthetic structures, depending on the sex for all patients. Descriptive statistics of the data is presented in table 5.

Table 5. Descriptive statistics, made by gender

Group Descriptives

	Group	N	Mean	Median	SD	SE
24 hours	male	26	4.96	5.00	0.424	0.424
	female	26	3.731	3.5	1.867	0.366
48 hours	male	26	2.81	3.00	1.86	0.364
	female	26	1.423	1.5	1.391	0.273
96 hours	male	26	1.19	1.00	1.39	0.272
	female	26	0.462	0.00	0.706	0.138

The table shows differences in the average sizes of the traumatic lesions in men and women. In order to determine the choice of a test, which will confirm or reject the statistical significance of these differences, a Normality test (Shapiro-Wilk) and Homogeneity of Variances Test (Levene's) are made for the dependent variables (the wound size for the 3 periods). The data for 24 hours is normally distributed, but for 48 and 96 hours one of the assumptions is not met. The Levene's test is not met for 96 hours. For this reason, the 3 different tests are made for the three dependent variables. The Student's t test is made for 24 hours, the Mann-Whitney U test for 48 hours and Welch's t test for 96 hours. The results are shown on table 6.

Table 6. Test report, about the difference of the wound size in dependance of the sex

		Statistic	df	p
24 hours	Student's t	2.20	50.0	0.033
48 hours	Mann-Whitney U	191		0.006
96 hours	Welch's t	2.40	37.2	0.022

No statistically significant differences were observed between both groups (male and female). Because the p-value is less than 0.05, it is assumed that the difference in the average sizes of the le-

sions is not significant, taking into account the influence of sex.

Table 7 presents the mean values for the size of the lesions after 24, 48 and 96 hours in the Study (SG) and Control (CG) groups, depending on the sex of the patients.

Table 7. Mean wound size for Men and Women for Study and Control groups

Sex	Wound size at 24h [mm]	Wound size at 48h [mm]	Wound size at 96h [mm]
Men	4,92(SG) 5(CG)	2,67(SG) 2,93 (CG)	1,67(SG) 0,79(CG)
Women	3,8(SG) 3,64(CG)	1,33(SG) 1,55(CG)	0,4(SG) 0,55(CG)

The effect of the gel on the size of the lesion after 24, 48 and 96 hours has been studied separately for men and women. Table 7 shows that the mean values of the size of the wound when the gel was applied and when it was not applied during the healing process do not differ significantly. Only in men the average size of the wound after 96 hours is twice as large in the SG. The Mann-Whitney U was applied to all three measurements of the size of the lesion separately for both sexes. In both males and females, the results of the test proved that the differences in the sizes of the lesions were not statistically significant.

The difference of the size of the lesion between the two sexes and whether the gel has an effect on it was statistically investigated. The results of the Mann-Whitney U test ($p=0.0234<0.05$, $U= 210.5$) for the patients in the Study group after 96 hours, taking into account the gender, show with a prolongated gel treatment, the healing process of the lesions in females is faster than in males.

4. CONCLUSION

The study establishes that 93% of patients applying 0.20% chlorhexidine gel, with traumatic lesion with a size less than 5mm, have recovered completely after 96 hours. From them 84.6% have already recovered fully on the second day.

The number of recovered patients in the Control group after 96 hours is 50%. An improvement in both groups has been reported after 48 hours at the earlies.

From the obtained results it can be concluded that oral mucosal lesions with a size of less than 5mm are positively affected by the application of 0.20% chlorhexidine gel.

Lesions in women that have used the gel, 96 hours after the placement of the prostheses heal faster than in men, which proves the influence of gender on the healing process.

References

[1] S. Saraswati, P. Razdan, M. Aggarwal, D. Bhowmick and P. Priyadarshni, "Traumatic ulcerations frequencies and postinsertion adjustment appointments in complete denture patients", Journal of Pharmacy and Bioallied Sciences, 13 (Suppl 2), 2021, pp. 1375-1380.

[2] B. Khanal, S. M. Sapkota, S. N Thakur, and R. Chaulagain, "Evaluation of traumatic ulcerations frequency and site in post-insertion adjustment recall visits in complete denture patients visiting a dental college in Chitwan", Journal of Chitwan Medical College, 13(3), 2023, pp. 18-20.

[3] D. L. Brunello and MN. Mandikos, Construction faults, age, gender, and relative medical health: Factors associated with complaints in complete denture patients. J Prosthet Dent, 79(5):545-54. 1998, doi: 10.1016/s0022-3913(98)70176-3. PMID: 9597608

[4] P. Kivovics, M. Jáhn, J. Borbély and K. Márton, Frequency and location of traumatic ulcerations following placement of complete dentures. Int J Prosthodont 2007;20:397-401

[5] S. Jain, N. Oberoi, A. Kumar, A. Aggarwal and K. Kaur, "A study to evaluate the location and frequency of denture-related ulcerations and postinsertion adjustments in complete denture patients", Indian Journal of Dental Sciences, 9(1), 2017, pp. 16-21.

[6] G. Özkan, K. Y. Yasin and P. Okyay, "The relationship of oral mucosal lesions and removable prostheses: quantitative and qualitative study", Balkan Journal of Dental Medicine, 24(3), 2020. pp. 161-169.

[7] M. Fay and M. Proschan, "Wilcoxon-Mann-Whitney or t-test? On assumptions for hypothesis tests and multiple interpretations of decision rules." Statist. Surv. 4 1 - 39, 2010. https://doi.org/10.1214/09-SS051

[8] M. Şahin and E. Aybek, "Jamovi: An Easy to Use Statistical Software for the Social Scientists", International Journal of Assessment Tools in Education, 6(4), 2020, pp. 670-692, https://doi.org/10.21449/ijate.661803

[9] King and R. Eckersley, "Statistics for Biomedical Engineers and Scientists: How to Visualize and Analize Data", ISBN 978-0-08-102939-8, Elseiver Ltd., 2019, pp. 1– 52, pp. 77–113, pp. 132-167, https://doi.org/10.1016/C2018-0-02241-0

ESTIMATION OF FOREST FIRE PARAMETERS BY JOINT USE OF GEOSPATIAL DATA AND GEODETIC METHODS

Svetlin I. Antonov[1], Hrisimir Dochev[2], Ivan S. Antonov[3]

Technical University of Sofia,
8 St. Kliment Ohridski blvd, 1000 Sofia, Bulgaria

[1] https://orcid.org/0000-0002-1698-8506; E. svantonov@yahoo.com;

[2] hdochev@mail.bg

[3] https://orcid.org/0000-0002-4636-2168; E. mfantonov@abv.bg;

Abstract

The article presents the results of the research carried out for the analysis and assessment of the main parameters of a forest fire, by applying a computer method for rapid remote coordination of a forest fire contour, by joint use of an existing 3D digital model of the terrain, GPS and a total station. Applications of the forest fire hazard assessment method are indicated.

1. INTRODUCTION

Forecasting of the basic parameters of the forest fire at any point in time during its development is a practical and an actual task, the correct solution of which allows the successful fight against it.

The availability of reliable information about the shape, area, contour, front, speed and intensity of development of a forest fire, as well as the direction of its most dangerous spread, is essential for making correct management decisions by the manager of firefighting, both for the correct organization of firefighting actions and for the successful evacuation of the endangered people.

In practice, many theoretical models describing the forest fire phenomenon have found application. The practical use of the latter to assess the development of forest fires is possible, but a rather complex mathematical apparatus is available. This determines the requirement that the work with the theoretical models describing the forest fires should be carried out mainly by highly qualified specialists [1], [2].

In parallel with the purely theoretical models, other methods have also found application in the practice for monitoring, evaluating and forecasting the development of forests fires, such as:

- space monitoring - when large forest fires are detected and their development is monitored by studying satellite images;
- aviation monitoring - in this case, the detection of forest fires and the subsequent monitoring is carried out with the help of aviation means; [3]
- ground monitoring - the detection of forest fires and the obtaining of information about their development is carried out with the help of ground means.

The problem of predicting the parameters of large forest fires and assessing their consequences, based on the information obtained from the photographs by means of satellite monitoring, at the moment has not yet found its satisfactory solution. The difficulty of solving it is determined by various factors, the most important of which are: [3], [4].

- low resolution of satellite images;
- insufficient efficiency of the process of monitoring and transmission of data (up to 4 times a day) and the need for additional time, in some cases over the course of hours, for processing and providing the information;
- the need of a significant number of fire points in the area of the forest fire, necessary for its detection (up to 1 ha);
- impossibility of providing information in conditions of cloudiness and heavy smog;
- the satellite monitoring system is an effective tool for monitoring the growth of forest fires in flat outdoor terrain (grain fields, non-forested areas / dry grasses, bushes), as there are difficulties in the detection of the

development of a low-level fire under a forest hillside;

- a balance has not yet been found between the high sensitivity for detecting thermal anomalies and excluding to the greatest extent the possibility of false alarms for forest fires.

Despite the long-standing practice, through the use of both manned and unmanned aircraft, aerial monitoring of forest fires is also accompanied by a number of problems, such as: [3]

- significant financial costs necessary for the irrigation of a certain forest area;
- low efficiency of the unmanned aircraft used, resulting from the extremely high price and their limited applicability for patrolling over the area of a developed forest fire;
- limited patrolling time of the aircraft, resulting from the limited amount of fuel;
- insufficient sensitivity of the used scanning devices, which is inversely dependent on their field of vision;
- aviation monitoring of forest fires is strongly influenced by meteorological conditions.

Modern ground monitoring of forest fires, despite its varieties, can be conditionally divided into visual monitoring with the help of fire watchers, apparatus-instrumental sounding of a given forest territory, through various technical means, as well as a combination of them. The main problems in their application are related to: [3]

- influence of the human factor, related to a decrease in the attention of the fire watchers, unregulated dismissal from the posts, submission of inaccurate data;
- submitting false alarms.

The new challenges in preventing and fighting forest fires in Bulgaria require, in parallel with the improvement of traditional methods, the search and application of flexible approaches and new models combining scientific innovations and information efficiency. Based on these circumstances, a "Methodology for remote 3D coordination of fire control" was developed.

2. METHODOLOGY FOR REMOTE 3D COORDINATION OF FIRE CONTROL

The application of this methodology provides fast (5÷15min) and at the same time remote (from 100 to 5000m) 3D coordination of the contour of a fire, through the joint use of:

- existing 3D digital model of the terrain; [5]
- total station;
- Global Navigation Satellite System - GNSS (a GPS antenna, receiver and controller are used, operating in RTK mode with a subscription to the permanent GPS networks existing in the Republic of Bulgaria);
- laptop or tablet.

An example scheme of the proposal is given in Fig. 1.

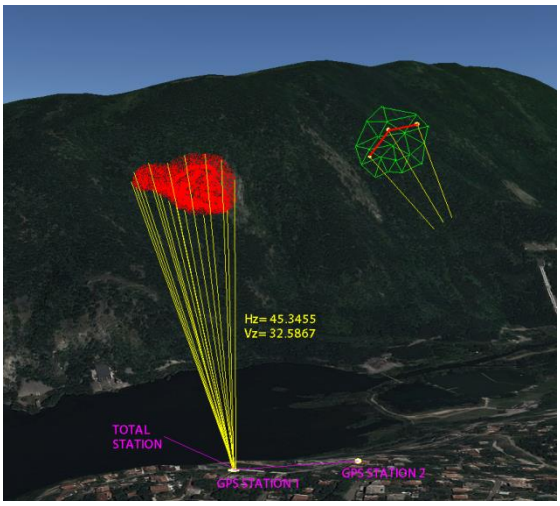

Figure 1. Practical demonstration of the applicability of the Methodology for remote 3D coordination of a fire contour for a forest fire that occurred in a terrain located above Lake "Pancharevo" [5].

During the research, the following practical tasks were set for solution:

- predicting the shape of the contour of the forest fire;
- prediction of the characteristic components of the contour of the forest fire
- area and perimeter;
- predicting the direction of the most dangerous spread of the forest fire at any point in time after its discovery.

Solving these tasks will contribute to the provision of up-to-date, objective and complete data necessary for the proper organization of forest fire fighting.

3. METHODOLOGY FOR REMOTE 3D CONTOUR COORDINATION OF FIRES

Classical geodetic methods for coordinating contours with GPS or total stations require the immediate presence of a person with a GPS antenna or reflector prism at contour points. The use of non-reflector total stations is applicable at distances (50÷200) m and with certain requirements for the reflective surface and low smoke.

In the conditions of a fire, this is practically impossible, which is why a new methodology for remote coordination has been developed, in which the 3D coordinates of the contour are obtained as an intersection point of a 3D sighting beam from the total station (defined with a starting point Xo, Yo, Zo , vertical angle Vz, horizontal angle Hz) and a corresponding 3D triangle (defined by three points X1,Y1,Z1, X2,Y2,Z2, X3,Y3,Z3) from the digital terrain model available to the team.

To implement the technology, one operator with working level total station and GPS skills is required

For the practical application of the method, preliminary preparation of the following technical and software tools is necessary:

- a 3D (XYZ) Digital Terrain Model (DTM) in WGS84 - GRS80 ellipsoid system is required;
- In the presence of digital models in other coordinate systems (UTM, BG1970) [6], their preliminary transformation to the accepted world rectangular geocentric system WSG84 is necessary. For the exact transformation of the elevations from the Baltic Height System in EVRS, it is also necessary to acquire a grid digital model of the quasi-geoid adopted for the measurement area;
- development of specialized software for the operating system of the adopted computer configuration - (for notebook computers - "Windows 10,11" or MAC OS) (Apple tablets and smartphones - iOS 5,6,7; for the rest Android").

The software is required to perform the following functions:

- storage in a binary file of a previously compiled 3D digital model of the terrain in an area around the location of the fire;
- selection of a sub-area of 3D DTM around the contour of the fire, in order to quickly find the intersection of the viewing beam with the plane of the corresponding triangle;
- successively searching for the intersections of the 3D ray from the total station with the plane of each of the triangles and finding that triangle for which its intersection with the 3D ray lies inside it.

In principle, we are looking for a point Xp,Yp,Zp which simultaneously satisfies:

- the equation of the 3D line (the line of sight from the total station);
- the equation of the plane of a triangle from a 3D DTM;
- lies within the contour of the triangle from the 3D DTM – determined depending on the sign (+,-) of the determinant of the coordinates of each line and the coordinates of the intersection point.

Finding the intersections with the planes of the triangles from the 3D DTM is done according to the methodology and by applying the formulas specified in [5].

The practical work for carrying out the necessary measurements on the terrain in the event of a forest fire is carried out in the following sequence:

- point Station_1 is selected from the locality, from which it will be possible to effectively observe the fire with the total station for an extended period of time;
- the point is coordinated in the WGS84 system by GPS operating in RTK mode (the duration of the measurement is about 1 min., and the accuracy is about 5 mm);
- a second point is selected - Station_2 at a distance (100÷300) m from Station_1, which is coordinated in the WGS84 system, via GPS;
- the Total Station is positioned at the Station_1 point and oriented to the already known coordinates of the Station_2 point;
- a visual polygonal "walk" of the contour of the fire is started with the visual beam of the total station through distances (approximately (20÷100) m) consistent with the de-

sired accuracy of contour determination - for each point of the contour, the coordinates are recorded in a file - vertical angle - Vz and horizontal angle - Hz (the required time for the walk depends on the area of the fire and on the operator and is approximately (5÷20) min);

- after completing the "tour", the file with the set of 3D rays is overwritten in a laptop or tablet, where the corresponding intersections lying in the triangles of the 3D DTM are determined - the contour of the fire is drawn;
- as an option, it is possible to transform the points - intersections of the rays from geocentric coordinates XYZ system WGS84 into geographic coordinates Latitude, Longitude, H and a file is generated in KML format for visualization in Google Earth; [5].
- after an expertly determined time, the contour is photographed and drawn again, which makes it possible to determine the geometric and temporal gradients and parameters of the fire;
- since the method works in the world coordinate system WGS84, the 3D results are also compatible with other satellite or aviation observations in the same coordinate system. For this purpose, an analysis was made of the existing geodetic and cartographic materials and data and ways of converting them into the currently operating "Bulgarian Geodetic System 2005" (BGS 2005) [6].

4. CONCLUSION

The presented results of the research are based on the analysis and assessment of the main parameters of a forest fire. Some applications of the forest fire hazard assessment method are shown. A computer method for rapid remote coordination of a forest fire contour is applied including 3D digital model of the terrain, GPS and a total station.

Several tasks are resolved, as: prediction the shape of the contour of the forest fire; prediction of the characteristic components of the contour; the area and the perimeter of the fire; predicting the direction the spread of the fire at any point after its detection.

Solving the tasks listed above contributes to the provision of up-to-date, objective and complete data necessary for the proper organization of forest fire fighting. The application of the methods provides fast and remote 3D coordination of the fire contour. The proposed methods are applicable to fighting fires in open space and protecting the power transmission and cable telecommunication network.

5. ACKNOWLEDGMENTS

The authors would like to thank the Research and Development Sector at the Technical University of Sofia for the financial support.

References

[1] Antonov, S. I, Mathematical modeling of the dynamics and radiant energy transfer in fire, 2023, Bulgaria, Sofia, Alexandra-Bakiev, ISBN: 978-954-92423-7-9, 2023.

[2] Antonov S., Impact of the wildfires on the power supply networks, HiTech 2021 - Proceedings, IEEE, ISBN: 978-166544873-4,
DOI: 10.1109/HiTech53072.2021.9614216, 2021.

[3] Rafael Bailon-Ruiz, Arthur Bit-Monnot, Simon Lacroix, Real-time wildfire monitoring with a fleet of UAVs, Robotics and Autonomous Systems, Vol. 152, ISSN 0921-8890, DOI: 10.1016/j.robot.2022.104071, 2022.

[4] G. Zagalikis, Remote sensing and GIS applications in wildfires, geographic information systems - data science approach, IntechOpen,
DOI: 10.5772/intechopen.111616, 2023.

[5] www.google.com/earth/

[6] Instruction No. RD-02-20-25/ 20.09.2011 for determining geodetic points using global navigation satellite systems, Ministry of Regional Development and Public Works, D.V. no. 79, 2011.

FRAMEWORK FOR A GAMIFIED PUBLIC TRANSPORTATION APPLICATION TO PROMOTE SUSTAINABLE TRAVEL IN SMART CITIES

Milen Sotirov

Nikola Vaptsarov Naval Academy
Varna, Bulgaria
m.sotirov@naval-acad.bg

Valentina Petrova, Assoc. Prof. PhD

Nikola Vaptsarov Naval Academy
Varna, Bulgaria
v.petrova@naval-acad.bg

Donika Nikolova-Sotirova

Technical University – Varna
Varna, Bulgaria
donika.sotirova@tu-varna.bg

Abstract

This paper explores the integration of gamification into public transportation systems to promote sustainable travel behaviors within smart cities. By incorporating game elements such as points, badges, and leaderboards, public transportation applications can motivate users to choose eco-friendly options. The study examines the potential of gamification to enhance user engagement, analyzing key findings from recent research and real-world examples. A proposed framework for a gamified public transportation application is presented, along with the essential specifications and methodologies required for development. The application also includes features to support national security, disaster management, and emergencies, highlighting the multifaceted benefits of gamification in urban mobility.

1. INTRODUCTION

The rising demand for sustainable urban mobility solutions has led to the exploration of innovative approaches to enhance public transportation systems. Gamification, the use of game design elements in non-game contexts, has emerged as a promising strategy to increase user engagement and promote sustainable behaviours. This paper aims to investigate the application of gamification in public transportation, focusing on its potential to encourage eco-friendly travel habits within smart cities. By reviewing recent literature and analysing successful real-world implementations, this study provides insights into the effective integration of gamification elements and proposes a comprehensive framework for developing a gamified public transportation application.

2. LITERATURE REVIEW

Gamification has emerged as an effective tool for boosting user engagement and promoting sustainable behaviors. This literature review examines gamification in public transportation to support eco-friendly travel in smart cities. By using points, badges, and leaderboards, transportation apps can encourage users to choose sustainable options. Key findings, successful strategies, and challenges in implementing gamification for sustainable transportation are highlighted.

Bitrián, Buil, and Catalán [1] Their study examines gamification's impact on mobile application engagement, focusing on points, badges, and leaderboards. They found ease of use, usefulness, and enjoyment key for engagement, while convenience was not. A well-designed gamified application can enhance user retention and satisfaction.

Wang et al. [2] This study identifies key gamification elements, benefits, and challenges in transportation. Goals, challenges, points, rewards, and social engagement effectively promote sustainable behaviour. The study highlights the need for tailored gamification strategies for specific issues.

Dias Daniel, Junqueira, and Coelho Rodrigues [3] They examined a gamified application promoting walking and cycling. Using quantitative research, they found that perceived usefulness positively influenced attitudes towards soft mobility. Instrumental attitudes, subjective norms, and perceived behavioural control significantly impacted the intention to use soft mobility.

Kazhamiakin et al. [4] study introduces a gamification platform to influence daily transportation choices and promote sustainable behaviours. Integrating Geo localized and temporal data, the platform balances mobility demand and supply. Personalized strategies can achieve long-term engagement and behaviour change.

Henrik Olofsson [5] His thesis explores gamification in public transportation to enhance engagement, conducted with Kalmar Länstrafik. Evaluating game elements in the GoOn application, he found positive impacts of points, levels, and achievements. He concludes that gamification can increase engagement and appeal, stressing careful design and user-centric approaches.

The literature shows that gamification can influence transportation behaviors. Effective gamified apps boost engagement, promote sustainable habits, and improve user experience. Success relies on careful design and user-focused approaches.

3. REVIEW OF REAL-WORLD GAMIFICATION IN PUBLIC TRANSPORTATION

Numerous real-world initiatives have effectively integrated gamification into public transportation systems to promote sustainable travel behaviours:

Transport for London (TfL) "Oyster Pay-As-You-Go": In London, the Oyster card system lets riders load credit for buses, trains, and the Underground. Riders earn points per trip, redeemable for ride discounts, event access, or merchandise. [6]

Metropolitan Transportation Authority (MTA) in New York: The MetroCard Bonus program offers savings, including unlimited ride and pay-per-ride options, plus discounts for students, seniors, and the disabled. The eTix application allows trip history viewing [7].

These programs succeed by aligning incentives with objectives like increasing ridership, reducing car usage, and promoting sustainable behaviour. They also simplify tracking progress and collecting rewards, enhancing rider motivation and engagement.

4. METHODOLOGY

The study will be conducted as a case study in Varna, Bulgaria, focusing on proposing a gamified concept and framework for a public transportation application. This application will aim to promote sustainable transportation behaviour by incorporating loyalty programs, rewards, badges, and leaderboards.

Figure 1 illustrates the proposed mobile app interface, displaying key gamification features designed to enhance user engagement and promote sustainable travel behaviours.

Figure 1. Gamified public transportation mobile application user interface

4.1. Conceptual framework

The conceptual framework for gamifying a public transportation application will involve a combination of research and design, as well as the implementation of gamification elements that are tailored to the needs of the target audience. The goal of the gamification is to encourage sustainable transportation behavior and to provide a fun and engaging user experience for users of the application showcased in Fig. 2.

The diagram illustrates the gamification framework proposed for enhancing public transportation engagement and promoting sustainable travel behaviours. The framework is divided into two primary sections: the current non-gamified system and the proposed gamified system.

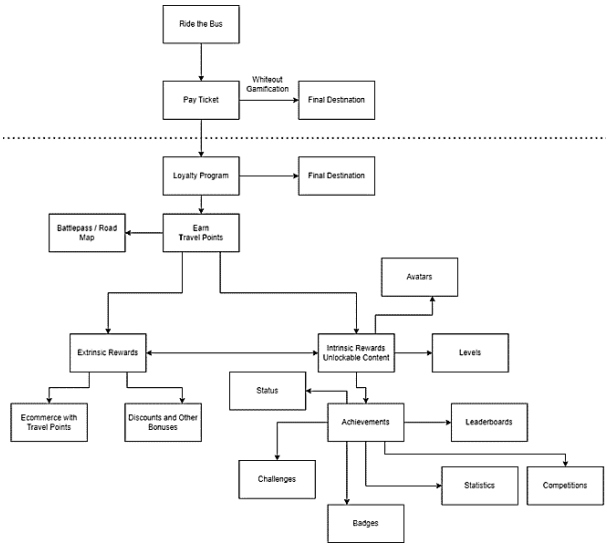

Figure 2. Gamification Framework for Public Transportation

CURRENT SYSTEM (WITHOUT GAMIFICATION)

Ride the Bus: This represents the initial action where a user decides to take the bus.

Pay Ticket: The user pays for their ticket.

Final Destination: The user reaches their destination without any additional engagement or rewards.

PROPOSED GAMIFIED SYSTEM

The proposed system introduces various gamification elements to enhance user engagement and promote sustainable behavior.

Loyalty Program: A 5-day program to reward regular bus riders. Users earn points or badges for consecutive bus rides, redeemable for discounts, exclusive offers, or other incentives, encouraging sustainable transportation and providing data on ridership patterns.

Battle Pass/Road Map: Users complete challenges and milestones to earn rewards, progressing through tiers (Bronze, Silver, Gold, Platinum) based on their bus ride frequency. This system provides a sense of achievement and motivates users through exclusive rewards and competitions.

Earning Traveling Points (TP): Users earn points for actions like ticket purchases, referrals, reviews, and spending time in the application. Points can be redeemed for discounts, privileges, or merchandise, promoting long-term public transportation use, and reducing carbon footprints.

Intrinsic Rewards/Unlockable Content: Rewards that provide personal achievement, social recognition, and meaningful impact. Examples include levels, customizable avatars, achievements, and educational rewards.

Levels: Users progress through levels (e.g., Commuter, Pro, Eco-Warrior) by using public transportation. Each level offers new rewards and challenges, encouraging continuous application engagement.

Avatars: Personalized avatars reflecting user interests, adding a fun and engaging element to the application and fostering a sense of community.

Achievements: Milestones or specific tasks that users complete, displayed on their profiles, and shared with friends, adding social competition.

Status: Reflects user engagement and commitment, displayed on profiles, motivating continued use.

Challenges/Quests or Missions: Tasks encouraging creative use of public transportation, enhancing user engagement.

Competition: Leaderboards and challenges create friendly competition, motivating users to increase their public transportation usage.

Leaderboards: Users compare their public transportation usage with others, aiming to climb ranks, enhancing engagement.

Badges: Earned for milestones or specific tasks, displayed on profiles as sources of pride and accomplishment.

Educational Rewards: Access to resources or information about public transportation.

Extrinsic Rewards: Tangible incentives like discounts, free rides, priority seating, and merchandise. Users earn Traveling Points (TP) for activities and redeem them for these rewards.

Referral Program: Incentivizes users to refer friends with reward points, leaderboards, and sharing tools, promoting application engagement and sustainable transportation.

Mini Games: Adds entertainment and educational value, with games related to sustainable transportation, enhancing user engagement.

Incorporating Local Facts: Challenges involving Varna's landmarks, cultural heritage, transportation network, and local events make the application more engaging and relevant for users.

This gamification framework aims to enhance user engagement, promote sustainable transportation, and support smart city initiatives by making public transportation more appealing and rewarding.

By integrating these gamification elements, the proposed system aims to make public transportation more engaging and rewarding, thereby encouraging users to adopt sustainable travel habits. A gamified public transportation application can effectively influence sustainable transportation behavior. The application will include the following key features:

- ***User-Friendly Interface***: The design will focus on ease of use, with intuitive navigation and streamlined ticket purchases.
- ***Social Interaction***: Features like a news feed, direct messaging, and the ability to follow other users.
- ***Feedback Mechanism***: Users can provide feedback and suggest improvements through a rating system.

5. APPLICATION SPECIFICATION FOR GAMIFIED PUBLIC TRANSPORTATION

This section outlines the essential specifications for developing a gamified public transportation application aimed at promoting sustainable travel behaviors. The application will incorporate various gamification elements such as loyalty programs, rewards, badges, and leaderboards. Below is a detailed table specifying the key features, development requirements, and OS availability for the application displayed in Table 1.

Table 1. Application Specification

Feature	Development Requirements
User-Friendly Interface	UI/UX design, front-end development
Loyalty Program	Backend database, points tracking system
Battle Pass/Road Map	Gamification engine, progression tracking
Travel Points	Points management system, backend integration
Unlockable Content	Content management system, gamification elements
Rewards	Reward management system, e-commerce integration
Achievements	Achievement tracking system
Challenges/ Quests	Task management system, user engagement tracking
Competitions	Leaderboard system, competition management
Leaderboards	Ranking algorithm, data analytics
Badges	Badge management system
Referral Program	Referral tracking system, reward allocation
Social Interaction	Social media integration, messaging service
Feedback Mechanism	Feedback collection system, data analysis
Mini Games	Game development, educational content creation

The successful development of this gamified public transportation application requires careful planning and integration of various features [8] that promote user engagement and sustainable travel behaviors. By ensuring compatibility across iOS and Android platforms, the application will reach a broader audience, contributing to the goal of enhancing public transportation use and supporting smart city initiatives. Additionally, robust security features such as data encryption, secure user authentication [9], and privacy protection mechanisms will be crucial in maintaining user trust and safeguarding sensitive information.

6. GAMIFICATION FOR NATIONAL SECURITY, DISASTERS AND EMERGENCIES

Gamification can be leveraged by the administration for national security, disaster management, and emergencies. Conducted under the "Security and Defense" program, this research showcases tools for preventing incidents and accidents. The gamified public transportation application will notify users of potential natural disasters, accidents, and crises in Bulgaria, educating [10] them on modern information protection techniques, human factors in security, and societal support. It gathers public opinions on security and defense, aiding state and local authorities in monitoring and prevention. The focus includes assisting authorities during emergencies, alerting the public, and training them for self-protection. Users earn points, rewards, social statuses, etc. supporting national security.

7. CONCLUSION

The integration of gamification elements in public transportation applications offers a promising approach to promoting sustainable transportation behaviors within smart cities. By incorporating loyalty programs, rewards, badges, and leaderboards, these applications can significantly enhance user engagement and motivation. The proposed gamifi-

cation framework aims to make public transportation more appealing and rewarding, encouraging users to adopt eco-friendly travel habits. Additionally, the application can support national security, disaster management, and emergency preparedness by providing timely notifications and educational content. Future research and development should focus on refining these gamification strategies and exploring their long-term impacts to maximize their effectiveness in supporting sustainable urban mobility. The success of this initiative will depend on careful design, user-centric approaches, and robust security measures to protect user data and maintain trust.

The report is in implementation of the National Scientific Program "Security and Defense", adopted with RMS No. 731/21.10.2021, and financed by the Ministry of Education and Science of the Republic of Bulgaria according to Agreement No. D01-74/ 19.05.2022.

References

[1] P. Bitrián, I. Buil, and S. Catalán, "Enhancing user engagement: The role of gamification in mobile apps," J Bus Res, vol. 132, pp. 170–185, Aug. 2021, doi: 10.1016/J.JBUSRES.2021.04.028.

[2] W. Wang, H. Gan, X. Wang, H. Lu, and Y. Huang, "Initiatives and challenges in using gamification in transportation: a systematic mapping," European Transport Research Review, vol. 14, no. 1, pp. 1–19, Dec. 2022, doi: 10.1186/S12544-022-00567-W/TABLES/10.

[3] A. D. Daniel, M. Junqueira, and J. C. Rodrigues, "The influence of a gamified application on soft mobility promotion: An intention perspective," J Clean Prod, vol. 351, p. 131551, Jun. 2022, doi: 10.1016/J.JCLEPRO.2022.131551.

[4] R. Kazhamiakin, E. Loria, A. Marconi, and M. Scanagatta, "A Gamification Platform to Analyze and Influence Citizens' Daily Transportation Choices," IEEE Transactions on Intelligent Transportation Systems, vol. 22, no. 4, pp. 2153–2167, Apr. 2021, doi: 10.1109/TITS.2021.3049792.

[5] Olofsson Henrik, "Gamification for public transportation - Improving attractiveness with interactive game elements," Bachelor Thesis, Linnaeus University, Kalmar, 2021.

[6] "Oyster pay as you go - Transport for London." Accessed: Feb. 09, 2023. [Online]. Available: https://tfl.gov.uk/fares/how-to-pay-and-where-to-buy-tickets-and-oyster/pay-as-you-go/oyster-pay-as-you-go#on-this-page-1

[7] "More affordable. More flexible. More fair." Accessed: Feb. 09, 2023. [Online]. Available: https://new.mta.info/fares/how-to-save-money

[8] M. Sotirov and V. Petrova, "The Nine-Steps Gamification Process: Increasing Student Engagement in LMS," in 2023 International Conference Automatics and Informatics (ICAI), IEEE, Oct. 2023, pp. 496–501. doi: 10.1109/ICAI58806.2023.10339063.

[9] D. Dimitrova and I. Dimitrov, "Security analysis of lightweight cryptographic algorithms," 15th International Scientific and Practical Conference "Environment. Technology. Resources," 2024.

[10] M. Sotirov, V. Petrova, and D. Nikolova-Sotirova, "Implementing Gamified Learning in University Environment," in 2023 International Conference Automatics and Informatics (ICAI), IEEE, Oct. 2023, pp. 476–480. doi: 10.1109/ICAI58806.2023.10339098.

GAMIFICATION OF PUBLIC TRANSPORTATION: DEVELOPING A COMPREHENSIVE TAXONOMY FOR A MOBILE APPLICATION AND AN ECOMMERCE PLATFORM FOR REDEEMING TRAVEL POINTS

Milen Sotirov

Nikola Vaptsarov Naval Academy
Varna, Bulgaria
m.sotirov@naval-acad.bg

Valentina Petrova, Assoc. Prof. PhD

Nikola Vaptsarov Naval Academy
Varna, Bulgaria
v.petrova@naval-acad.bg

Donika Nikolova-Sotirova

Technical University – Varna
Varna, Bulgaria
donika.sotirova@tu-varna.bg

Abstract

This paper explores the integration of gamification into public transportation platforms to promote sustainable travel behaviors within smart cities. By incorporating game elements such as points, badges, and leaderboards, these platforms can motivate users to choose eco-friendly options. The study reviews key findings from recent literature, proposes a comprehensive taxonomy for organizing platform features, and details an ecommerce website for redeeming travel points. Additionally, it examines the role of gamification in enhancing national security, disaster management, and emergency response.

1. INTRODUCTION

The demand for sustainable urban mobility solutions has led to the exploration of innovative approaches to enhance public transportation systems. Gamification [1], which involves using game design elements in non-game contexts, has shown significant potential in increasing user engagement, and promoting eco-friendly behaviours. This paper investigates the application of gamification in public transportation, focusing on its ability to support sustainable travel habits within smart cities. It synthesizes recent research, proposes a detailed taxonomy for a public transportation platform, and discusses the development of an ecommerce website for redeeming travel points. The paper also explores how gamification can aid national security and disaster management efforts.

2. LITERATURE REVIEW

This literature review examines the impact of gamification on public transportation and its potential to support sustainable travel behaviors within smart cities. By integrating game elements such as points, badges, and leaderboards, transportation platforms can motivate users to adopt eco-friendly travel options. This review synthesizes key findings from recent studies, highlighting successful strategies and identifying challenges in implementing gamification for sustainable transportation.

Yen, Mulley, and Meza [2] This study examines attitudes and perceptions influencing participation in gamification schemes for travel demand management in Taipei City. Using structural equation modeling, they identify perceived enjoyment, ease of use, and social norms as critical for engagement, providing insights for designing effective strategies.

Yen, Mulley, and Burke [3] Their examination of gamification in transportation emphasizes its transformative potential. They propose a framework for gamified strategies to enhance travel behavior change, highlighting the importance of integrating psychological and design elements.

Bellotti et al. [4] They explore gamification to enhance user experience and efficiency of on-demand public transportation. Implementing a system with points, badges, and leaderboards, they show significant improvements in satisfaction and participation, demonstrating gamification's potential to transform services.

Caroux et al. [5] This overview identifies key gamification elements and their role in promoting sustainable behaviors. Reviewing case studies and research, they highlight gamification's potential to enhance engagement and satisfaction, while discussing challenges like technological barriers and user acceptance.

Wang et al. [6] This study investigates the positive spillover of sustainable behaviors, emphasizing self-determination theory. Data from an online survey shows that competence, relatedness, and autonomy need mediate the relationship between pro-environmental preferences and eco-friendly behavior intentions.

Clipper Card Program in San Francisco Bay Area: This reusable card offers discounts for combining multiple transportation modes like bus and train journeys. [7]

SmarTrip Program in Washington, DC: Rewards riders with off-peak hour discounts, future rides, or free rides. Cards can be reloaded for multiple journeys. [8]

The reviewed literature shows that gamification significantly influences transportation behaviors. Well-designed gamified applications boost user engagement, promote sustainable habits, and improve user experience. Despite technological barriers and user acceptance challenges, the positive impacts on retention and satisfaction are clear. Future research should optimize gamification strategies, address barriers, and explore long-term effects. Overall, gamification is a promising approach for achieving smart city goals by encouraging eco-friendly transportation and improving urban mobility.

3. TAXONOMY AND FEATURES FOR A PUBLIC TRANSPORTATION PLATFORM

The proposed public transportation platform is showcased in Fig. 1 aims to enhance user experience by incorporating a comprehensive taxonomy that organizes its various features and functionalities. This taxonomy ensures that all relevant aspects are covered, making the platform user-friendly and intuitive.

Fig. 1. Suggested user interface of the mobile application

User Information

- **Account Creation and Management**: Enables users to create and manage their accounts.
- **Personal Details**: Stores user information such as name, age, and location.
- **Payment Information**: Manages payment methods including credit/debit cards and PayPal.
- **Travel History**: Tracks the user's past trips and travel patterns.

Trip Planning

- **Route Planning**: Assists users in planning their travel routes.
- **Fare Calculation**: Calculates the fare for planned trips.
- **Real-Time Arrival Times**: Provides real-time information on bus/train/ferry arrivals.
- **Schedules and Maps**: Offers access to transportation schedules and maps.

Rewards and Incentives

- **Traveling Points (TPs)**: Users earn points for using the platform and completing certain actions.

- **Badges and Achievements**: Rewards users with badges and achievements for reaching milestones.
- **Leaderboards**: Displays user rankings based on their earned points.
- **Challenges and Missions**: Engages users through various challenges and missions.
- **Intrinsic and Extrinsic Rewards**: Provides both personal and tangible rewards to motivate users.

Social Engagement

- **Friend-Finding and Referral Program**: Encourages users to refer friends and connect with others.
- **Sharing Travel Stories and Photos**: Allows users to share their travel experiences.
- **Public/Private Leaderboards**: Offers leaderboards for competitive engagement.

Feedback and Support

- **Customer Support**: Provides help and support for users.
- **Feedback and Ratings**: Collects user feedback and ratings for continuous improvement.
- **Suggestions and Bug Reports**: Allows users to report issues and suggest enhancements.
- **FAQs and Help Center**: Offers a knowledge base for common questions and support.

User Management: The platform features a robust user management system that stores all user data, including the number of points each user has earned.

Point System: A point system rewards users for their sustainable transportation behavior. Points can be earned through platform usage, participating in challenges, and completing missions.

Ecommerce Integration: The platform includes an ecommerce section where users can redeem their points for discounts and bonuses on various products. This enhances user engagement and promotes eco-friendly practices.

Products: The ecommerce section offers a range of products, including eco-friendly and transportation-related items. The product catalogue is regularly updated to ensure the availability of the latest products.

Payment System: A secure payment system allows users to purchase products using their earned points or other payment methods like credit cards or PayPal.

Analytics: A comprehensive analytics system tracks user behavior, purchase history, and points earned. This data helps improve user experience and optimize the point system.

Personal Dashboard: A personal dashboard [9] provides users with easy access to their stats and progress in the loyalty program. It includes:

- Number of trips taken
- Points earned
- Rewards redeemed
- Progress towards rewards
- Leaderboard ranking
- Carbon offset
- Number of referrals
- Personalized recommendations

Feedback System: Incorporating a feedback and rating system gathers valuable information from users about their experiences with the loyalty program. This feedback helps improve the program's effectiveness and user satisfaction.

By integrating these features and functionalities, the public transportation platform aims to provide a comprehensive and engaging user experience. The taxonomy serves as a foundation for organizing the platform's elements, ensuring that all aspects are addressed to promote sustainable transportation behavior and enhance urban mobility.

4. ECOMMERCE WEBSITE FOR REDEEMING TRAVEL POINTS

To enhance the user experience and incentivize sustainable transportation behaviors, the public transportation platform includes an ecommerce website. This website allows users to redeem the travel points they have earned through various ac-

tions within the platform. By providing a diverse range of rewards, the ecommerce section not only encourages continued engagement but also supports eco-friendly practices. Figure 2 suggests user interface of the ecommerce website for redeeming travel points in a gamified public transportation system.

Fig. 2. Ecommerce Platform for Travel Points Redemption

Features of the Ecommerce Website:

1. **Cashback Rewards** Users can redeem their travel points for cashback rewards, which can be applied to future purchases within the platform or as discounts on transportation services.
2. **Exclusive Discounts** The website offers exclusive discounts on a variety of products and services. These discounts are available only to users who redeem their travel points, providing a unique incentive for active participation in the platform.
3. **Free Shipping** To further entice users, the ecommerce website includes options for free shipping on selected items. This makes the rewards more accessible and attractive, encouraging users to make more eco-friendly transportation choices.
4. **Early Access to New Products** Users who redeem their points can gain early access to new and innovative products. This feature creates a sense of exclusivity and motivates users to continue earning and redeeming points.
5. **Gift Cards** The ecommerce section offers gift cards that can be used for various purchases. These gift cards can be an excellent option for users looking to treat themselves or others, adding flexibility to the reward system.
6. **Limited Edition Items** Special limited-edition items are available for users who redeem their travel points. These exclusive products are designed to appeal to users' desire for unique and collectible rewards, further driving engagement.
7. **Premium Membership** Users can use their travel points to obtain premium membership status within the platform. Premium members enjoy additional benefits such as enhanced features, priority support, and exclusive content.
8. **Personalized Recommendations** The ecommerce website provides personalized recommendations based on users' travel behavior and preferences. This tailored approach ensures that the rewards are relevant and appealing, enhancing the overall user experience.

Benefits of the Ecommerce Website: The ecommerce website is designed to provide numerous benefits to users, including:

- **Increased Engagement**: By offering a variety of attractive rewards, the website keeps users motivated and engaged with the platform.
- **Promotion of Sustainable Behaviors:** The reward system encourages users to adopt sustainable transportation habits, contributing to the goal of reducing carbon emissions and promoting eco-friendly practices.
- **Enhanced User Satisfaction**: With a diverse range of rewards, users are likely to find something that appeals to them, increasing their satisfaction with the platform.
- **Support for Smart City Initiatives**: By promoting sustainable transportation and rewarding eco-friendly behaviors, the ecommerce website supports broader smart city goals.

The ecommerce website is a critical component of the public transportation platform, providing users with a tangible incentive to engage in sustainable

travel behaviors. By offering a wide range of rewards that can be redeemed with travel points, the website enhances user engagement, satisfaction, and supports the overall mission of promoting eco-friendly transportation within smart cities.

5. GAMIFICATION ELEMENTS FOR NATIONAL SECURITY, DISASTERS AND EMERGENCIES

The implementation of gamification on a dedicated website can enhance national security, disaster management, and emergency response efforts. As part of the national scientific program "Security and Defense," this initiative showcases various tools for preventing and managing incidents, disasters, and accidents. Users can access real-time notifications about potential natural disasters, accidents, and crises across Bulgaria directly through the website. The platform also educates users on modern information protection techniques, the impact of human factors on security, and the importance of societal support for national security.

The website serves as a hub for gathering public opinions on security and defense matters in Bulgaria, providing valuable insights for improving these measures. It supports state and local administration bodies by facilitating the monitoring and prevention of incidents and disasters. The focus areas include assisting authorities during emergencies, alerting the public, and providing training on self-protection methods.

By engaging with the website, users earn points and rewards, which include both intrinsic and extrinsic benefits, such as social status and recognition. These gamification strategies increase user engagement and support the broader goals of national security and disaster preparedness in Bulgaria.

6. CONCLUSION

The integration of gamification elements into public transportation platforms presents a promising approach to promoting sustainable transportation behaviors within smart cities. By incorporating loyalty programs, rewards, badges, and leaderboards, these platforms can significantly enhance user engagement and motivation. The development of an ecommerce website for redeeming travel points further incentivizes eco-friendly travel habits. Additionally, gamification can support national security and disaster management efforts by providing real-time notifications, educational content, and gathering public feedback. Future research and development should focus on refining gamification strategies, addressing technological barriers, and exploring their long-term impacts to maximize effectiveness in supporting sustainable urban mobility and broader smart city initiatives.

The report is in implementation of the National Scientific Program "Security and Defense", adopted with RMS No. 731/21.10.2021, and financed by the Ministry of Education and Science of the Republic of Bulgaria according to Agreement No. D01-74/ 19.05.2022.

References

[1] M. Sotirov, V. Petrova, and D. Nikolova-Sotirova, "Implementing Gamified Learning in University Environment," in 2023 International Conference Automatics and Informatics (ICAI), IEEE, Oct. 2023, pp. 476–480. doi: 10.1109/ICAI58806.2023.10339098.

[2] B. T. H. Yen, C. Mulley, and G. Meza, "Exploring the attitudes and perceptions influencing user participation in gamification schemes for TDM," Research in Transportation Economics, vol. 99, p. 101300, Jun. 2023, doi: 10.1016/J.RETREC.2023.101300.

[3] B. T. H. Yen, C. Mulley, and M. Burke, "Gamification in transport interventions: Another way to improve travel behavioural change," Cities, vol. 85, pp. 140–149, Feb. 2019, doi: 10.1016/J.CITIES.2018.09.002.

[4] R. Drakoulis et al., "A Gamified Flexible Transportation Service for On-Demand Public Transport," IEEE Transactions on Intelligent Transportation Systems, vol. 19, no. 3, pp. 921–933, Mar. 2018, doi: 10.1109/TITS.2018.2791643.

[5] L. Caroux, A. Arguel, M. Sacher, and C. Lemercier, "Gamification in transportation and mobilities: a preliminary overview of scientific literature," in 21st Triennial Congress of International Ergonomics Association - IEA 2021, Vancouver, 2021.

[6] J. Wang, X. Yang, A. Bailey, and J. Wang, "Positive spillover of consumers' sustainable behaviors: The mediating role of self-determination need satisfaction," J Clean Prod, vol. 317, p. 128436, Oct. 2021, doi: 10.1016/J.JCLEPRO.2021.128436.

[7] "Muni | Clipper." Accessed: Feb. 09, 2023. [Online]. Available: https://www.clippercard.com/ClipperWeb/muni.html

[8] "About SmarTrip® | WMATA." Accessed: Feb. 09, 2023. [Online]. Available: https://www.wmata.com/fares/smartrip/

[9] M. Sotirov, D. Nikolova-Sotirova, T. Georgieva, and V. Petrova, "From Dungeons to Dashboards: Integrating Game-Based Character Sheet in University Environment," in 2023 7th International Symposium on Innovative Approaches in Smart Technologies (ISAS), IEEE, Nov. 2023, pp. 1–6. doi: 10.1109/ISAS60782.2023.10391326.

EVALUATING THE EFFICACY OF GAMIFIED PUBLIC TRANSPORTATION SYSTEMS: A FRAMEWORK FOR EFFICIENCY AND IMPACT MODELLING

Milen Sotirov

Nikola Vaptsarov Naval Academy
Varna, Bulgaria
m.sotirov@naval-acad.bg

Valentina Petrova, Assoc. Prof. PhD

Nikola Vaptsarov Naval Academy
Varna, Bulgaria
v.petrova@naval-acad.bg

Donika Nikolova-Sotirova

Technical University – Varna
Varna, Bulgaria
donika.sotirova@tu-varna.bg

Abstract

This paper explores the integration of gamification into public transportation systems to promote sustainable travel behaviors within smart cities. By incorporating game elements such as points, badges, and leaderboards, these platforms can motivate users to choose eco-friendly options. The study reviews key findings from recent literature, proposes a comprehensive framework for evaluating gamification effectiveness, and develops a mathematical model to quantify its impact on user engagement and sustainability. Additionally, it examines the role of gamification in enhancing national security, disaster management, and emergency response.

1. INTRODUCTION

The demand for sustainable urban mobility solutions has led to the exploration of innovative approaches to enhance public transportation systems. Gamification, which involves using game design elements in non-game contexts, has shown significant potential in increasing user engagement and promoting eco-friendly behaviors. This paper investigates the application of gamification [1][2] in public transportation, focusing on its ability to support sustainable travel habits within smart cities. It synthesizes recent research, proposes a detailed framework for evaluating gamification effectiveness, and discusses the development of an ecommerce website for redeeming travel points. The paper also explores how gamification can aid national security and disaster management efforts.

2. LITERATURE REVIEW

Gamification has increasingly been recognized as a valuable tool for influencing user behaviors across various domains, particularly in promoting sustainable transportation.

Deterding et al. [3] They differentiate gamification from "serious games" and "playful design," focusing on using game design elements in non-game contexts. This distinction helps understand how gamification can effectively motivate and engage users.

Reindl et al. [4] Their literature review explores how gamification influences sustainable commuting. Identifying elements like points, leaderboards, and badges, they find these elements encourage behavioral change. Further research is needed to measure long-term impact and effectiveness.

Fonseca [5] examines gamification's role in promoting sustainable urban mobility, highlighting adoption challenges. Reviewing digital applications, the study identifies effective game elements and emphasizes personalization, user engagement strategies, and integration with existing systems.

Zimmermann et al. [6] They investigate digital nudging to shift commuters from car use to public transportation. Using choice-based conjoint analysis,

they find that trip recommendations via a mobility app significantly influence preferences, highlighting the importance of contextual factors and personalized approaches.

University of Warwick's Sustainable Transportation Initiative: Uses gamification to promote sustainable transportation among students, awarding points and badges for eco-friendly modes like bicycling and public transit. [7]

This literature review explores key studies that highlight the effectiveness of gamification in encouraging eco-friendly travel behaviors and identifies the critical elements and challenges associated with its implementation in public transportation systems.

3. FRAMEWORK FOR EVALUATING GAMIFICATION EFFECTIVENESS

To ensure the success of a gamified public transportation system, it is crucial to evaluate the effectiveness of the implemented gamification elements. This section proposes a comprehensive framework using specific metrics and statistical methods to assess the impact of these elements on user behavior and sustainability.

Engagement Rate: Measures the level of user interaction with the gamified platform over time. Key metrics include Daily Active Users (DAU), Monthly Active Users (MAU), and session length. Statistical methods such as trend analysis and cohort analysis are used to track and understand engagement patterns.

Retention Rate: Indicates the percentage of users who continue using the platform over a certain period. High retention rates are essential for long-term success. Metrics include 1-day, 7-day, and 30-day retention rates, analyzed using survival analysis and churn rate calculation.

Sustainability Impact: Measures the reduction in carbon emissions and other environmental benefits resulting from increased public transportation use. Metrics include public transportation usage, emission reduction, and miles traveled. Comparative and regression analyses are employed to assess the relationship between platform engagement and sustainability.

Data Collection: Utilizes app analytics tools to gather detailed data on user engagement, retention, and behavior patterns. Collaboration with local transportation authorities is essential for comprehensive data on public transportation usage and emissions.

Data Analysis: Applies statistical methods to rigorously analyze collected data, uncovering trends and correlations in user behavior and engagement with gamified features.

Reporting and Feedback: Regular reports summarize findings, insights, and recommendations, which are shared with stakeholders. User feedback [8] is incorporated to continuously enhance and refine gamification elements.

The proposed framework provides a holistic view of user engagement, retention, and sustainability impact, supporting informed decision-making and continuous improvement in promoting sustainable transportation behaviors.

4. MATHEMATICAL MODEL OF GAMIFICATION IMPACT

To quantify the impact of gamification on user engagement and sustainable transportation behavior, we develop a mathematical model based on user behavior dynamics. Let *U(t)* represent the number of active users at time *t*.

Differential Equation Model

The rate of change of active users can be modeled using a differential equation:

$$\frac{\mathrm{dU(t)}}{dt} = \alpha \mathrm{G(t)} - \beta \mathrm{U(t)}$$

where:

- *α* is the rate at which new users are attracted due to gamification elements.
- *G(t)* represents the gamification factor, a function of time that incorporates the effects of points, badges, leaderboards, and rewards.
- *β* is the rate at which users lose interest and stop using the app.

Gamification Factor

The gamification factor G(t) can be modeled as:

$$\mathrm{G(t)} = \mathrm{P(t)} + \mathrm{B(t)} + \mathrm{L(t)} + \mathrm{R(t)}$$

where:

- *P(t)* is the points earned by users over time.
- *B(t)* is the impact of badges and achievements.

- *L(t)* represents leaderboard effects.
- *R(t)* is the rewards system.

Solution and Analysis

Solving the differential equation provides insights into user engagement trends:

$$U(t) = \frac{\alpha}{\beta} G(t)(1 - e^{-\beta t})$$

This solution shows how user engagement stabilizes over time based on the balance between attraction and attrition rates.

Framework for Evaluating Effectiveness

We propose a framework to evaluate the effectiveness of the gamification elements using the following metrics:

1. **Engagement Rate**:

$$E(t) = \frac{U(t)}{N}$$

where *N* is the total number of registered users.

2. **Retention Rate**:

$$R(t) = \frac{U(t)}{U(0)}$$

where *U(0)* is the number of users at the initial time.

3. **Sustainability Impact**: Calculate the reduction in carbon emissions *C(t)* due to increased public transportation usage:

$$C(t) = \gamma(\sum_{i=1} \frac{U(t)}{} d_i)$$

where *γ* is the average emission reduction per user and d_i is the distance traveled by user *i*.

The mathematical model developed quantifies the impact of gamification on user engagement and sustainable transportation behaviour. By using differential equations to represent user behaviour dynamics, we can predict how gamification elements like points, badges, leaderboards, and rewards influence user retention and attraction. The proposed framework, including metrics for engagement rate, retention rate, and sustainability impact, offers a structured approach to evaluating the effectiveness of these gamification strategies. This model provides valuable insights for optimizing gamification elements to enhance user engagement and promote sustainable transportation practices.

5. FUTURE RESEARCH

Future research in gamifying public transportation can focus on the following areas:

- **User Experience and Engagement:** Further study of the user experience and engagement levels.
- **Impact on Travel Behavior:** Determine the long-term impact of gamification on travel behavior and sustainability.
- **Personalization:** Research personalized gamification experiences based on user preferences and behaviors.
- **Integration with Other Transportation Modes:** Explore the impact of integrating gamification with other transportation modes.
- **Cost-Benefit Analysis:** Conduct an in-depth cost-benefit analysis of gamification in public transportation.
- **User Demographics:** Study the effectiveness of gamification across different user demographics.
- **Interaction with Public Transportation Providers:** Investigate the interaction between gamification, public transportation providers, and local governments.

The findings suggest that gamification can effectively promote sustainable transportation behavior and increase public transportation adoption. The platform will undergo continuous monitoring and refinement based on user feedback and engagement data, tracking key metrics to measure the effectiveness of gamification elements.

6. GAMIFICATION ELEMENTS FOR NATIONAL SECURITY, DISASTERS AND EMERGENCIES

The implementation of gamification on a dedicated website can enhance national security, disaster management, website and emergency response efforts. Part of the national scientific program "Security and Defense," this initiative showcases tools for preventing and managing incidents, disasters, and accidents. Users receive real-time notifications

about potential natural disasters, accidents, and crises across Bulgaria through the website. The platform educates users on modern information protection techniques, human factors in security, and societal support for national security.

The website gathers public opinions on security and defense matters in Bulgaria, providing insights for improving these measures. It supports state and local administration bodies in monitoring and preventing incidents and disasters. The focus areas include assisting authorities during emergencies, alerting the public, and providing training on self-protection methods.

By engaging with the website, users earn points and rewards, including intrinsic and extrinsic benefits such as social status and recognition. These gamification strategies increase user engagement and support broader national security and disaster preparedness goals in Bulgaria.

7. CONCLUSION

Integrating gamification into public transportation platforms presents a promising approach to promoting sustainable transportation behaviors within smart cities. By incorporating loyalty programs, rewards, badges, and leaderboards, these platforms can significantly enhance user engagement and motivation. The development of an ecommerce website for redeeming travel points further incentivizes eco-friendly travel habits. Additionally, gamification can support national security and disaster management efforts by providing real-time notifications, educational content, and gathering public feedback. Future research and development should focus on refining gamification strategies, addressing technological barriers, and exploring their long-term impacts to maximize effectiveness in supporting sustainable urban mobility and broader smart city initiatives.

The report is in implementation of the National Scientific Program "Security and Defense", adopted with RMS No. 731/21.10.2021, and financed by the Ministry of Education and Science of the Republic of Bulgaria according to Agreement No. D01-74/ 19.05.2022.

References

[1] M. Sotirov, V. Petrova, and D. Nikolova-Sotirova, "Implementing Gamified Learning in University Environment," in 2023 International Conference Automatics and Informatics (ICAI), IEEE, Oct. 2023, pp. 476–480. doi: 10.1109/ICAI58806.2023.10339098.

[2] M. Sotirov and V. Petrova, "The Nine-Steps Gamification Process: Increasing Student Engagement in LMS," in 2023 International Conference Automatics and Informatics (ICAI), IEEE, Oct. 2023, pp. 496–501. doi: 10.1109/ICAI58806.2023.10339063.

[3] S. Deterding, D. Dixon, R. Khaled, and L. Nacke, "From game design elements to gamefulness: Defining 'gamification,'" Proceedings of the 15th International Academic MindTrek Conference: Envisioning Future Media Environments, MindTrek 2011, pp. 9–15, 2011, doi: 10.1145/2181037.2181040.

[4] A. Reindl, M. Juppe, P. Graf, L.-M. Putz-Egger, and W. Schildorfer, "The use of gamification to change commuters mobility behavior: A literature review," GamiFIN Conference, 2023.

[5] X. Fonseca, "Sustainable Mobility: How to Gamify and Factors to Better Success," EAI/Springer Innovations in Communication and Computing, vol. Part F633, pp. 115–134, 2023, doi: 10.1007/978-3-031-30514-6_6.

[6] S. Zimmermann, T. Schulz, A. Hein, H. Gewald, and H. Krcmar, "Motivating change in commuters' mobility behaviour: Digital nudging for public transportation use," J Decis Syst, vol. 33, no. 1, pp. 79–105, Jan. 2024, doi: 10.1080/12460125.2023.2198056.

[7] "Smarter Travel for Solihull | Smarter Travel Ltd." Accessed: Feb. 09, 2023. [Online]. Available: https://www.smartertravel.uk.com/smarter-travel-for-solihull/

[8] M. Sotirov, D. Nikolova-Sotirova, T. Georgieva, and V. Petrova, "From Dungeons to Dashboards: Integrating Game-Based Character Sheet in University Environment," in 2023 7th International Symposium on Innovative Approaches in Smart Technologies (ISAS), IEEE, Nov. 2023, pp. 1–6. doi: 10.1109/ISAS60782.2023.10391326.

IMPLEMENTING GRADIENT EDGE DETECTION IN FPGA: AN APPROACH TO MAXIMIZING OPERATING FREQUENCY AND MINIMIZING THE NUMBER OF CLOCK CYCLES

Dimitre Kromichev

Department of Marketing and International Economic Relations, University of Plovdiv
24 Tzar Asen Str, Plovdiv 4000, Bulgaria
dkromichev@yahoo.com

Abstract

For demanding applications, filtering is an indispensable stage in the computational flow of gradient based edge detection. Of the two main filtering techniques – linear and nonlinear, the former, represented generally by the Gaussian weighted average function, is preferred due to its capability to handle various noise types, thus rendering the gradients based edge detection universally usable. In the speed domain, when implemented in FPGA Gaussian filter, with respect to its mathematics, presents two capital problems: 1) it defines the optimal clock frequency of the entire edge detection method; 2) it determines the pipelining efficiency of the whole computational flow in terms of the minimum number of clock cycles required to produce a Gaussian filtered image pixel. This paper proposes an organization of Gaussian filtering computations which guarantees the maximizing of operating frequency and the minimizing of the number of clock cycles in FPGA based gradient edge detection without using embedded memory.

1. INTRODUCTION

There are various approahes to filtering in gradient edge detection [2][17][19][20]. The most prominent representatives of the nonlinear domain – median [3][22] and binominal [14][24] filters with their modifications [21], provide good results only for specific noise types. The most widely used linear filter in gradient edge detection is the Gaussian weighted average function [15][25]. In FPGA, Gaussian filtering mathematics presents problems in terms of both clock frequency and number of clock cycles [1][4][18][23]. The highest reported clock frequencies in FPGA are 65.044 MHz in Vertex 4 and 38.725 MHz in Spartan 6 [16] The number of clock cycles is not specified.

This paper proposes an organization of Gaussian filtering computations focused on accomplishing the following tasks: 1) design an organization of computations in FPGA based Gaussian filtering which is an optimal solution to the problem of speed in FPGA based gradient edge detection without using embedded memory; 2) investigate the proposed organization of computations for maximum operating frequency $F_{\max}$ and minimum number of clock cycles taken to sacure the result $nTclk_{\min}$; 3) define the value of $F_{\max}$ in FPGA gradient edge detection which uses Gaussian filtering. The tools used in the investigations are: Quartus, TimeQuest Timing Analyzer, ModelSim, Scilab. The hardware description language is VHDL. Ten Intel (Altera) FPGA families are used to obtain the experimental data. The analyses and conclusions are relevant for gray scale images.

2. DEFINING THE OPTIMAL VALUE OF $F_{\max}$ IN FPGA BASED GRADIENT EDGE DETECTION

Methodology:

- Differentiate between the two capital approaches to the FPGA based Gaussian filtering computations
- Prove the speed superiority of the selected approach with respect to the FPGA implementation
- Investigate the speed of the proposed organization of computations on a comparative basis.

FPGA based Gaussian filtering has three input variables: 1) size of input image; 2) size of filter; 3) magnitude of coefficients. All of them have a direct impact on speed and resource utilization. Basic assumptions of the proposed organization are: 1) every clock cycle a pixel is set at the Gaussian filter's input; 2) image is processed in a row-wise fashion; 3) pixels within the square neighbourhood are set by columns, left to right.

The integer arithmetic in Gaussian filtering producing the deepest logic defines F_{max} of FPGA based gradient edge detection [11][12]. It is proved that the integer division algorithm in [6] is not impacted by the magnitude of $dividenc$ because the largest $quotien$ is always 2^8-1. Experiments in [5], [7], [8], [9], [10], [13] prove that under equal test conditions multiplication produces the deepest logic. Thus, hard miltiplier's maximum operating frequency $F_{max}(hard)$ defines the optimal value of maximum operating frequency of Gaussian filtering $F_{max}(G)$. $F_{max}(hard)$ depends on miltiplier's size. The selection of size is according to the criteria: 1) it must be supported by all FPGA families; 2) it must accommodate the widest possible range of coefficients' magnitudes. Therefore, $F_{max}(hard)$ of 18 x 18 multiplier in its fastest speed grade defines the optimal value of $F_{max}(G)$ and, hence, the optimal value of F_{max} of FPGA based gradient edge detection.

2. GAUSSIAN FILTERING: ORDER OF ARITHMETIC OPERATIONS AND PARALLEL COMPUTATIONS

In FPGA, F_{max} is a function of input data width. It depends on the order in which arithmetic operations are executed. For a filter of size zxz there are two general approaches with respect to the position of division:

- Division is executed on the sum of all consecutive multiplication results

$$\frac{\sum_{i=1}^{N_C} R_{C_i}}{s} \quad (1)$$

where

Nc is the number of multiplications for a filter's size,

Rc is a multiplication result,

s is the sum of filter's coefficients.

- Division is executed on the result of each consecutive multiplication

$$\cdot \sum_{i=1}^{N_C} \frac{R_{C_i}}{s} \quad (2)$$

Experiments prove that (2) is possible only when the division algorithm in [6] is used. Division with variable $divisor$ and division by multiplying with the reciprocal of $divisor$ are not applicable. In (2) $F_{max}(G)$ cannot be impacted by the filter's size and coefficients' magnitude, and $nTclk_{min}(G)$ is a constant at $F_{max}(G)$.

The functional model of the proposed parallel Gaussian filtering is in Figure 1.

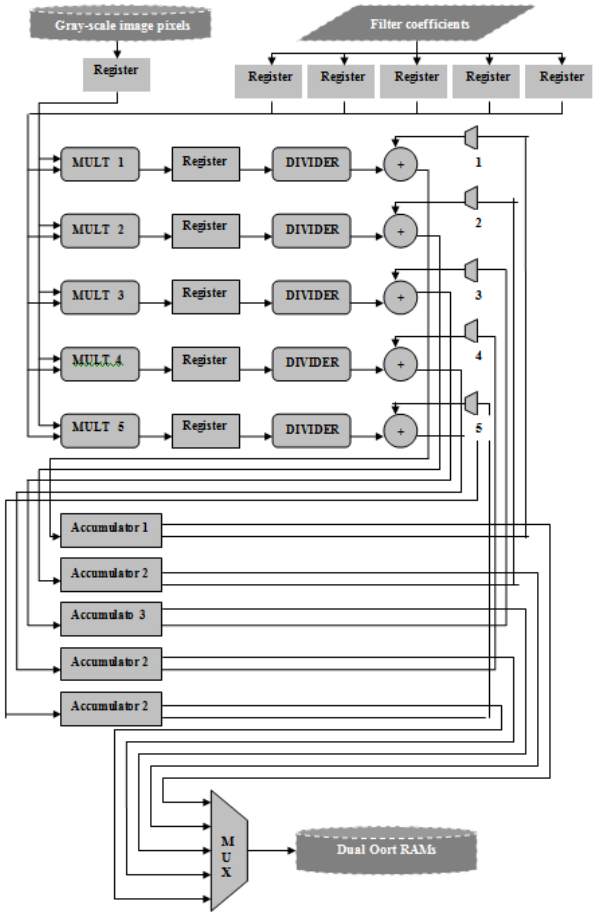

Figure 1. Functional model of parallel execution of operations in Gaussian filtering for 5x5 filter

The RTL design of Gaussian filtering for one accumulator is in Figure 2. The RTL design of the entire model of parallel Gaussian filtering computations for filter of size 5x5 is presented in Figure 3.

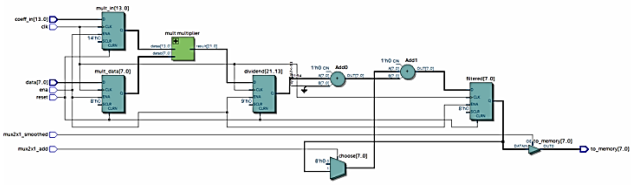

Figure 2. RTL design of Gaussian filtering for a single accumulator

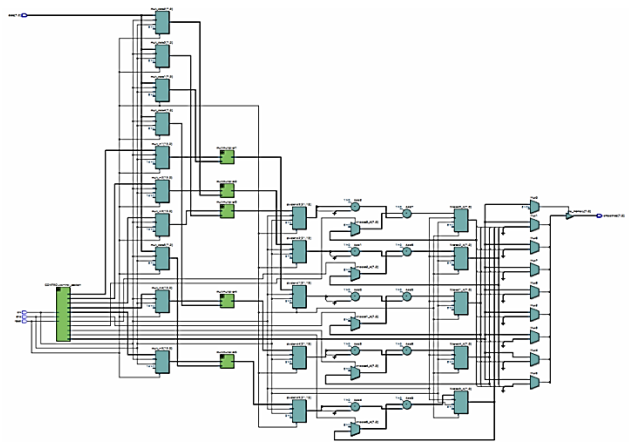

Figure 3. RTL design of the entire Gaussian filtering for 5x5 filter

The resource utilization of the RTL design in Figure 3 is presented in Table 1.

Table 1. Resource utilization for parallel Gaussian filtering with 5x5 filter

FPGA family	Resource utilization of parallel Gaussian filtering computations and control section for Gaussian filter of size 5x5				
	Logic utilization (in LEs/ ALUTs/ALMs)	Total registers	Total memory bits	Total DSP blocks	Embedded multiplier 9 bit elements
Cyclone	590 (LEs)	-	0	-	-
Cyclone II	512 (LEs)	316	0	-	10
Cyclone III	487 (LEs)	284	0	-	10
Cyclone IV	487 (LEs)	284	0	-	10
Cyclone V	189 (ALMs)	292	0	5	-
Stratix	562 (LEs)	337	0	3	-
Stratix II	408 (ALUTs)	309	0	3	-
Stratix III	394 (ALUTs)	288	0	3	-
Stratix IV	394 (ALUTs)	288	0	3	-
Stratix V	185 (ALMs)	291	0	2	-

3. INVESTIGATING THE SPEED OF THE PROPOSED GAUSSIAN FILTERING TECHNOLOGY IN FPGA

Methodology:

- The proposed organization of computations are tested by using various integer division algorithms: with a single division operation for a pixel, and with *z* number of division operations for a pixel
- The available organizations of computations are comparatively tested on the basis of $nTclk_{\min}(G)$ for optimal $F_{\max}(G)$
- Gaussian filter used in the tests: *z* = 5, central coefficient = 159

The results are in Table 2 and Table 3.

Table 2. Speed of the designed organization of Gaussian filtering computations for various integer division algorithms

FPGA family	Speed of designed organization of Gaussian filtering computations for various integer division algorithms					
	Advanced integer division algorithm		Integer division with *divisor* which is a variable implementing array divider		Integer division by multiplication with the reciprocal of *divisor*	
	$F_{\max}(G)$ (in MHz)	$nTclk_{\min}(G)$	$F_{\max}(G)$ (in MHz)	$nTclk_{\min}(G)$	$F_{\max}(G)$ (in MHz)	$nTclk_{\min}(G)$
Cyclone	132	6	19	8	45	8
Cyclone II	248	6	34	8	120	8
Cyclone III	291	6	41	8	138	8
Cyclone IV	159	6	44	8	140	8
Cyclone V	295	6	46	8	248	8
Stratix	278	6	37	8	163	8
Stratix II	401	6	57	8	259	8
Stratix III	503	6	68	8	317	8
Stratix IV	505	6	82	8	320	8
Stratix V	507	6	80	8	479	8

Table 3. $nTclk_{\min}(G)$ of Gaussian filtering at $F_{\max}(G)$ by using various computational approaches

Organization of computations in Gaussian filtering	$nTclk_{\min}(G)$ at $F_{\max}(G)$ by using various computational approaches		
	Advanced integer division algorithm	Integer division with *divisor* which is a variable implementing array divider	Integer division by multiplication with the reciprocal of *divisor* With rounding executed wothon a separate clock cycle
Sequential	-	34	28
Separanility without applying distributive low by columns & rows	-	36	30
Separanility with applying distributive low by columns & rows	-	32	26
Symmetry with simultaneous multiplication	-	34	28
Symmetry with sequential multiplication	-	36	30
Designed organization of computations	6	-	-

4. ANALYSIS OF RESULTS

According to the data in Table 2 the optimal value of $F_{\max}(G)$ of the proposed organization of computations is achieved only on the basis of using the integer division algorithm in [6]. For Cyclone II-V and Stratix I-V, $F_{\max}(G)$ when using the division algorithm in [6] is from 84.3% to 86.3% higher than $F_{\max}(G)$ when using division with $divisor$ which is a variable. For Cyclone, $F_{\max}(G)$ using the division algorithm in [6] is 85.7% higher.

In Cyclone II-V and Stratix I-V, $F_{\max}(G)$ when using the division algorithm in [6] is from 5.6% to 51.7% higher than $F_{\max}(G)$ when using integer division by multiplication with the reciprocal of $divisor$. This large difference in percentage terms is due to the following:

- There is no proportionality between the number of bits in $divisor$ and the number of bits in the integer representing the reciprocal of $divisor$. In this case, the number

of bits in the reciprocal of $divisor$is larger than 17 bits

- In Cyclone II-IV, the largest multiplier size is 18x18. Therefore, two hard multipliers must be cascaded to execute division. Hence, $F_{max}(G)$ is more than 50% lower.
- In Cyclone V and Stratix V there is 27x27 multiplier. Hence, in Cyclone V $F_{max}(G)$ is 15.7% lower, and in Stratix V $F_{max}(G)$ is 5.6% lower.
- In Stratix I - IV there is no 27x27 multiplier. Therefore, the difference in $F_{max}(G)$ is based on the difference between 18x18 multiplier and 36x36 multiplier.

In Cyclone, $F_{max}(G)$ when using division algorithm in [6] is 66% higher than $F_{max}(G)$ using integer division by multiplication with the reciprocal of $divisor$. This is due to the fact that multiplier here is logic elements based. For this width of the reciprocal of $divisor$ the optimal value of $F_{max}(G)$ is achieved for 5 clock cycles. In the proposed organization of computations multiplication must be executed within a single clock cycle.

The data in Table 2 shows that for all tested integer division algorithms $nTclk_{min}(G)$ is a costant. Because in division with $divisor$ which is a variable and division by multiplication with the reciprocal of $divisor$ there is a rounding operation, and rounding is executed within a separate clock cycle, filtering an image pixel with the division algorithm in [6] requires two clock cycles less.

Table 3 shows that for $nTclk_{min}(G)$ the proposed organization of computations is from 81.3 to 83.4% faster than the approaches to Gaussian filtering when using division with $divisor$ which is a variable, and from 77% to 80% faster than the other approaches to Gaussian filtering when using division by multiplication with the reciprocal of $divisor$

5. CONCLUSION

Proposed is an organization of Gaussian filtering computations for FPGA based gradient edge detection without using embedded memory. Experiments in ten Intel (Altera) FPGA families prove that $F_{max}(G)$ is defined by F_{max} of 18x18 hard multiplier and $nTclk_{min}(G)$ is equal to the side of Gaussian filter plus one.

References

[1] Arun Mahajan, "Paramveer Gill, 2D Convolution Operation with Partial Buffering Implementation on FPGA", International Journal of Image, Graphics and Signal Processing (IJIGSP), 12, 2016, pp. 55-61

[2] Cao, Yiqin, Wu Dan, Dan Duan, Yeyu, "A new image edge detection algorithm based on improved Canny", Journal of Computational Methods in Sciences and Engineering, vol. 20, no. 2, 2020, pp. 629-642

[3] Chang-Yong Lee, Young-Hyung Kim, and Yong-Hwan Lee Optimized "Hardware Design using Sobel and Median Filters for Lane Detection", Journal of JAITC, Vol. 9, No. 1, 2019, pp.115-125

[4] Deepak Raj, Poonam Singal, "Reducing the Computational Complexity of a 2d Gaussian Filter for Image Processing (An Overview) ", International Journal of Advance Research, Ideas and Innovations in Technology, Volume 3, Issue3, 2017, pp. 514-517

[5] Dimitre Kromichev, "An Approach to Computing the Gradients in FPGA Based Edge Detection Focused on Ultimate Execution Speed and Exactness of Detected Contours", Proceedings of 16th International Engineering Conference on Communications, Electromagnetics and Medical Applications (CEMA'23), 2023, pp. 47-51

[6] D. Kromichev, "FPGA Based Edge Detection: Integer Division Algorithm with a Constant Divisor", 2022 13th National Conference with International Participation (ELECTRONICA), Bulgaria, 2022, pp. 1-4

[7] Dimitre Kromichev, "FPGA Based Edge Detection: Integer Square Root Algorithm", Proceedings of 16th International Engineering Conference on Communications, Electromagnetics and Medical Applications (CEMA'22), 2022, pp. 25-29

[8] Dimitre Kromichev "FPGA Based Edge Detection: Integer Inverse Tangent Algorithm", Proceedings of16th International Engineering Conference on 'Communications, Electromagnetics and Medical Applications' (CEMA'22), 2022, pp. 30-34

[9] Dimitre Kromichev, "Investigation of Different Multipliers Focused on Ultimate Execution Speed in FPGA Based Edge Detection", Computer Science and Technologies, ISSN 1312- 3335, Vol. 1, 2022, pp. 6-14

[10] Dimitre Kromichev, "Study of Different Adders Focused on Ultimate Execution Speed in FPGA Based Edge Detection", Journal of the Technical University - Sofia, Plovdiv Branch "Fundamental Sciences and Applications", vol. 28(1), 2022

[11] Dimitre Kromichev, "Ultimate Execution Speed in FPGA Based Edge Detection: Technology of Accurate Rounding in Integer Division with a Variable Divisor", Computer Science and Technologies, ISSN 1312- 3335, Vol. 1, 2022, pp. 15-24

[12] Dimitre Kromichev, "Ultimate Execution Speed in FPGA Based Edge Detection: Investigating the Speed Parameters of Iterative Integer Division", Computer Science and Technologies, ISSN 1312- 3335, Vol. 1, 2022, pp. 25-35

[13] Dimitre Kromichev, "Ultimate Execution Speed in FPGA Based Edge Detection: Comparative Investigation of Four FPGA Specific Integer Multipliers", Computer Science and Technologies, ISSN 1312- 3335, Vol. 1, 2023, pp. 38-47

[14] El Houssain Ait Mansour, Francois Bretaudeau, "A novel edge detection method based on efficient gaussian binomial filter", International Journal of Advances in Intelligent Informatics, Vol. 7, No 2, 2021, pp. 62-68

[15] Gian Domenico Licciardo, Carmine Cappetta, Luigi Di Benedetto, "FPGA optimization of convolution-based 2D filtering processor for image processing", 2016 8th Computer Science and Electronic Engineering (CEEC), 2016, pp. 668-676

[16] Harshal Prajapati, "RTL Implementation of Gaussian Filter Using VHDL", International Journal of Engineering Sciences & Research Technology, 2016, pp. 813-817

[17] Huang, S. C. Hoang, Q. V. Le, T. H. Peng, Y. T. Huang, C. C. Zhang, C. Fung, B. C. M. Cheng, K. H. Huang, S. W. "An Advanced Noise Reduction and Edge Enhancement Algorithm", Sensors, 21, 5391, 2021, pp. 1-12

[18] L. Rao, Bin Zhang, Jizhong Zhao, "Hardware Implementation of Reconfigurable 1D Convolution", Journal of Signal Processing Systems, 2016, pp. 232-237

[19] Min Wang, Shudao Zhou, Zhanhua Liu, "Adaptive Image Denoising with Block-Rotation-Based SVD Filtering and Edge Detection", International Journal of Remote Sensing, Volume 42, 2021 - Issue 8, 2021, pp. 3166-3179

[20] Ng Kok Soon, Zuraida Abal Abas, Asmala Ahmad, Hidayah Rahmalan, "Improvement of the Traditional Canny Edge Detection Algorithm by using Combination of Arithmetic Mean Filter, Harmonic Mean Filter and Geometric Mean Filter", International Journal of Innovative Technology and Exploring Engineering (IJITEE), Volume-9 Issue-2, 2019, pp. 486-490

[21] P. Taghinia Jelodari, M. Parsa Kordasiabi, S. Sheikhaei and B. Forouzandeh, "FPGA implementation of an adaptive window size image impulse noise suppression system", Journal of Real-Time Image Processing, vol. 16, no. 6, 2017, pp. 2015-2026

[22] P. Topno and G. Murmu, "An Improved Edge Detection Method based on Median Filter", 2019 Devices for Integrated Circuit (DevIC), 2019, pp. 378-381

[23] Sa'ed Abed, "Implementation of Edge Detection Algorithm using FPGA Reconfigurable Hardware", Journal of Engineering Research, Vol 8, No 1, 2020, pp.867-872

[24] S. D. Dabhade, G. N. Rathna and K. N. Chaudhury, A Reconfigurable and Scalable "FPGA Architecture for Bilateral Filtering", in IEEE Transactions on Industrial Electronics, vol. 65, no. 2, 2018 pp. 1459-1469

[25] Tarun Tyagi, Vishal Mishra, "2D Gaussian Filter for Image Processing: A Study", IJSTE - International Journal of Science Technology & Engineering, Volume 3, Issue 06, December 2016, pp. 74-82

INVESTIGATING THE UPPER LIMIT OF SPEED IN TRADITIONAL NON-MAXIMUM SUPPRESSION WITH SIMULTANEOUS DYNAMIC THRESHOLD COMPUTATION IN FPGA BASED GRADIENT EDGE DETECTION

Dimitre Kromichev

Department of Marketing and International Economic Relations, University of Plovdiv
24 Tzar Asen Str, Plovdiv 4000, Bulgaria
dkromichev@yahoo.com

Abstract

A single pixel thin contours and continuous contours are two important criteria for precision in edge detection. Satisfying these criteria by applying the traditional (John Canny's) approach requires the addressing of two specific problems in FPGA based gradient edge detection: 1) the traditional mathematics of edge thinning leads to up to 50% of false negatives in a number of cases for various image statistics. This problem was addressed, thoroughly analyzed and resolved by proposing a correction to the non-maximum suppression mathematics; 2) the threshold calculation in a sequential fashion by using the entire image statistics is incompatible with the concept of speed and the use of FPGA based gradient edge detection for demanding applications in real time. The latter is dealt with and resolved in this paper by proposing a non-maximum suppression with simultaneous dynamic threshold computation. The organization of computations is investigated for its upper speed limit in ten Intel (Altera) FPGA families

1. INTRODUCTION

There is a nunber of approaches to the problem of thrershold computation in gradient edge detection. They can be summarized as: 1) within-class variance method, 2) customized threshold function; 3) self-adaptive threshold computation; 4) connected component analysis algorithm, 5) genetic algorithm, 6) adaptive threshold computation by doing a differential operation on amplitude gradient histogram, 6) adaptive threshold selection method, 7) adaptive dual-threshold detection method; 8) self-adaptive threshold; 9) type-2 fuzzy set-based technique; 10) S-membership function [16]. All of them are executed as a separate stage after the entire image has been non-maximum suppressed [6][11][12] [13]. The most widely applied is the within-class variance method used for adaptive thresholding based on calculating: 1) the gray level gradient histogram; 2) the probability of background and object; 3) the maximum between-cluster variance of different regions; 4) the threshold with maximum between-cluster variance σ; 5) the low threshold as the high threshold value multiplied by 0.4 or 0.5 [2][10][19]. Automatic selection of the thresholds relies on gradient histogram concavity analysis. High threshold is selected between the largest peak and the second largest peak by using a non-uniform quantizer [8], [17]. The following disadvantage is pointed out: use of gradient calculation to define the angle of suppression [18]. In FPGA implementations there are several general approaches. In distributed Canny [14][15] an intermediate classification threshold is calculated based on a set of pixels with gradient magnitudes larger than a defined value; then the 64-bin uniform discrete histogram is used for the high threshold calculation. Low threshold is 40% of the high threshold. 128x128, 256x256 and 512x512 images are used. Maximum reported clock frequency is 100 MHz. No counting methodology is provided, and, therefore the total number of clock cycles for executing the distributed Canny is not specified. When derivative and smoothing operations are combined into a single mask high and low thresholds are fixed to constant values [9]. In block level implementation standard non-maximum suppression is used, and then uniformly quantized gradient magnitude histograms are computed on overlapped blocks. Adaptive thresholding is based on block classification [7].

Although the concept of selecting the largest value pixel as a technique to thin the detected contour had been in circulation for quite some time it is the John Canny's paper of 1986 [1] that defined this approach as a required stage in gradient edge detection. The approach in [1], referred to as traditional, presents two capital problems to the FPGA im-

plementation of gradient edge detection: 1) the mathematics of edge thinning given in [1] leads to 50% of false negatives in a number of cases and various image statistics. This problem was addressed, thoroughly analyzed and resolved in [3] by proposing a correction to the non-maximum suppression mathematics; 2) the threshold calculation in a sequential fashion by using the entire image statistics is incompatible with the concept of speed and the use of FPGA based gradient edge detection for demanding applications in real time. The latter is addressed and resolved in this paper by proposing a non-maximum suppression technology with simultaneous dynamic threshold computation. The upper speed limit of the proposed organization of computations is experimentally investigated. The analyses and conclusions are relevant for gray scale images. Ten Intel (Altera) FPGA families are employed in the investigations to obtain the experimental data and draw the relevant conclusions by using the follwing tools: Quartus, TimeQuest Timing Analyzer, ModelSim, Scilab. The hardware description language is VHDL.

2. DYNAMIC THRESHOLD COMPUTATION

The goal here is to execute accurate threshold computation in a dynamic fashion, and simultaneously with the non-maximum suppression. The steps are:

1) Defined is a closed interval of integers TH such that

$$[(N_{\max}+1)-N_{\min}=RTH]\&[\frac{RTH}{7})=$$

$$[0]\&[N_{\max}+N_{\min}<2^8-1] \qquad (1)$$

where

$N_{\max}$ is the rightmost value in TH ,

$N_{\min}$ is the leftmost value in TH ,

RTH is the result of $(N_{\max}+1)-N_{\min}$.

2) TH is divided into subintervals $SUB\_TH's$ in which the ratio between the rightmost value $SUB\_N_{\max}$ and the leftmost value $SUB\_N_{\min}$ is defined by the equation

$$(SUB\_N_{\max}+1)-SUB\_N_{\min}=6\ . \qquad (2)$$

3) Each SUB_TH subinterval is associated with a reference table value RTV which is defined as

$$RTV=(SUB\_N_{\max}-3)=SUB\_N_{\min}+3 \qquad (3)$$

4) Defined is a set of table values – they are integers calculated by dividing the values in the interval [5, 250] by these five values $\{2,2.2,2.5,2.8,3\}$.

5) Defined is a set of counters $COUNT\_SUB\_TH$ Each counter is associated with a concrete SUB_TH. Starting with non-maximum suppressed image pixel #1, each pixel value PV is checked for

$$SUB\_N_{\max}\geq PV\geq SUB\_N_{\min} \qquad (4)$$

If (4) is true, then

$$COUNT\_SUB\_TH=$$
$$COUNT\_SUB\_TH+1 \qquad (5)$$

6) When the entire image is non-maximum suppressed the values in the counters are compared to select the two largest among them. Selected are the two $SUB\_TH's$ and their $RTV's$ which correspond to these two largest values. For the computation of the high threshold the smaller of the two – $SUB\_TH_{smaller}$ and its $RTV_{smaller}$, is used. The high threshold is associated with a set of table values which are precalculated by using a divisor from $\{2,2.2,2.5,2.8,3\}$. The selected table value is the low threshold.

3. FPGA BASED NON-MAXIMUM SUPPRESSION WITH SIMULTANEOUS DYNAMIC THRESHOLD COMPUTATION

Organization of computations in non-maximum suppression focuses on: 1) maximum operatimg frequency $F_{\max}(NMS)$ and minimum number of clock cycles $nTclk_{\min}(NMS)$; 2) simultaneous dynamic threshold computation; 3) pipelining efficiency.

The organization of computations is based on: 1) mid-level pipelining (Figure 1); 2) low level parallelism (Figure 2); 3) number of uses of a single pixel (Figure 3) [4][5].

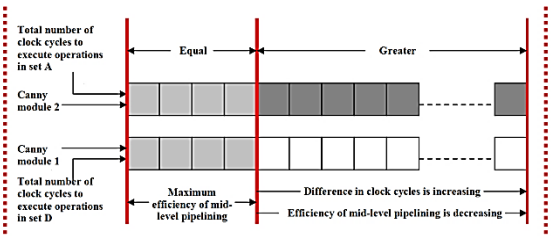

Figure 1. Model of mid-level pipelining

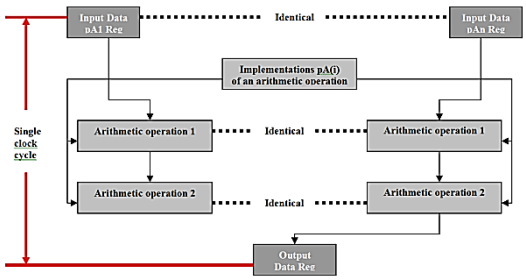

Figure 2. Model of low level parallelism (single clock cycle)

The functional model of the proposed technology in FPGA is shown in Figure 4.

When the last image pixel is non-maximum suppressed the thresholds are already dynamically computed. Therefore, thresholding can start immediately after the last image pixel is non-maximum suppressed. This contributes to the optimal value of $nTclk_{\min}$ in FPGA based gradient edge detection. Using VHDL, the resultant

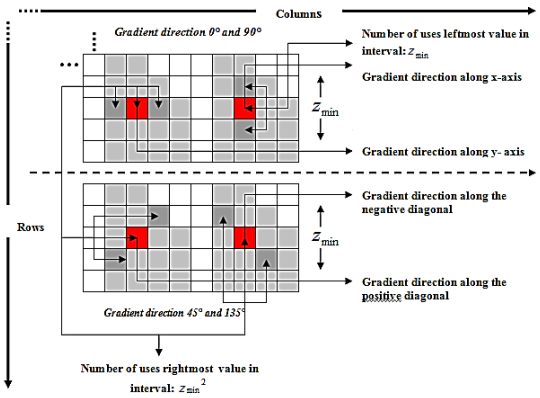

Figure 3. Model of minimum number of uses of a single pixel from the square neighbourhood

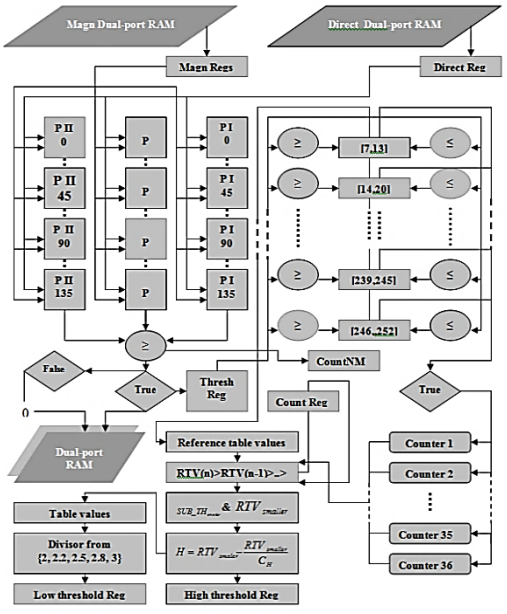

Figure 4. Functional model of non-maximum suppression with dynamic threshold computation

RTL design of non-maximum suppression with simultaneous dynamic threshold computation is (Figure 5):

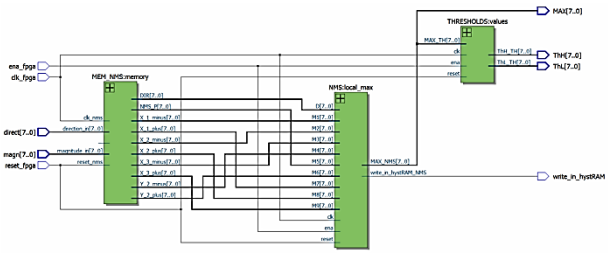

Figure 5. RTL design of non-maximum suppression with dynamic threshold computation

Resource utilization for non-maximum suppression with simultaneous dynamic threshold computation and memory control section is shown in Table 1.

Table 1. Resource utilization for non-maximum suppression with dynamic threshold computation

FPGA family	Resource utilization of non-maximum suppression, dynamic threshold computations and memory control section				
	Logic utilization (in LEs/ ALUTs/ALMs)	Total registers	Total memory bits	Total DSP blocks	Embedded multiplier 9 bit elements
Cyclone	2809 (LEs)	-	65536	-	-
Cyclone II	2741 (LEs)	1378	65536	-	0
Cyclone III	2672 (LEs)	1283	65536	-	0
Cyclone IV	2672 (LEs)	1283	65536	-	0
Cyclone V	1022 (ALMs)	1308	65536	0	-
Stratix	2440 (LEs)	1422	65536	0	-
Stratix II	2215 (ALUTs)	1341	65536	0	-
Stratix III	2045 (ALUTs)	1279	65536	0	-
Stratix IV	2045 (ALUTs)	1279	65536	0	-
Stratix V	1012 (ALMs)	1303	65536	0	-

4. INVESTIGATING THE SPEED OF NON-MAXIMUM SUPPRESSION WITH DYNAMIC THRESHOLD COMPUTATION IN FPGA

All available approaches to threshold computation are characterized by two facts: 1) an entire new module is inserted in FPGA based gradient edge detection; 2) FPGA based computations stop executing until the entire non-maximum suppressed image is processed. On that basis, $F_{\max}(NMS)$ and $nTclk_{\min}(NMS)$ of the proposed organization of computations cannot be tested comparatively. The specifics of non-maximum suppression with dynamic threshold computation requires two levels of presenting the test results for $nTclk_{\min}$: 1) $nTclk_{\min}(NMS)$` which defines the minimum number of clock cycles required to process a single image pixel with non-maximum suppression; 2) $nTclk_{\min}(Thresh)$ – the minimum number of clock cycles required by the threshold computation.

The obtained results are in Table 2.

5. ANALYSIS OF RESULTS

Because the largest value in a counter is guaranteed to be within 17 bits on the basis of satisfying the inequality (4), the obtained data shown in Table 2 represents the worst case scenario for $F_{max}(NMS)$. The requirements of mid-level pipelining, low level parallelism and the number of uses of a single pixel having been satisfied, $nTclk_{min}(Thresh)$ takes only the last 39 clock cycles of the execution of the non-maximum suppression computations. Therefore, the most important achievement of the proposed organization of computations in terms of minimizing the number of clock cycles in the entire FPGA based gradient edge detection is that the non-maximum suppression computations and the threshold computation end simultaneously.

Table 2. $F_{max}(NMS)$, $nTclk_{min}(NMS)$ and $nTclk_{min}(Thresh)$ of the designed organization of non-maximum suppression with dynamic threshold computation

FPGA family	Speed of the designed organization of non-maximum suppression with dynamic computation of high and low thresholds		
	$F_{max}(NMS)$ (in MHz)	$nTclk_{min}(NMS)$ required to non-maximum suppress a single image pixel	$nTclk_{min}(Thresh)$ required to calculate the low threshold
Cyclone	232	1	39
Cyclone II	319	1	39
Cyclone III	367	1	39
Cyclone iV	370	1	39
Cyclone V	388	1	39
Stratix	331	1	39
Stratix II	464	1	39
Stratix III	589	1	39
Stratix IV	637	1	39
Stratix V	685	1	39

7. CONCLUSION

Proposed in this paper is a non-maximum suppression technology with simultaneous dynamic threshold computation. The upper speed limit of the proposed organization of computations is experimentally investigated in ten Intel (Altera) FPFA families. On the basis of applying mid-level pipelining, low level parallelism and the number of uses of a single pixel approaches for minimizing the required number of clock cycles it is ascertained that the entire threshold computation takes only 39 clock cycles to execute. Most importantly, the non-maximum suppression computations and the threshold computation end simultaneously under all test conditions.

References

[1] Canny J., A., "Computational Approach to Edge Detection", IEEE Transaction on Pattern Analysis and Machine intelligence, No. 6, 1986, pp. 679-698

[2] Cao, Yi qin, Wu Dan, Dan Duan, Yeyu, "A new image edge detection algorithm based on improved Canny", Journal of Computational Methods in Sciences and Engineering, vol. 20, no. 2, 2020, pp. 629-642

[3] Dimitre Kromichev, "Gradient Based Edge Detection: Investigating the Problem of False Negatives in Terms of Edge Thinning", Proceedings of 16th International Engineering Conference on Communications, Electromagnetics and Medical Applications (CEMA'23), 2023, pp. 52-57

[4] Dimitre Kromichev, "Speed Focused FPGA Based Canny Computations: Pipelining", Journal of the Technical University Sofia, Plovdiv Branch, Fundamental Sciences and Applications, ISSN 1310-8271, Volume 26 No 1 (2020)

[5] Dimitre Kromichev, "Parallelism in Speed Focused FPGA Based Canny Computations Journal of the Technical University Sofia, Plovdiv Branch, Fundamental Sciences and Applications, ISSN 1310-8271, Volume 26 No 1 (2020)

[6] D. J. Bora, "An optimal color image edge detection approach", 2017 International Conference on Trends in Electronics and Informatics (ICEI), 2017, pp. 342-347

[7] Enzeng Dong, Yao Zhao, Xiao Yu, Junchao Zhu, Chao Chen, "An Improved NMS-Based Adaptive Edge Detection Method and Its FPGA Implementation", Hindawi Publishing Corporation Journal of Sensors, Volume 10, 2016, pp. 512-520

[8] Ferdous Hossain, Mithun Kumar P.K., Mohammad Abu Yousuf, "Hardware Design and Implementation of Adaptive Canny Edge Detection Algorithm", International Journal of Computer Applications, Volume 124 (9), 2015, pp. 62-68

[9] Gao Jie and Liu Ning, "An improved adaptive threshold canny edge detection algorithm", IEEE Transactions, International Conference on Computer Science and Electronics Engineering (ICCSEE), Vol. 1, 2012, pp.164-168

[10] Kewen Liu, Kang Xiao, and Hongxia Xiong, "An Image Edge Detection Algorithm Based on Improved Canny", 5th International Conference on Machinery, Materials and Computing Technology (ICMMCT 2017), 2017, pp. 533-537

[11] Lin Zhang, "Image Adaptive Edge Detection Based on Canny Operator and Multiwavelet Denoising", 2014 International Conference on Computer Science and Electronic Technology (ICCSET 2014), 2014, pp. 335-338

[12] L. Rao, Bin Zhang, Jizhong Zhao, "Hardware Implementation of Reconfigurable 1D Convolution", Journal of Signal Processing Systems, 2016, pp. 232-237

[13] Ojashwini R. N., Gangadhar Reddy R., Rani R.N., Pruthvija B., "Edge Detection Canny Algorithm Using

Adaptive Threshold Technique", Intelligent Data Engineering and Analytics. Advances in Intelligent Systems and Computing, vol. 1177, 2021, pp. 202-210

[14] Rinjo A. J. and Remya K. P., "FPGA Implementation of Distributed Canny Edge Detector for Low Clarity Images", IJISET - International Journal of Innovative Science, Engineering & Technology, Vol. 3, Issue 6, June 2016, pp. 618-622

[15] R. Jayarani, "Edge Detection using Distributed Canny Algorithm and Implementation in FPGA", International Journal of Research in Engineering, Science and Management, Volume-2, Issue-5, May-2019, pp. 1043-1047

[16] Shwetha.V,. C.H.Renu Madhavi, "Design Techniques for Improvement of Canny Edge Detection Algorithm", International Journal of Creative Research Thoughts (IJCRT), Volume 8, Issue 8, August 2020, pp. 1224-1231

[17] Sun Tao and Chang Zhi Gao, "An Improved Canny Edge Detection Algorithm", Applied Mechanics and Materials, vol. 291–294, Trans Tech Publications, Ltd., Feb. 2013, pp. 2869–2873

[18] Tao Yang, Yue-hong Qiu, "Improvement and implementation for Canny edge detection algorithm", Proc. SPIE 9631, Seventh International Conference on Digital Image Processing (ICDIP 2015), 6 July 2015, pp. 845-854

[19] Xiang Wu, Weibo Yu, Xiaotong Liu and Keping Liu, "A Newly Improved Canny Algorithm of Image Edge Detection", International Conference on Information Engineering for Mechanics and Materials (ICIMM 2016), 2016, pp. 501-510

AUTHOR INDEX